AFFDL-TR-79-3157

LEVEL II

AD A082335

INFLUENCE OF PITCHING MOMENT CHARACTERISTICS ON DEPARTURE AND UNCOORDINATED ROLL REVERSAL BOUNDARIES FOR FIGHTER CONFIGURATIONS

W. BIHRLE, JR.
B. BARNHART

BIHRLE APPLIED RESEARCH, INC.
400 JERICHO TURNPIKE
JERICHO, NEW YORK 11753

FEBRUARY 1980

DTIC
ELECTE
S
MAR 27 1980
D
E

DDC FILE COPY

80 3 24 105

ROBERT B. CROMBIE, 1Lt, USAF
Project Engineer
Control Dynamics Branch
Flight Control Division

VERNON O. HOEHNE, Acting Chief
Control Dynamics Branch
Flight Control Division

FOR THE COMMANDER

MORRIS A. OSTGAARD
Acting Chief
Flight Control Division

REPORT DOCUMENTATION PAGE	READ INSTRUCTIONS BEFORE COMPLETING FORM

1. REPORT NUMBER	2. GOVT ACCESSION NO.	3. RECIPIENT'S CATALOG NUMBER
AFFDL-TR-79-3157		

4. TITLE (and Subtitle)	5. TYPE OF REPORT & PERIOD COVERED
Influence of Pitching Moment Characteristics on Departure and Uncoordinated Roll Reversal Boundaries for Fighter Configurations.	Final rept. May 78 — June 79
	6. PERFORMING ORG. REPORT NUMBER

7. AUTHOR(s)	8. CONTRACT OR GRANT NUMBER(s)
William/Bihrle, Jr. Billy/Barnhart	F33615-78-C-3609

9. PERFORMING ORGANIZATION NAME AND ADDRESS	10. PROGRAM ELEMENT. PROJECT, TASK AREA & WORK UNIT NUMBERS
Bihrle Applied Research, Inc. 400 Jericho Turnpike Jericho, N.Y. 11753	P.E. 62201F 24030520 05

11. CONTROLLING OFFICE NAME AND ADDRESS	12. REPORT DATE
Air Force Flight Dynamics Laboratory/FGC Air Force Systems Command Wright-Patterson AFB, Ohio 45433	Feb 1980
	13. NUMBER OF PAGES
	117

14. MONITORING AGENCY NAME & ADDRESS(if different from Controlling Office)	15. SECURITY CLASS. (of this report)
	Unclassified
	15a. DECLASSIFICATION/DOWNGRADING SCHEDULE

16. DISTRIBUTION STATEMENT (of this Report)

Approved for public release; distribution unlimited.

17. DISTRIBUTION STATEMENT (of the abstract entered in Block 20, if different from Report)

18. SUPPLEMENTARY NOTES

19. KEY WORDS (Continue on reverse side if necessary and identify by block number)

Flying Qualities	Departure	Dynamic Stability
Stability and Control	Roll Reversal	
High Angle of Attack	Large-Angle Motions	
Statically Unstable Aircraft	Control Configured Vehicles	

20. ABSTRACT (Continue on reverse side if necessary and identify by block number)

A study is reported which generated design charts and developed associated boundaries for identifying departure and uncoordinated roll-reversal flight characteristics as a function of aerodynamic rolling and yawing moment co-efficients typical of fighter airplanes for various pitching moment characteristics. This information should be valuable for specification, design and evaluation purposes.

The investigation utilized a large angle, six-degree-of-freedom digital computer program to simulate the motions of a fighter performing a severe air combat

DD FORM 1 JAN 73 **1473** EDITION OF 1 NOV 65 IS OBSOLETE

maneuver. The results showed that the developed uncoordinated roll reversal boundaries may be applied to any fighter configuration and that the developed departure boundaries are applicable to fighter configurations exhibiting static pitch stability. Unaugmented airframes having pitch instability impose more stringent requirements on the rolling and yawing moment coefficients to avoid departure susceptibility. A simple angle-of-attack feedback augmentation system can markedly improve the departure resistance of both stable and unstable airframes given sufficient control authority.

FOREWORD

This report was prepared for the United States Air Force by Bihrle Applied Research, Inc., Jericho, New York, in fulfillment of Contract F33615-78-C-3600, "Departure Trends of Control Configured Vehicle Aircraft," Project 2403, Task 05, Work Unit 24030520. The work reported herein was performed during the period May 1978 through June 1979 under the sponsorship of the Air Force Flight Dynamics Laboratory, Wright-Patterson Air Force Base, Ohio, 45433. Gary K. Hellmann and Lt Robert B. Crombie were the Air Force Project Engineers who monitored this study during different periods of time.

The NASA Langley Research Center CDC6600 computer was used to generate the time histories described in this report. The excellent computer services furnished by NASA-LRC are gratefully acknowledged.

Accession For

NTIS GRA&I	☒
DDC TAB	
Unannounced	
Justification	

By

Distribution/

Availability Codes

| Dist | Avail and/or special |
| A | |

iii

TABLE OF CONTENTS

LIST OF ILLUSTRATIONS

LIST OF TABLES

LIST OF SYMBOLS

b — wing span, ft

m — mass, slugs

q — pitch rate, rad/sec

$\bar{q}$ — free-stream dynamic pressure, lb/ft^2

S — wing area, ft^2

V — free-stream velocity, ft/sec

$\bar{c}$ — wing mean aerodynamic chord, ft

C_{L_α} — lift curve slope at trim alpha, $\partial(\text{lift}/\bar{q}S)/\partial\alpha$, deg^{-1}

C_ℓ — rolling moment coefficient, rolling moment/$(\bar{q}Sb)$

C_m — pitching moment coefficient, pitching moment/$(\bar{q}S\bar{c})$

C_n — yawing moment coefficient, yawing moment/$(\bar{q}Sb)$

C_{ℓ_β} — lateral stability derivative, $\partial C_\ell/\partial\beta$, deg^{-1}

$C_{m_{|\beta|}}$ — pitch due to sideslip derivative, $\partial C_m/\partial|\beta|$, deg^{-1}

$C_{m_{\delta_e}}$ — longitudinal control effectiveness at trim alpha, $\partial C_m/\partial\delta_e$, deg^{-1}

C_{n_β} — directional stability derivative, $\partial C_n/\partial\beta$, deg^{-1}

$C_{n_{\delta_a}}$ — yaw due to lateral control derivative, $\partial C_n/\partial\delta_a$, deg^{-1}

C_{m_q} — pitch damping derivative, $\partial C_m/\partial(q\bar{c}/2V)$, rad^{-1}

i_s — longitudinal control deflection, positive to produce nose-down (negative) pitching moment, deg

I_X, I_Y, I_Z — moment of inertia about the X, Y and Z body axis, respectively, slug-ft^2

I_{XZ} — product of inertia, slug-ft^2

α, alpha   angle of attack, positive when X body axis is above projected relative wind vector, deg

β, beta   sideslip angle, positive when relative wind vector is to the right of the X-Z plane, deg

ΔCG   center-of-gravity shift measured from the basic airplane CG location along body X-axis, $X_{CG}/\bar{c}$, positive forward

δ_a lateral control deflection, positive to produce left (negative) rolling moment, deg

δ_e longitudinal control deflection, positive to produce nose-down (negative) pitching moment, deg

NADC   Naval Air Development Center

SECTION I

INTRODUCTION

High angle-of-attack capability has been shown to signif-
icantly enhance the air combat maneuvering effectiveness of
fighter airplanes. Unfortunately, it had not been possible
to design for such a capability with a modicum of confidence
because there was no criterion available with which to identify
accurately a specific design's susceptibility to depart from
controlled flight during severe rolling maneuvers at high angles
of attack. The study reported in Reference 1 endeavored to
overcome this condition by generating design charts and devel-
oping associated boundaries for identifying departure and un-
coordinated roll-reversal flight characteristics as a function
of three aerodynamic parameters. These parameters were the
rolling and yawing moment coefficients associated with sideslip
and yawing moment coefficient due to lateral control deflection.

The investigation cited utilized a large angle, six-degree-
of-freedom digital computer program to simulate the motions of
a fighter performing a severe air combat maneuver for different
combinations of the lateral-directional parameters while main-
taining a representative set of longitudinal characteristics.
The present study, a logical extension of that investigation,
determines the extent to which the pitching moment character-
istics, i.e. static stability, pitch damping (C_{m_q}) and the
pitch cross-derivative $(C_{m_{|\beta|}})$, affect the boundaries de-
veloped in Reference 1. The results are presented herein. Be-
cause of the increasing interest in control configured vehicles
which exhibit various levels of static instability at trim, the
static stability study included different levels of trim in-
stability. Fortunately, obtaining desired levels of instability
at trim does not preclude the existence of an inherently stable
airframe in pitch at high angles of attack as was modelled in

1

the previous and present study.

Since airplanes with relaxed static stability must be flown in a stability augmentation mode, this study also determined the control characteristics required of a simple pitch augmentation system to maintain, at different levels of trim instability, the applicability of the departure boundaries developed in Reference 1 for an unaugmented statically stable airplane.

Departure boundaries based on a severe rolling maneuver at high angles of attack (alphas) are, of course, superfluous for an airplane that departs during a simple longitudinal maneuver because of a pitch-up characteristic. Normally such airplanes are equipped with an angle-of-attack limiting device. Airframes so equipped deny full use of an inherent air combat maneuvering capability that may exist at higher alphas due to favorable lateral-directional characteristics. It was, therefore, decided to explore briefly the possibility of allowing such an airframe to perform rolling maneuvers at high alphas by employing a high-authority augmentation system instead of a hard limiter.

SECTION II

TECHNICAL APPROACH

A. INTRODUCTION

The analysis herein is based on large angle, six-degree-of-freedom computations since the departure and attendant incipient spin motions are large amplitude, coupled motions reflecting the influence of gyroscopic and kinematic effects. The departure phenomenon could not, therefore, be identified by employing linearized, limited degree-of-freedom equations of motion.

Earlier studies had determined that several aerodynamic parameters were important in promoting a spin. A large angle six-degree-of-freedom analytical study sponsored by Naval Air Systems Command in 1967 (reported in Reference 2) had identified adverse yaw due to aileron deflection, dihedral effect and directional stability to be instrumental in spin development. Subsequent analytical and flight test investigations corroborated these findings. Another large angle, six-degree-of-freedom analytical study sponsored by the Naval Air Development Center in 1977 (Reference 1) demonstrated the role played by the relative magnitudes of these three aerodynamic parameters and their variations with angle of attack in promoting control-induced departures.

The first phase of the NADC study covered the selection of C_ℓ, C_n and $C_{n_{\delta_a}}$ models to be investigated. High angle-of-attack, high Reynolds number data for fighter-type airplanes were collected. All the data fell into broad bands throughout the angle-of-attack range so that it was possible to represent the aerodynamic characteristics for the spectrum of fighter-type airplanes with four C_ℓ, three C_n, and three $C_{n_{\delta_a}}$ models. These lateral-directional aerodynamic models have been utilized

herein. However, the present study is limited to the adverse $C_{n_{\delta_a}}$ model (Figure A9) which is characteristic of most lateral controls at high angles of attack.

As stated in Section I, one goal of the present effort was to amplify the results of Reference 1 by determining the extent to which changing the pitching moment characteristics would modify the previously developed boundaries. To accomplish this, a study was performed for each of the variables of interest, i.e., C_{m_q}, $C_{m_{|\beta|}}$ and static stability/instability levels. Since all these studies were concerned with the previously developed departure and uncoordinated roll reversal boundaries, the technical approach reported in Reference 1 was employed:

- o generate, analytically, airplane maneuvering time histories for combinations of the lateral-directional aerodynamic models,

- o tabulate and analyze the results,

- o construct departure susceptibility design charts, and

- o develop departure boundaries from these charts.

The goal of the augmentation control characteristics investigation was to determine the magnitude of the augmentation control authorities and rates required to maintain, for different levels of trim instability, the applicability of the boundaries developed in Reference 1. This investigation also invoked the above cited technical approach for different control characteristics. In addition, the results were cross-plotted to determine the authority requirements as a function of trim instability.

Table 1 shows: (a) the range of study variables explored relative to the pitching moment and augmentation control characteristics investigations, and (b) the matrix of lateral-directional aerodynamic models investigated for each of these study variables.

4

TABLE 1

LATERAL-DIRECTIONAL AERODYNAMIC MODELS AND STUDY VARIABLES INVESTIGATED

Static Margin	C_{m_q}	$C_{m|\beta|}$	C_n Stable	C_n Neutral	C_n Unstable	Comments
			C_ℓ Models			
9%	−25	Basic	A B C D	A B C D	A B C D	C_{m_q} Study
	−15		B C D	A B C D	A B C	
	−10		A B C D	A B C D	A B C D	
	−9		A B C D	A B C D	A B C D	
	−7		A B C D	A B C D	A B C D	
	−5		B C D	A B C D	A B C D	
	Basic	Positive	A B C D	A B C D	A B C D	$C_{m|\beta|}$ Study
		Zero	A B C D	A B C D	A B C D	
		Negative	A B C D	A B C D	A B C D	
1%		Basic	A B C D	A B C D	A B C D	Static Margin Study (Unaugmented)
−5%			A B C D	A B C D	A B C D	
−10%			A B C D	A B C D	A B C D	

TABLE 1 (Concluded)

Static Margin	Control Authority deg	Rate Limit deg/sec	C_n Stable	C_n Neutral	C_n Unstable	Comments
				C_ℓ Models		
1%	10	10	A B C D	A B C D	A B C D	Control Re-quirement Study (Aug-mented),
-5%	20	30	A B C D	A B C D	A B C D	
	30	30	A B C D	A B C D	A B C D	
	30	15	A B C D	A B C D	A B C D	
-10%	30	30	A B C D	A B C D	A B C D	
	45	45	A B C D	A B C D	A B C D	
	60	60	A B C D	A B C D	A B C D	
	60	30	A B C D	A B C D	A B C D	
	60	45			A B C D	
	45	30			A B C D	
-2%			A B C D	A B C D	A B C D	Pitch-up Study (Unaugmented)
	60	60	A B C D	A B C D	A B C D	(Augmented)

6

B.   AERODYNAMIC MODEL

The longitudinal and lateral force and control character-
istics, as well as the dynamic derivatives presented in the
Appendix, are typical of those associated with many current
fighter airplanes and, except for C_{m_q}, were not varied during
this study. The rolling, yawing, and pitching moment charac-
teristics that were varied are discussed in the following
paragraphs.

Rolling Moment Coefficient

The rolling moment coefficient, C_ℓ, was modelled as a
function of alpha and beta as shown in Figure 1. Each of the
four models had the same stable value at zero angle of attack
and became progressively more stable with increasing angle of
attack up to 12 degrees. Above 12 degrees, the models differed.
The magnitude of model B remained at the 12 degree alpha value,
whereas models C and D decreased to their constant high angle-
of-attack levels. Model A, chosen as representative of a
slatted configuration, continued to increase in magnitude up
to an alpha of 30 degrees after which it decreased and re-
turned to the level of model B at 48 degrees alpha.

Yawing Moment Coefficient

The yawing moment coefficient, C_n, was also modelled as
a function of alpha and beta. As shown in Figure 2, one of the
three models was identically zero. The other two models had
the same constant stable value up to 12 degrees angle of attack,
after which one model continued to be invariant with increas-
ing alpha and the other decreased to an unstable value which
was then held constant above an alpha of 21 degrees.

Pitching Moment Characteristics

The basic C_{m_q} model varied in magnitude as a function of
angle of attack. To determine the coefficient's influence
on departure susceptibility, six constant (i.e. invariant with

alpha) models having values of -5, -7, -9, -10, -15 and -25 per radian were considered. The basic C_{m_q} model and the six constant models are presented in Figure 3.

The basic and the three alternate models investigated during the $C_{m_{|\beta|}}$ study are presented in Figure 4. One model had a zero value up to an angle of attack of 20 degrees. It then became increasingly positive between 20 and 38 degrees alpha, after which it was held constant. Another model was identically zero. The third model had a negative value and was invariant with angle of attack.

As shown in Figure 5, the pitching moment coefficient, C_m, was modelled as a function of alpha and longitudinal control deflection. The different pitching moment vs. alpha relationship shown for each stability level studied was the result of a shift in center of gravity, in the pitch axis only, to provide the desired static margin $\left(- \dfrac{C_m}{C_L} \right)$ at trim alpha. An alternate pitching moment coefficient was also examined briefly. The C_m variation with angle of attack of this model was typical of a vehicle exhibiting a pitch-up characteristic and is presented in Figure 6. The functional dependence on sideslip of the basic C_m model was maintained for the alternate model.

C. INERTIA PARAMETER MODEL

The mass is distributed along the fuselage reference axis for fighters to varying degrees. During the NADC study (Reference 1), three inertia parameter models were considered which ranged from an airplane whose mass was concentrated heavily in the fuselage to one in which the mass was distributed only slightly more in the fuselage than in the wings. The following inertia parameter model (representing the mean value for fighters) was chosen for the investigation reported herein:

$(I_X-I_Y)/mb^2 = -0.067$

$(I_Y-I_Z)/mb^2 = -0.012$

$(I_Z-I_X)/mb^2 = 0.079$

The mass and inertial characteristics used in the equations of motion were:

$I_X = 25,000$ slug ft^2

$I_Y = 135,000$ slug ft^2

$I_Z = 155,000$ slug ft^2

$I_{XZ} = 0$

m= 1025 slugs

D. FLIGHT CONDITION AND MANEUVER

The initial flight condition and maneuver utilized herein were the same as those used during the NADC investigation. The airplane was trimmed in a 60-degree bank-angle turn at 35,000 feet and Mach 0.9. A rolling pull-out maneuver was then performed. Control inputs for the maneuver were:

o Full trailing-edge-up longitudinal control deflection commanded at time equal zero, at 30 degrees per second.

o Full lateral control deflection initiated 1.5 seconds into the maneuver at a rate of 30 degrees per second in the direction to unbank the airplane.

o Rudder undeflected.

The controls were kept fully deflected for a duration sufficient to allow the airplane motions to develop, at which time both the longitudinal and lateral controls were returned to trim at 30 deg/sec. Nominally, the return of the controls to zero was initiated at eight seconds into the time history, which provided at least three oscillations for the alpha trace.

However, as the static margin was made negative, the period of the angle-of-attack oscillations increased to the point where less than three peaks occurred prior to eight seconds. To circumvent this, the time span over which the pilot control inputs were maintained was extended for some cases by an additional two seconds, allowing three angle-of-attack peaks to occur.

E.   TIME HISTORY COMPUTATIONS

To evaluate the lateral-directional aerodynamic models, 20-second time histories of the airplane motions were generated in response to the previously described control inputs. As mentioned previously, these motions were computed using a large angle, six-degree-of-freedom digital computer program. The program used nonlinear tabulated data for the aerodynamics, atmospheric properties (density and speed of sound), and control inputs. Aerodynamic parameter tables could be programmed as functions of up to three independent variables (e.g., angle of attack, sideslip angle and control deflection). Control deflection input tables were programmed as a function of time.

The resultant vehicle response to the control inputs was plotted on a CALCOMP drum plotter. Up to 64 output parameters could be plotted against time for each computer run. For this study, the following sixteen parameters were plotted:

pitch angle	elevator deflection
bank angle	lateral control deflection
yaw angle	flight path angle
pitch rate	altitude change
roll rate	range position
yaw rate	dynamic pressure
angle of attack	total velocity
sideslip angle	total rotation rate

F.   PROCEDURES FOR DEVELOPING DESIGN CHARTS AND BOUNDARIES

The NADC study found the following time history parameters

10

to be useful in determining boundaries:

o last alpha peak value prior to lateral control removal

o approximate second-order damping ratio of alpha trace

o peak yaw rate magnitude and sign

o incremental peak bank angle prior to lateral control removal

These four parameters are presented in design charts for each computed time history. An airplane's tendency to depart from controlled flight or experience an uncoordinated roll reversal was ascertained by reviewing this information.

Yaw rate alone is not a reliable indicator of departure, since many combinations of the lateral-directional aerodynamic models investigated result in yaw rates that are opposite (unfavorable) to the commanded lateral control displacement, and are accompanied by a roll reversal. Consequently, the airplane rolls in the same direction in which it yaws and contrary to command. This roll reversal is not a departure; it is actually the "safety valve" that precludes departure and presents a strong signal to the pilot to use his rudder pedals to coordinate the maneuver.

A significant aspect of departure is that it is a high angle-of-attack phenomenon in which inertial and kinematic coupling generate uncommanded motions. Departure criteria chosen, in the previous study, to obviate departure were based on two characteristics of the angle-of-attack time history trace and were as follows:

1. The last peak of the angle-of-attack trace, prior to returning the controls to trim, must be less than 50 degrees (i.e. within 15 degrees above the static trim value of 35 degrees). The choice of the last angle-of-attack peak prior to removal of controls, the third peak

11

in this instance, was based on examining flight test time histories over many years. It was observed that this peak was indicative of the ensuing motion. The selection of a specific cutoff alpha value to predict an ensuing departure for every possible situation is, of course, impossible (see Section IIIB1).

2. The approximate damping ratio of the angle-of-attack trace, calculated by assuming a second-order system, must be greater than zero.

The bases for these criteria were re-examined for use in this study. The angle-of-attack time history parameters presented in the design charts of Reference 1 were employed to construct boundaries predicated on the last peak alpha being 40, 50, 60 or 70 degrees and the approximate damping ratio being .02, 0, or -.04. These plots are presented in Figures 7, 8 and 9 for proverse, neutral and adverse $C_{n_{\delta_a}}$ characteristics, respectively.

It can be seen that the peak angle-of-attack curves representing 60 and 70 degrees generally lie in the region of negative damping. Negative damping and the successively larger alpha peaks associated with it is patently undesirable due to the repeated excursions into the angle-of-attack region where autorotative rolling and yawing moments due to rotary flow, which induce spins, may be encountered. The 45 degree peak curve, conversely, is always indicative of a damped oscillation and would seem to be overly conservative. The 50 degree criterion therefore appears to be justified in all instances.

For the neutral $C_{n_{\delta_a}}$ model, the zero damping criterion is seen to be essentially redundant while for the other two $C_{n_{\delta_a}}$ models it is generally less conservative than the bound-

12

ary based on 50 degrees alpha. Consequently, as shown in
Figure 10, the boundaries based on the previous Reference 1
criteria and those based on the single 50-degree alpha peak
criterion are effectively superimposed for the proverse and
adverse $C_{n_{\delta_a}}$ models and with an insignificant boundary shift
realized for neutral $C_{n_{\delta_a}}$. Hence, the departure boundaries
in this study are based only on the peak angle-of-attack cri-
terion. The boundaries were developed therefore from cross-
plots of the design chart angle-of-attack peak information
and represent interpolations between or extrapolations from
the actual $C_{n_\beta}/C_{\ell_\beta}$ levels of the models. The validity of this
procedure is discussed in Section V.

It should be noted that the boundaries are only intended
to predict an airplane's susceptibility to depart from con-
trolled flight or to encounter roll reversal during an un-
coordinated maneuver. They do not indicate whether or not a
spin occurs, since they are based solely on transient aircraft
motions. A spin, on the other hand, is defined in terms of
quasi-steady aircraft motions that, as shown in Reference 3,
require the modelling of rotary aerodynamics, which is not the
case here.

Although the approximate angle-of-attack damping ratio
is unnecessary for departure boundary definition and the
trace does not truly reflect a simple second-order system
during large angle, coupled, six-degree-of-freedom motion,
it does give an insight into the status of the motion in most
instances and is therefore included in the design charts. If,
upon examining the design charts, a damping ratio appears to
fall out of place, it is because the measurement of an approx-
imate damping ratio was very difficult in that particular
case.

13

G. AUGMENTATION SYSTEM

The purpose of the augmentation study was to determine
if a simple pitch-axis augmentation loop could provide improved
departure resistance, during a high angle-of-attack rolling
maneuver, for an airframe exhibiting static trim instability.
If such were the case, the control authorities and rates re-
quired to maintain the applicability of the boundaries de-
veloped in Reference 1 were to be determined for different
levels of trim instability.

To accomplish these goals, a simple angle-of-attack feed-
back loop (see Figure 11) was modelled in the computer program.
Its purpose was to artificially provide the same stability
level at trim as the unaugmented 9% static margin airplane,
regardless of the actual airframe static margin. The feed-
back gain, a function of the difference in trim stability be-
tween the actual and desired pitching moment characteristics,
was derived as follows:

$$C_m = C_{m_o} + C_{m_\alpha} \alpha + C_{m_{\delta_e}} (\delta_e - k\alpha) + \ldots \tag{1}$$

where k represents the feedback gain. Rearranging,

$$C_m = C_{m_o} + (C_{m_\alpha} - kC_{m_{\delta_e}})\alpha + C_{m_{\delta_e}}\delta_e + \ldots \tag{2}$$

where the effective C_{m_α} of the augmented airframe is $C_{m_\alpha} - kC_{m_{\delta_e}}$.

If this effective C_{m_α} is equated to the desired C_{m_α}, then

$$k = (C_{m_\alpha} - C_{m_\alpha \text{ desired}})/C_{m_{\delta_e}} \tag{3}$$

Since the desired C_{m_α} is that of the nine-percent static margin
airplane, the difference between the actual and desired C_{m_α}
is the increment due to the center of gravity shift, $\Delta CG \cdot C_{L_\alpha}$.

Therefore,

$$k = \Delta CG \cdot C_{L_\alpha}/C_{m_{\delta_e}} . \tag{4}$$

14

The augmentation control authority and rate limits investigated for different levels of trim instability are presented in Table 1.

H. PRESENTATION OF RESULTS

For each study in the pitching moment characteristics investigation (i.e. C_{m_q}, $C_{m_{|\beta|}}$, static margin), four design charts and the resulting departure and uncoordinated roll reversal boundaries are presented. Except for the uncoordinated roll reversal boundaries, the same information is presented for the augmentation control characteristics investigation.

The design charts are presented on four separate pages, one for each of the four time history parameters. Each page contains three plots: one each for the unstable, neutral and stable C_n models investigated. Each plot, in turn, presents the value of the time history parameter as a function of the C_ℓ models for constant values of the study variable. To facilitate interpretation, the C_ℓ models are spaced along the abscissa according to the value of their post-stall C_{ℓ_β} slopes (taken between $\beta=0$ and $\beta=10$ degrees), with each model indicated by symbols according to the key. Because C_ℓ model A did not attain a constant value above 15 degrees angle of attack, as the other models did, its C_{ℓ_β} slope at the average angle of attack attained by the time histories using this model, 40 degrees, was used. Also, the C_ℓ value for model D (Figure 1) was zero at $\beta=10$ degrees, therefore the C_{ℓ_β} slope for this model was based on the value at the average β peak realized during this study, approximately 15 degrees.

The design charts are followed by the departure and uncoordinated roll reversal boundaries. The abscissa of these plots is again C_{ℓ_β}. The C_n models are spaced along the ordinate according to the value of their C_{n_β} slopes (taken between $\beta=0$ and $\beta=10$ degrees) above 21 degrees angle of attack.

15

SECTION III

PITCHING MOMENT CHARACTERISTICS INVESTIGATION

A. DESIGN CHARTS

Figures 12, 13 and 15 present the design charts derived for the C_{m_q}, $C_{m_{|\beta|}}$ and static margin studies, respectively. The basic airplane results from Reference 1 for the adverse $C_{n_{\delta_a}}$ model (Figure 10) are also included in each figure for comparison. The results for the basic airplane and the significance of the pitching moment characteristics on these results are discussed below.

Design data for the basic airplane show that for a stable C_n model the angle-of-attack time history traces are damped and the angle of attack approaches its trim value of approximately 35 degrees regardless of the C_ℓ model. For neutral or unstable yawing moment models, the rolling moment becomes significant in determining whether the alpha time history is convergent or divergent. If C_n is unstable above the stall, as is the case for most airplanes, a fairly high level of dihedral effect is required to prevent the airplane from diverging in angle of attack during an uncoordinated rolling maneuver at high alphas.

The direction that the basic airplane rolls and yaws in response to the control inputs also depends strongly upon the C_n characteristics. For a stable yawing moment, the basic airplane will roll in the direction commanded accompanied by a coordinating yaw rate, whereas it tends to yaw in the opposite direction for an unstable yawing moment inducing roll reversal.

These design charts show that a stable yawing moment characteristic is the most effective parameter governing departure prevention. It also tends to prevent roll reversal during an uncoordinated rolling maneuver at high alphas. A designer's recourse when confronted with a configuration directionally

16

unstable over some alpha range might be to insure a high level
of dihedral effect (lateral stability). For this combination
of aerodynamic characteristics, departures are eliminated at
the expense of inducing roll reversals during uncoordinated
maneuvers. This constitutes a trade-off between a safety-of-
flight condition (departure) and a flight characteristic that
might be regarded as annoying (i.e. requiring the use of rudder
pedals).

1. C_{m_q} Study

It is shown in Figures 12a and b that C_{m_q} has no signif-
icant influence on the angle of attack time history for C_{m_q}
levels more negative than -9 rad^{-1}. A C_{m_q} magnitude below -10
results in consistently larger angle of attack peaks for neutral
and stable C_n models accompanied, for a stable C_n, by essentially
zero damping of the angle-of-attack time history. Figures 12c
and d show that C_{m_q} has generally no significant influence on
the peak yaw rate or bank angle experienced during this maneuver.

2. $C_{m_{|\beta|}}$ Study

Figure 13a presents the angle-of-attack peak design chart
for the $C_{m_{|\beta|}}$ study. For a stable yawing moment, $C_{m_{|\beta|}}$ has
virtually no effect on the peak angle of attack experienced.
For neutral or unstable C_n's, the zero $C_{m_{|\beta|}}$ closely approx-
imates the results for the basic model, while a positive $C_{m_{|\beta|}}$
results in lower peak values and conversely for the negative
model. These latter effects become significant at a low value
of C_{ℓ_β}. Figures 13c and d show that, except for an unstable
C_n model and the neutral C_n model with low C_{ℓ_β}, $C_{m_{|\beta|}}$ does not
significantly affect the magnitudes of the peak yaw rate or
incremental bank angle experienced.

17

3. Static Margin Study

Figure 14 shows the effect produced on the pitching moment coefficient when the airplane's center of gravity is shifted aft: as the static margin decreases and becomes negative, with full nose-up control, the trim angle of attack increases, while the slope of the curve, C_{m_α}, decreases. The peak angle-of-attack design chart, Figure 15a, shows that, indeed, as the static margin is decreased the last angle-of-attack peak increases. For the nine percent static margin cases, the approximate damping ratios shown in Figure 15b are positive (stable) and negative (unstable) for the stable and unstable C_n models, respectively. These values then become less and more stable, respectively, for the stable and unstable C_n models when the static margin is reduced. That is, the stable damping ratio for stable C_n models decreases, while a stable increment is added to the unstable damping ratio for the unstable C_n model.

Figures 15 c and d present the peak yaw rate and incremental bank angle design charts. Decreasing the static margin generally tends to decrease the magnitude of the positive yaw rates experienced for unstable C_n models, but tends to produce slightly less negative or more positive yaw rates for a stable C_n. The incremental peak bank angle experienced becomes less negative for a stable C_n model and more positive (except at the lowest C_{l_β}) for an unstable C_n model as the static margin is decreased.

B. DEPARTURE BOUNDARY

Departure boundaries developed using the peak angle-of-attack criterion (Section IIF) for the C_{m_q}, $C_{m_{|\beta|}}$ and static margin studies are presented in Figures 16, 17 and 18, respectively, with the boundary for the basic (nine percent static margin) airplane. The departure boundary for the basic airplane shows that for large stable values of C_{l_β}, fairly large unstable

18

C_{n_β} values can be tolerated without departure susceptibility.
For low levels of C_{ℓ_β}, more stable (or at least less unstable)
C_{n_β} values would be required for a configuration to remain
departure resistant. For an airplane which exhibits positive
C_{n_β}, the influence of C_{ℓ_β} becomes unimportant except for a
configuration with virtually no dihedral effect (lateral sta-
bility).

The influence of each of the study variables on the basic
departure boundary is discussed below:

1. C_{m_q} Study

The design charts showed that C_{m_q} level did not influence
the angle-of-attack peak levels except for C_{m_q} magnitudes less
than -10 rad^{-1}. Consequently, as expected, only the least neg-
ative C_{m_q} models produced any significant change to the depar-
ture boundary of the basic airplane (see Figure 16). However,
the dashed portions of the boundaries for the -5 and -7 rad^{-1}
C_{m_q} models appear incongruous in that for increasing direction-
al stability (C_{n_β} becoming more positive) a corresponding in-
crease in dihedral effect is required to provide departure re-
sistance. The shape of this portion of the departure boundary
occurs since the alpha peak criterion value of 50 degrees is
exceeded for these C_{m_q} values at stable C_{n_β}'s. Examination
of the rest of the time history parameters indicates that,
though the angle-of-attack criterion is violated, in most in-
stances there is no roll reversal in this region and the yaw
rates experienced are generally low. This situation was
verified by computing additional time histories for cases in
the region above the dashed boundaries. The dashed portion
of the boundary therefore does not identify the motion of con-

19

cern in which the existence or direction of yawing motion is contrary to what had been anticipated, and the motion occurs so quickly that the airplane is in an incipient spin phase before a pilot could take corrective action. What is really experienced is a larger angle-of-attack excursion than would be expected. The region above the dashed boundary therefore identifies a controllable pitch excursion motion rather than an uncontrollable departure, and is an instance in which the use of a specific cutoff alpha value did not predict departure as defined herein (see also Section IIF).

For the higher C_{m_q} levels characteristic of some current airplane configurations, C_{m_q} is insignificant in promoting or preventing departure resistance; consequently, the basic departure boundary may be directly applied. For unaugmented airframes having C_{m_q} magnitudes lower than -10 rad^{-1}, the basic boundary would be unconservative. However, such airplanes do exhibit very high effective levels of C_{m_q} when their pitch dampers are engaged.

2. $C_{m_{|\beta|}}$ Study

Figure 17 presents the departure boundaries for the $C_{m_{|\beta|}}$ study. It can be seen that $C_{m_{|\beta|}}$ has an appreciable effect on the C_{n_β} levels required for departure resistance at low values of C_{ℓ_β}. A positive level of $C_{m_{|\beta|}}$ is seen to be favorable; a negative one unfavorable. Generally, airplane configurations to date are represented by the basic model, i.e. slightly negative at the low angles of attack, then becoming positive for higher angles of attack. Only academic curiosity prompted the investigation of a large negative value at high angles of attack. Consequently, the basic departure boundary can be applied to similar configurations having various realistic $C_{m_{|\beta|}}$ characteristics (although the boundary may be slightly conservative in some instances).

3. Unaugmented Static Margin Study

The departure boundaries for the basic nine percent static margin airplane, as discussed in Section IIF, were based on the value of the last angle-of-attack peak, prior to control removal, being less than 15 degrees above the static trim value. This criterion was applied to the unaugmented static margin study, despite the increases in the static trim alpha value with decreasing static margin, as shown in Figure 14. Figure 18 presents the departure boundaries for each of the static margins investigated.

In going from a positive to a negative static margin, the combinations of $C_{n_\beta}/C_{\ell_\beta}$ for which there is departure resistance are decreased appreciably. The departure boundary, however, is only slightly influenced by the static margin when stable. For the reasons discussed in Section IIIB1, departure is not realized in the region above the dashed portion of the boundaries. As was done for the C_{m_q} study, additional cases were investigated above the dashed boundary. In all instances, a controllable pitch excursion, no roll reversal and generally low yaw rates were experienced.

C. UNCOORDINATED ROLL REVERSAL BOUNDARY

Examination of the design charts shows that for a large group of the cases studied the airplane rolled in a direction opposite to that commanded. The initial motion was in the commanded direction, to varying degrees; then, as the sideslip angle increased, the motion reversed and the airplane rolled in the opposite direction. Using the bank angle information contained in the design charts, uncoordinated roll reversal boundaries can be generated in the same manner as was done for the departure boundaries. The uncoordinated roll reversal boundaries from Reference 1 are reproduced in Figure 19 for adverse, neutral and proverse $C_{n_{\delta_a}}$. As discussed in

21

Section IIF and IIIA, these boundaries are <u>not</u> departure
boundaries. Also shown on this figure are lateral control
departure parameter (LCDP= 0) boundaries (Reference 4):

$$\text{LCDP} = C_{n_\beta} - C_{\ell_\beta} \frac{C_{n_{\delta_a}}}{C_{\ell_{\delta_a}}} = 0.$$ As can be seen, the LCDP boundaries

closely approximate the uncoordinated roll reversal boundaries.
The LCDP parameter appears to be a convenient and accurate tool
for predicting uncoordinated roll reversal but not departure.

Figures 20, 21 and 22 present the uncoordinated roll re-
versal boundaries for the C_{m_q}, $C_{m_{|\beta|}}$ and static margin studies,
respectively, with the basic curve also shown for comparison.
The influence of C_{m_q}, $C_{m_{|\beta|}}$ or static margin on the uncoordinated
roll reversal boundary is slight. Since this boundary is evident-
ly independent of the pitching moment characteristics, the basic
boundary of Reference 1 may be applied to all airplane config-
urations.

SECTION IV

AUGMENTATION CONTROL CHARACTERISTICS INVESTIGATION

A.   BASIC C_m CURVE (NO PITCH-UP)

Elevator deflections commanded by the augmentation system
as a function of angle of attack can be calculated by using
the expression for the feedback gain presented in Equation (4),
Section IIG. The elevator deflection required to simulate the
nine percent static margin pitching moment curve can be gen-
erated from the pitching moment curves presented in Figures 5
and 14. Figure 23 presents plots of the steady-state deflection
commanded by the augmentation system and the deflection required
to statically match the nine percent static margin pitching
moment curve at zero sideslip for airplanes with static margins
of 1, -5, and -10 percent and pilot inputs of zero and -30
degrees. The augmentation commanded deflection is shown to
exceed the required deflection curves for all angles of attack
greater than six degrees.

Imposition of an augmentation authority limit would of
course determine the angle of attack range over which it would
be possible for the augmentation system to meet or exceed the
required control deflections shown in Figure 23. Figure 24
presents the effective static pitching moment curves at each of
the reduced static margins for various augmentation authorities.
The nine percent static margin curve is also shown. An in-
dication of the augmentation authority required to simulate the
nine percent static margin pitching moment, for a specific
alpha range, can be determined from these curves.

1. Design Charts

Figures 25, 26 and 27 present the design charts for 1,
-5 and -10 percent static margins, respectively, showing the
effect of various augmentation authority limits on selected

23

time history parameters. As would be expected from examination of the effective pitching moment curves (Figure 24), an increase in the augmentation authority limit decreases the last angle-of-attack peak prior to returning the controls to zero.

Large augmentation authorities can appreciably influence the peak yaw rates and incremental bank angles experienced, as can be seen in parts c and d of Figures 26 and 27.

2. Departure Boundaries

Since the augmentation study's aim was to determine the control characteristics needed to maintain the applicability of the previously developed (Reference 1) departure boundaries, the departure criterion used for the original static margin, i.e. a 50 degree angle-of-attack peak value, was used to construct departure boundaries for each of the control authorities simulated at the various static margins. Figures 28, 29 and 30 present these boundaries for 1, -5 and -10 percent static margins, respectively. Figure 28 shows that for a one percent static margin, a zero augmentation authority is insufficient, but a ten degree authority virtually duplicates the nine percent boundary. For a -5 percent static margin (Figure 29), 20 degrees authority is insufficient, while 30 degrees results in a great improvement over the nine percent airframe. Figure 30 shows that at -10 percent static margin, both 45 and 60 degree augmentation authorities produce a large favorable shift in the departure boundaries, whereas a 30 degree authority is ineffective.

The results of the previous three figures were cross-plotted to determine the augmentation control authority required, at each static margin, to maintain the validity of the nine percent airframe departure boundary. The results are shown in Figure 31. It must be noted that these results are dependent upon the C_m vs. alpha and longitudinal control

deflection characteristic above stall, as well as the pitch inertia, I_y, assumed for this study. These dependencies should be investigated to assess their effects on the required augmentation control authority before the results of Figure 31 may be applied to other airplanes with different longitudinal characteristics.

The augmentation rate limits assumed for the results shown in Figures 28 through 31 were equal to the authority limits; i.e. the full augmentation authority was available within one second. Time and computer resource limitations precluded an exhaustive analysis of the effects of lowered rate limits. As shown in Table 1, several different rate limits were nevertheless examined for selected cases. The results indicate that if this limit were set too low, severe rate limiting of the longitudinal control deflection trace would occur with a decidedly unfavorable impact on departure resistance.

B. ALTERNATE C_m CURVE (PITCH-UP CASE)

The alternate pitching moment curve, shown in Figure 6, has a pitch-up characteristic at 40 to 60 degrees angle of attack. For the control inputs assumed during this investigation, the unaugmented airframe would always reach angles of attack of 64 degrees or greater. A large stability augmentation control authority of 60 degrees was investigated with this alternate pitching moment curve. However, as shown in Figure 32, only a slightly increased nose-down pitching moment capability above 28 degrees angle of attack was realized in going from a 30 to 60 degree control augmentation authority due to the decrease in control effectiveness evident in Figure 6. If the higher control effectiveness of the original C_m curves shown in Figure 5 had been retained, a control authority of 40° rather than 60° would have been investigated.

1. Design Charts

Figure 33 presents the design chart information for the alternate pitching moment model with a 60 degree augmenta-

25

tion authority limit. For the unstable C_n model, all but the highest dihedral effect model show very large peak alphas. For the neutral and stable C_n models, angle of attack peaks less than 40 degrees (below the pitch-up region) are realized for all C_ℓ models. The angle of attack trace for the unstable C_n model is so rapidly divergent that it was impossible to measure damping ratios. For the neutral and stable C_n's, the damping ratios are very large for the high dihedral effect models and diminish rapidly as C_{ℓ_β} approaches zero.

The peak yaw rate and incremental bank angle plots (33c and d) show trends similar to those of the basic pitching moment model, except that for the neutral C_n model, the airplane rolls and yaws as commanded, instead of oppositely.

2. Departure Boundary

The departure boundary for the augmented airframe with the alternate pitching moment model, presented in Figure 34, is based on the criterion used for the basic (nine percent static margin) airframe: an angle of attack peak of 50 degrees. The 60 degree authority limit is generally sufficient to match or exceed the departure boundary of the unaugmented basic airplane.

SECTION V

VERIFICATION OF BOUNDARIES

As cited in Section IIF, the departure boundaries are
based on cross-plots of the design chart angle-of-attack peak
information and represent interpolations between or extrap-
olations from the models' actual $C_{n_\beta}/C_{\ell_\beta}$ levels. Since this
procedure might cause concern regarding the constructed bound-
ary's accuracy, it merited investigation, because this study
demonstrated the developed departure and uncoordinated roll re-
versal boundaries' general applicability to longitudinally
stable fighter configurations. Hence, a considerable number
of additional time histories were generated for $C_{n_\beta}/C_{\ell_\beta}$ combi-
nations in the vicinity of the departure boundaries presented
in Figure 10 for the proverse, neutral and adverse $C_{n_{\delta_a}}$ models.
These finalized departure boundaries, presented in Figure 35,
were compared to the boundaries derived using Reference 1 design
chart information.

Figures 35a and b show that the interpolation and extrap-
olation procedure incurred only minute shifts in the departure
boundaries so constructed for the proverse and neutral $C_{n_{\delta_a}}$
models, respectively. A more pronounced shift in the finalized
boundary was realized for the adverse $C_{n_{\delta_a}}$ model (Figure 35c).
The finalized boundary in this instance is somewhat more con-
servative than the originally constructed boundary.

The uncoordinated roll-reversal boundaries were assumed
to be valid for the following reasons and were not further
investigated:

o   no extrapolations were required in constructing these bound-
    aries.
o   whereas the departure boundaries are highly dependent on C_{ℓ_β},
    this is not the case for the uncoordinated roll reversal
    boundaries.

27

SECTION VI

CONCLUDING REMARKS

Design charts and departure and uncoordinated roll reversal boundaries were generated as functions of characteristic C_n and C_ℓ models for various levels of C_{m_q}, $C_{m_{|\beta|}}$ and static stability/instability for an adverse $C_{n_{\delta_a}}$ model. The results indicate that:

o the developed departure boundary is applicable to fighter configurations which are statically stable.

o the departure boundary would be non-conservative for unaugmented airframes with low C_{m_q} or unusual $C_{m_{|\beta|}}$ characteristics (C_{m_q} magnitudes less negative than -10 rad^{-1} or large negative $C_{m_{|\beta|}}$ values at high angles of attack).

o unaugmented airframes which are statically unstable in pitch impose more stringent requirements on the $C_{n_\beta}/C_{\ell_\beta}$ combinations to avoid departure susceptibility.

o for stable or unstable static margins, a simple angle-of-attack feedback augmentation system using a reasonable control authority can markedly improve departure resistance. However, if a pitch-up characteristic is associated with an unstable static margin, a very large augmentation authority could be required.

o the uncoordinated roll reversal boundary is not pronouncedly influenced by any of the aerodynamic parameters investigated and may be applied to any fighter configuration.

o the LCDP parameter appears to be a convenient and accurate tool for predicting uncoordinated roll reversal but not departure.

It is strongly anticipated that the departure and uncoordinated roll reversal boundaries for proverse and neutral

$C_{n_{\delta_a}}$'s would also be valid for a large range of pitching moment characteristics. Consequently, the basic boundaries derived in Reference 1 were verified and, where necessary, modified for the three $C_{n_{\delta_a}}$ models considered during that investigation. Figure 36a, b and c present composite plots of the departure and uncoordinated roll reversal boundaries for each of the proverse, neutral and adverse $C_{n_{\delta_a}}$ models, respectively.

From these plots, it can be seen that there are four distinct regions defining the airplane responses:

1. The region labelled no departure, lying above both the departure and uncoordinated roll reversal boundaries, indicates that for $C_{n_\beta}/C_{\ell_\beta}$ combinations in this region, no high angle-of-attack excursions are experienced and the airplane rolls and yaws as commanded.

2. The region labelled no departure - uncoordinated roll reversal, which lies between the two boundaries, indicates that the airplane is not departure susceptible in this region, but that without a coordinating rudder input, the airplane will roll and yaw opposite to command.

3. The region labelled departure indicates that the airplane will be departure susceptible in this region.

4. The final region, which extends along the left side of the figures until the two boundaries cross (i.e. above the un-coordinated roll reversal boundary and below the departure boundary), represents a high angle-of-attack excursion region. The airplane would roll as commanded, accompanied normally by only small yaw rates, but would be likely to experience higher angles of attack than would be anticipated.

a) β=10 deg
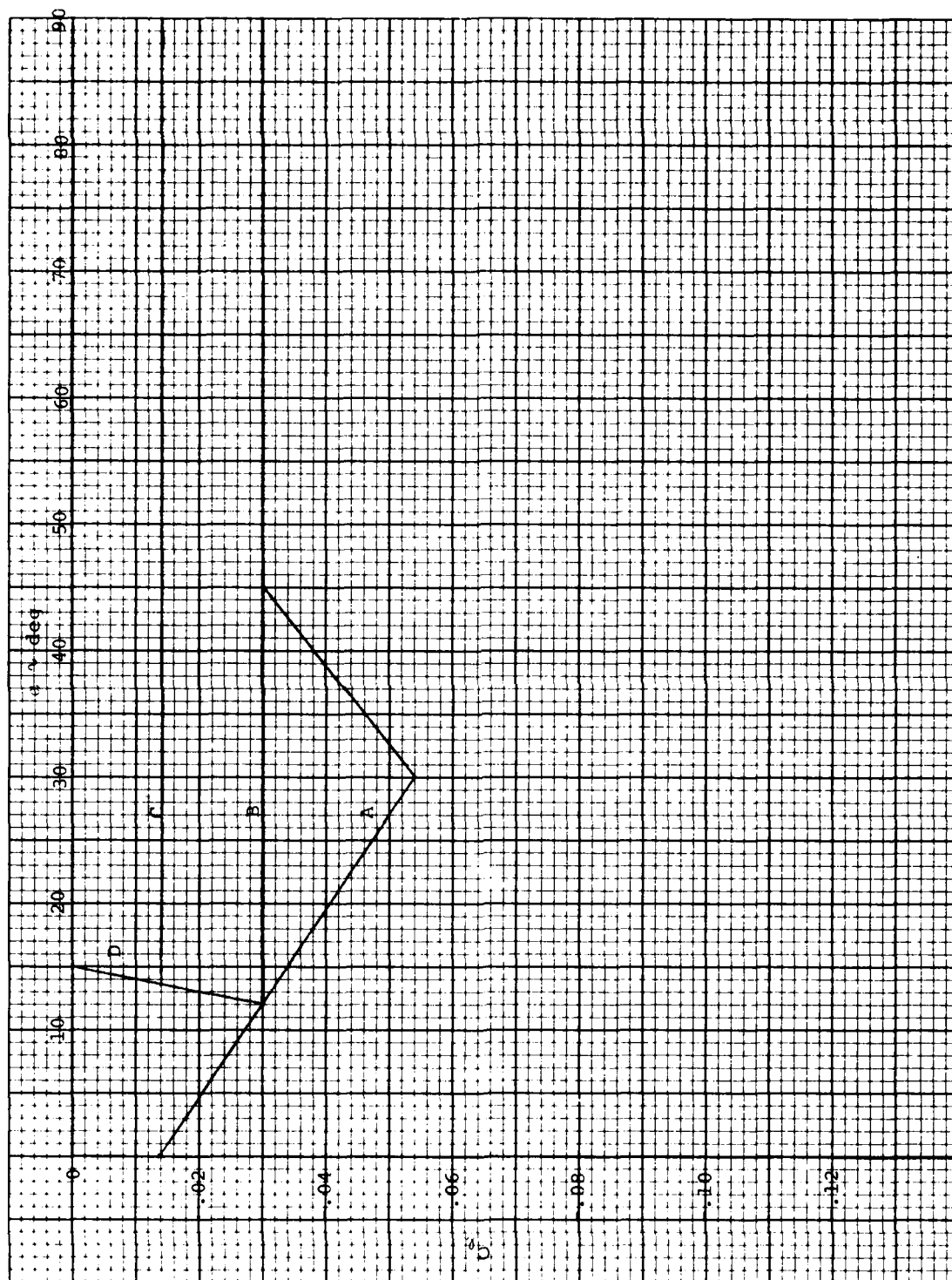
Figure 1. Rolling moment coefficient models

(b) $\delta = 25$ deg.
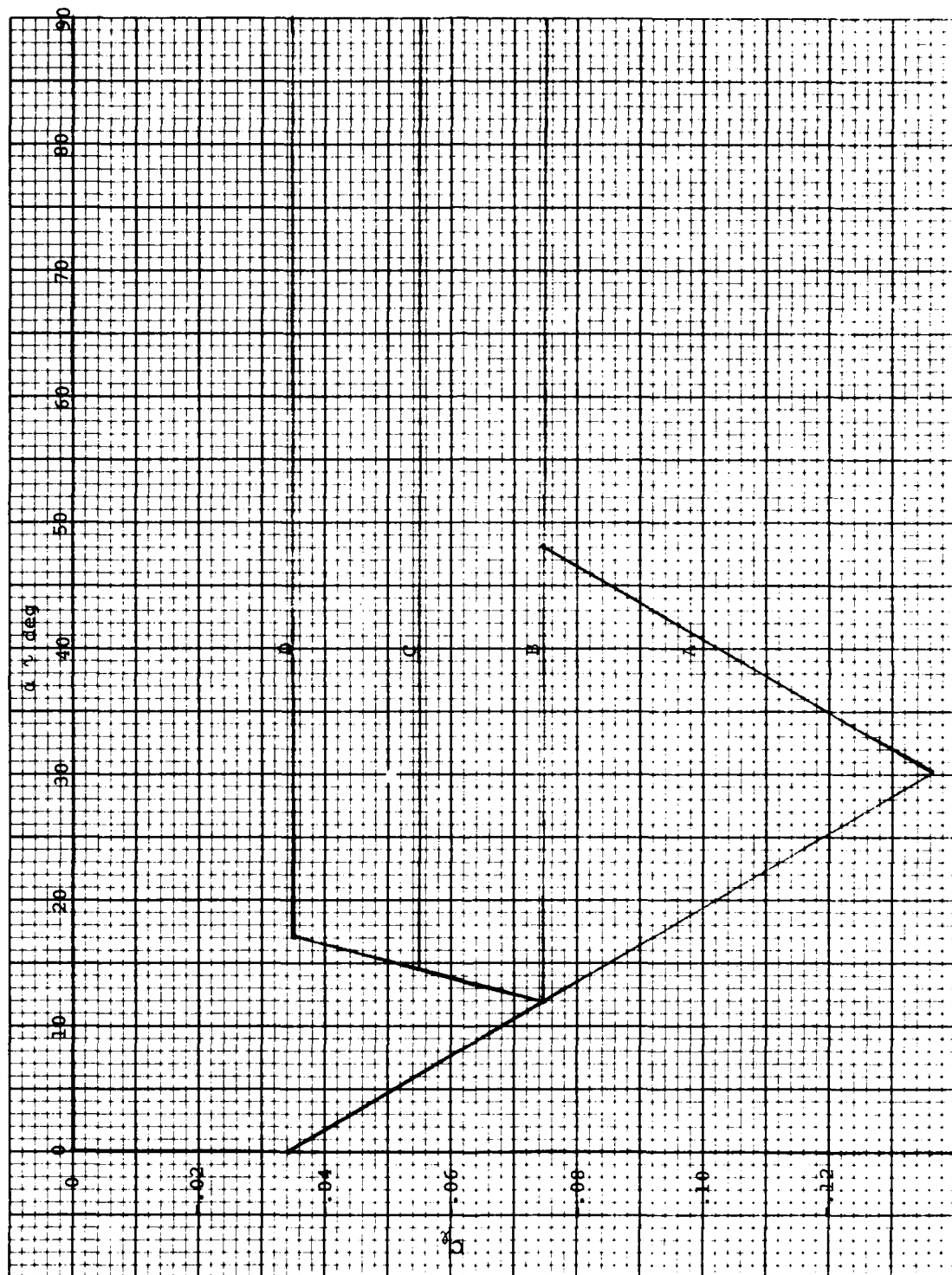
Figure 1. - (Concluded)
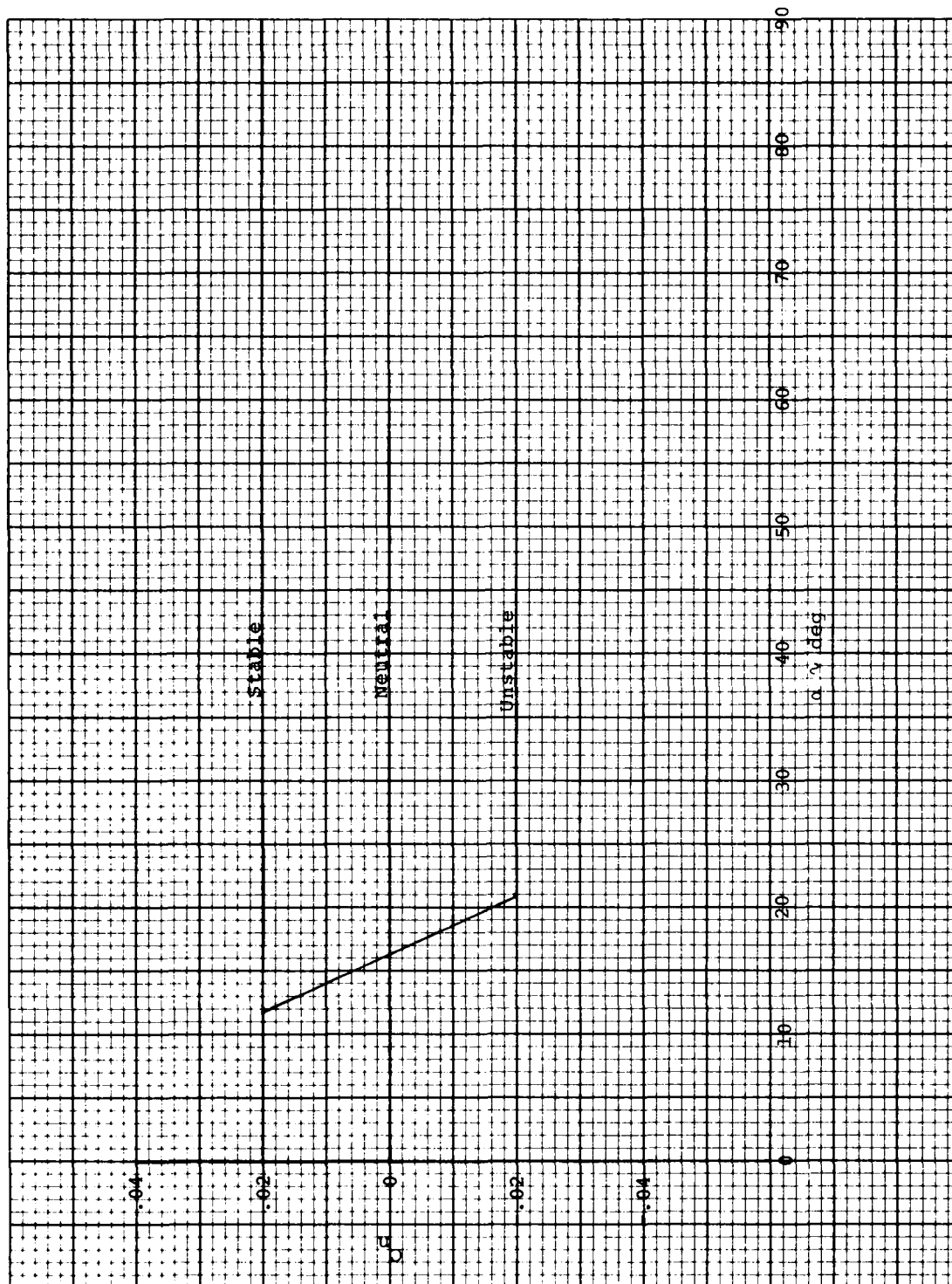
a) $\beta = 10$ deg

Figure 2. Yawing moment coefficient models

32

b) β=25 deg
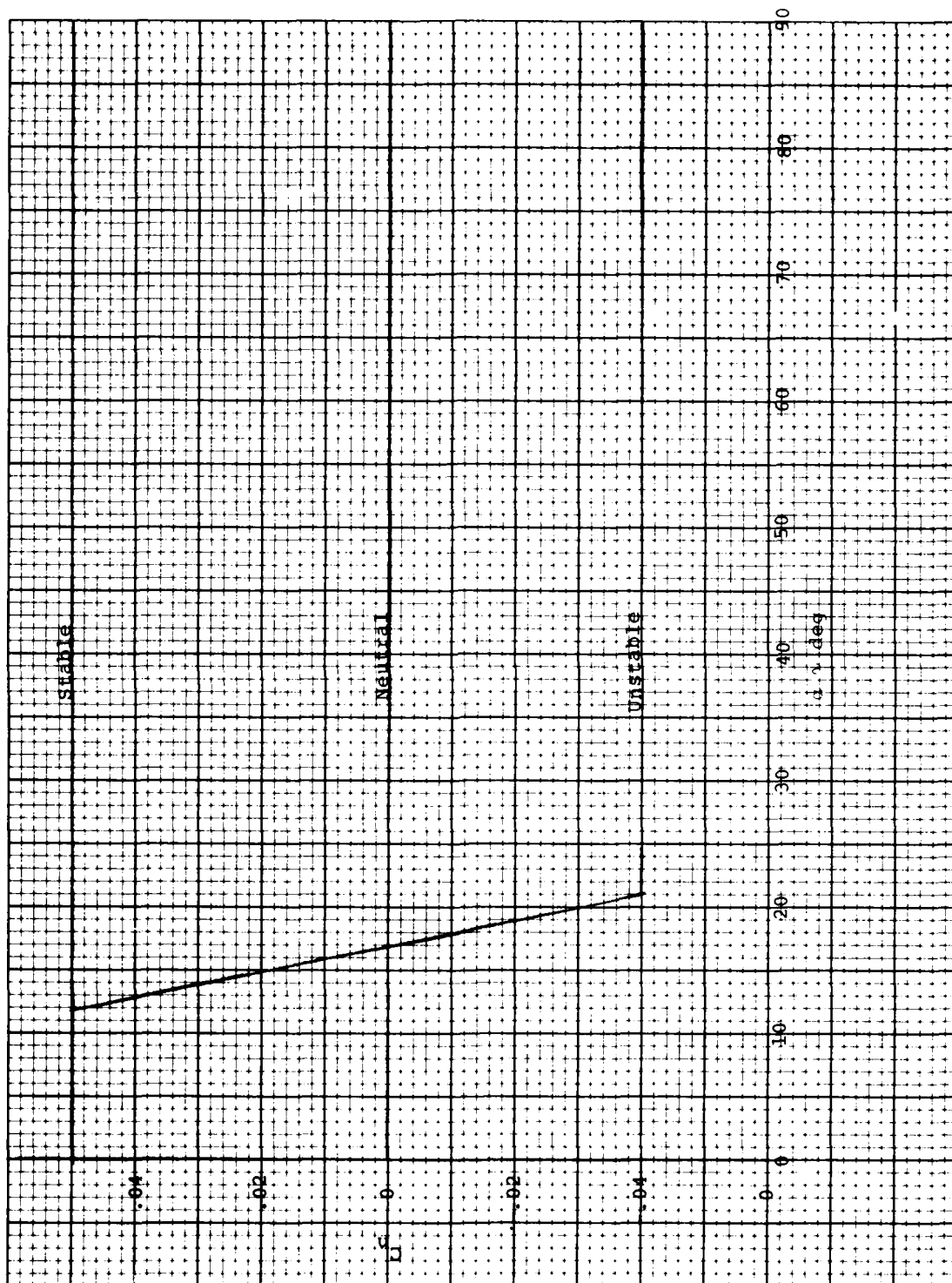
Figure 2. (Concluded)

33
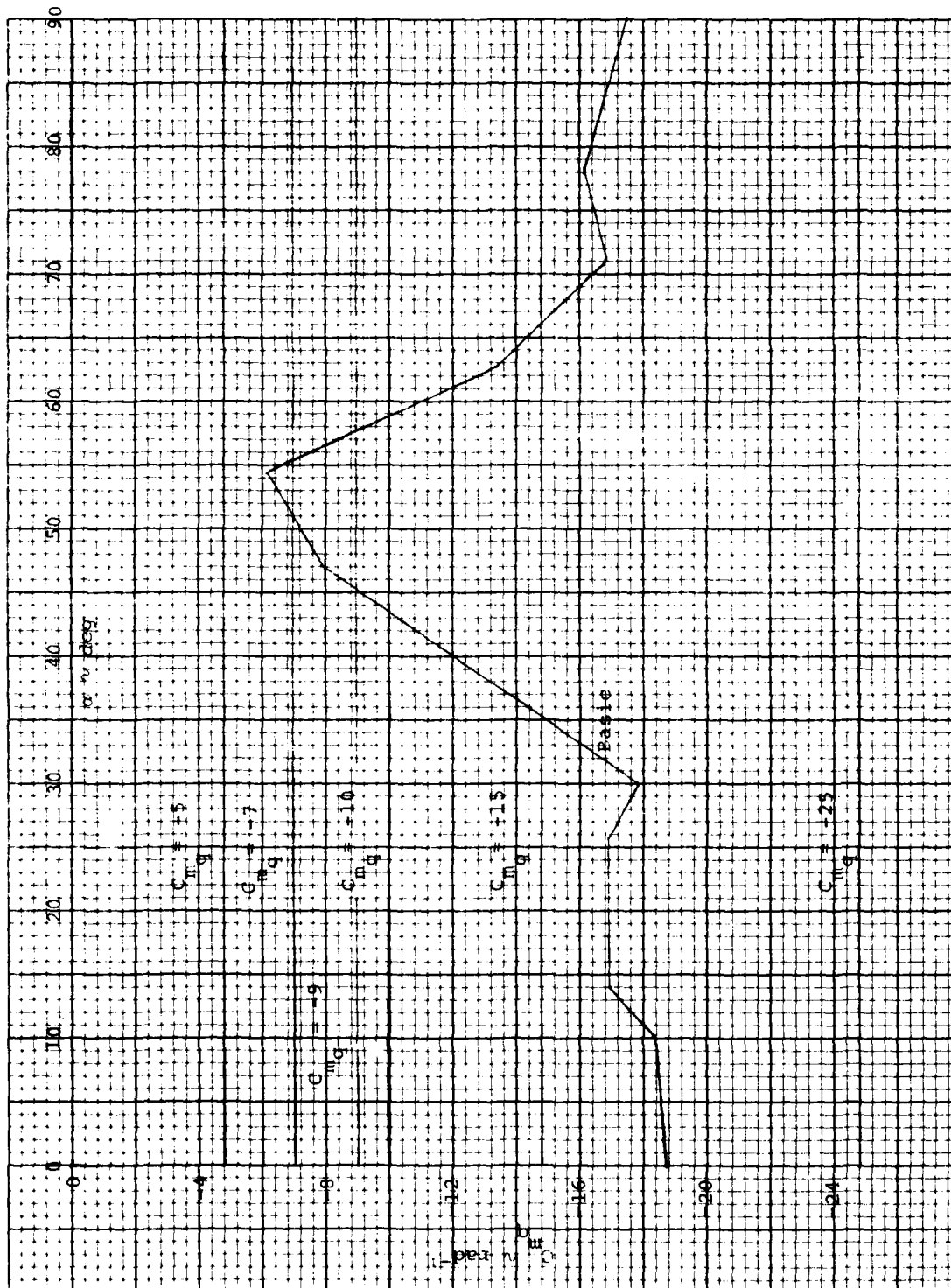
Figure 3. Pitch damping derivative, C_{m_q}, models
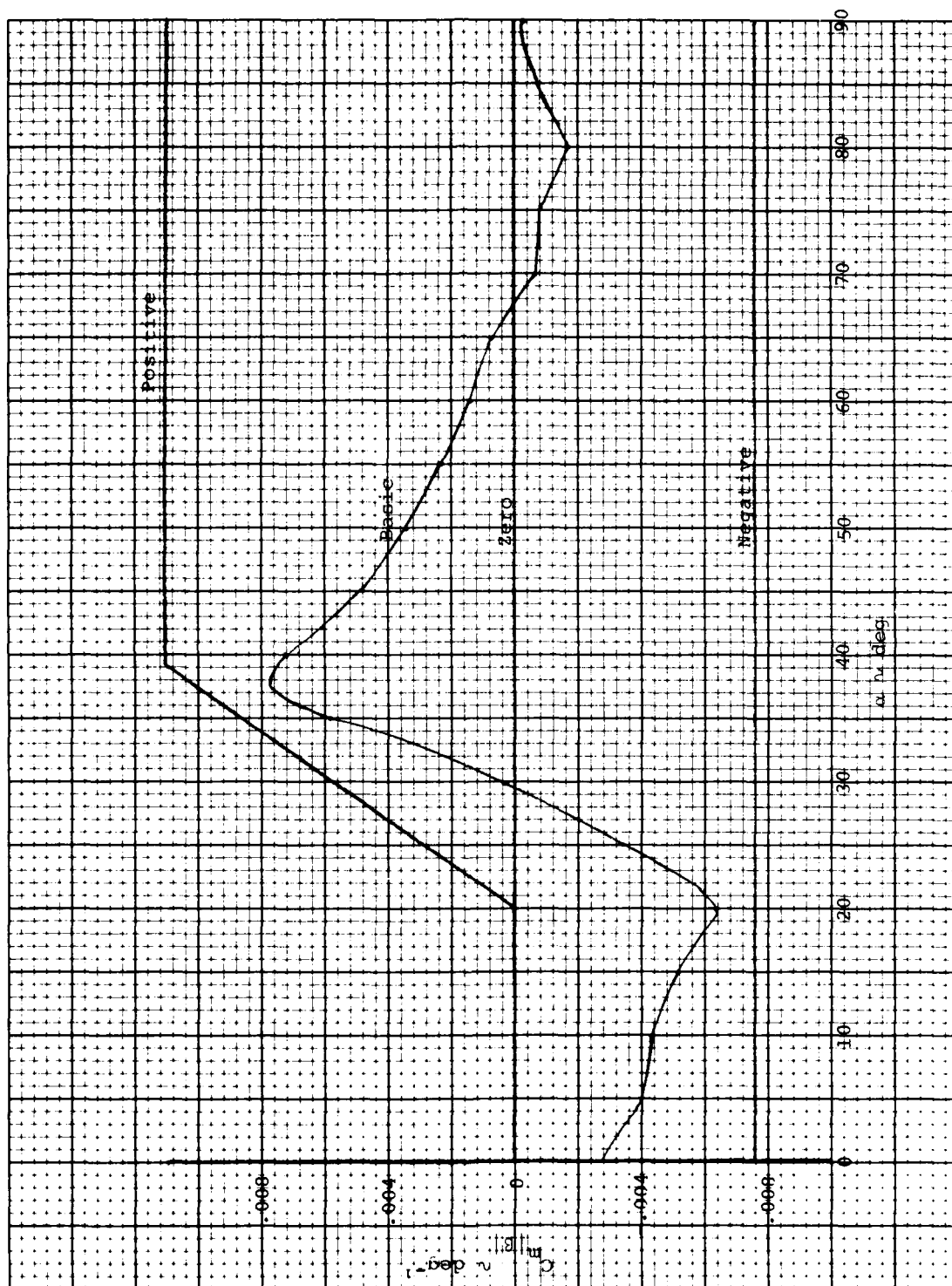
Figure 4. Pitching moment cross derivative, $C_{m_{|\beta|}}$, models
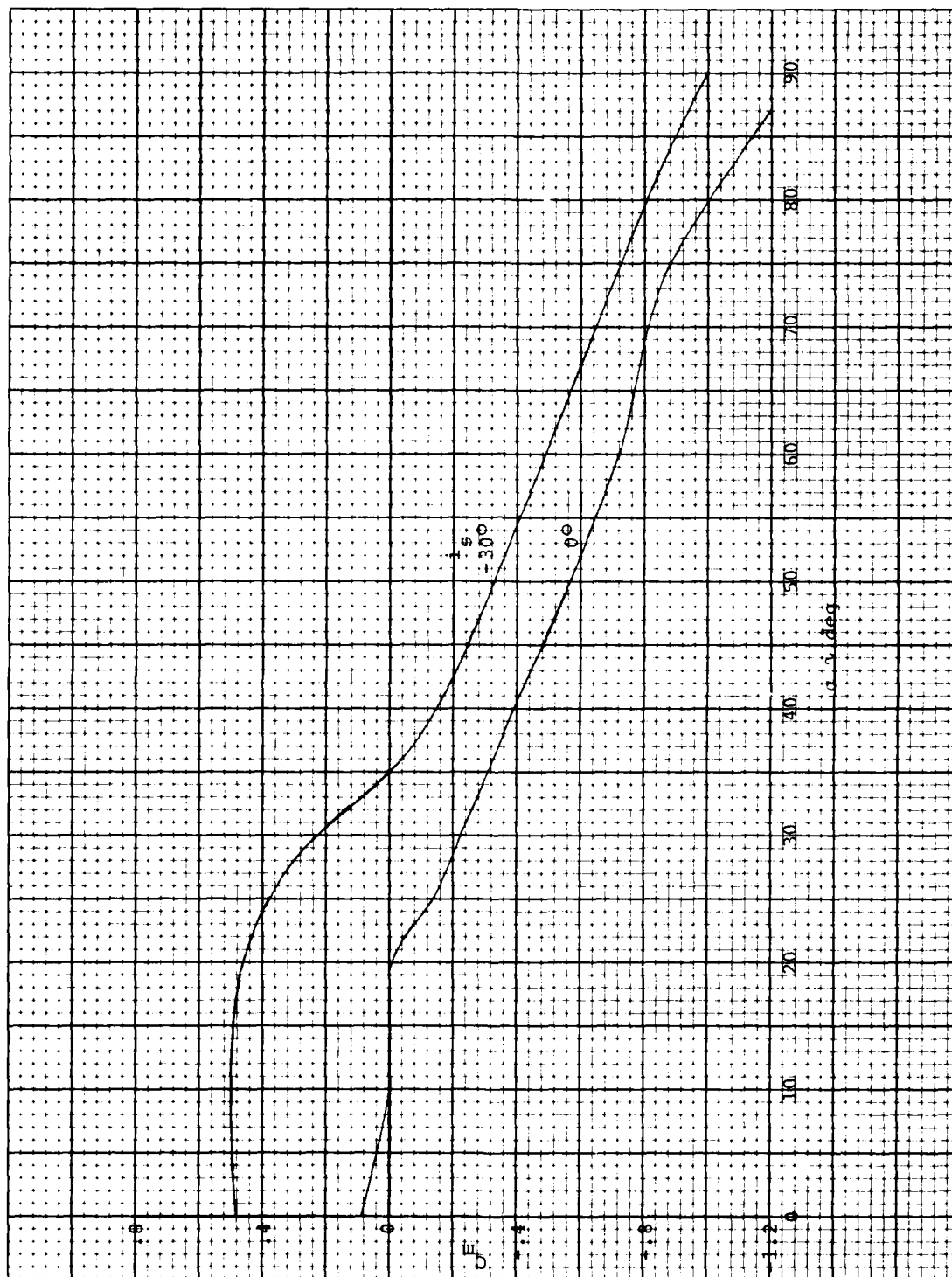
a) 9% static margin

Figure 5.   Pitching moment coefficient as a function of angle of attack
and longitudinal control deflection

b) i_s static margin

Figure 5. (Continued)

37
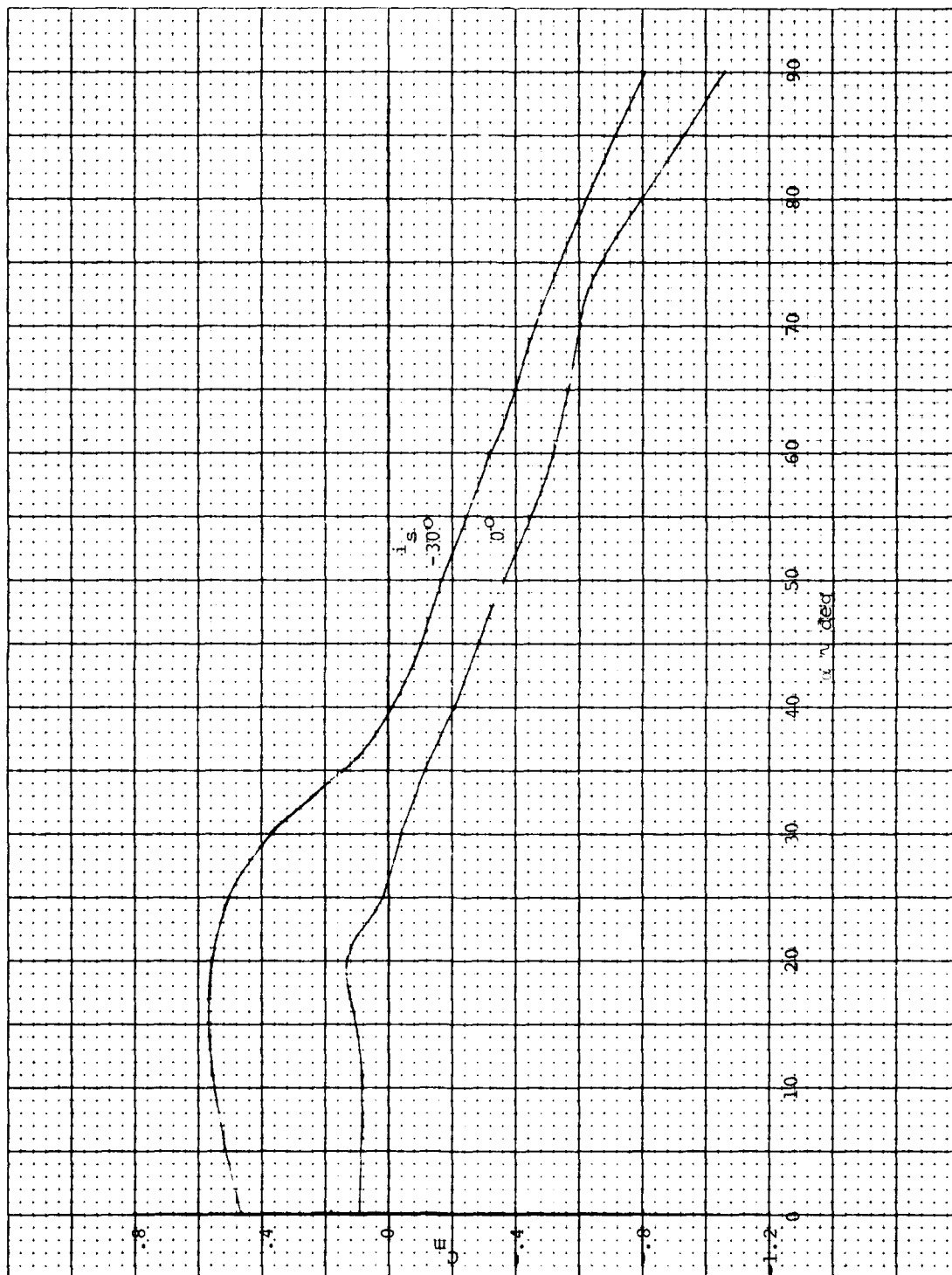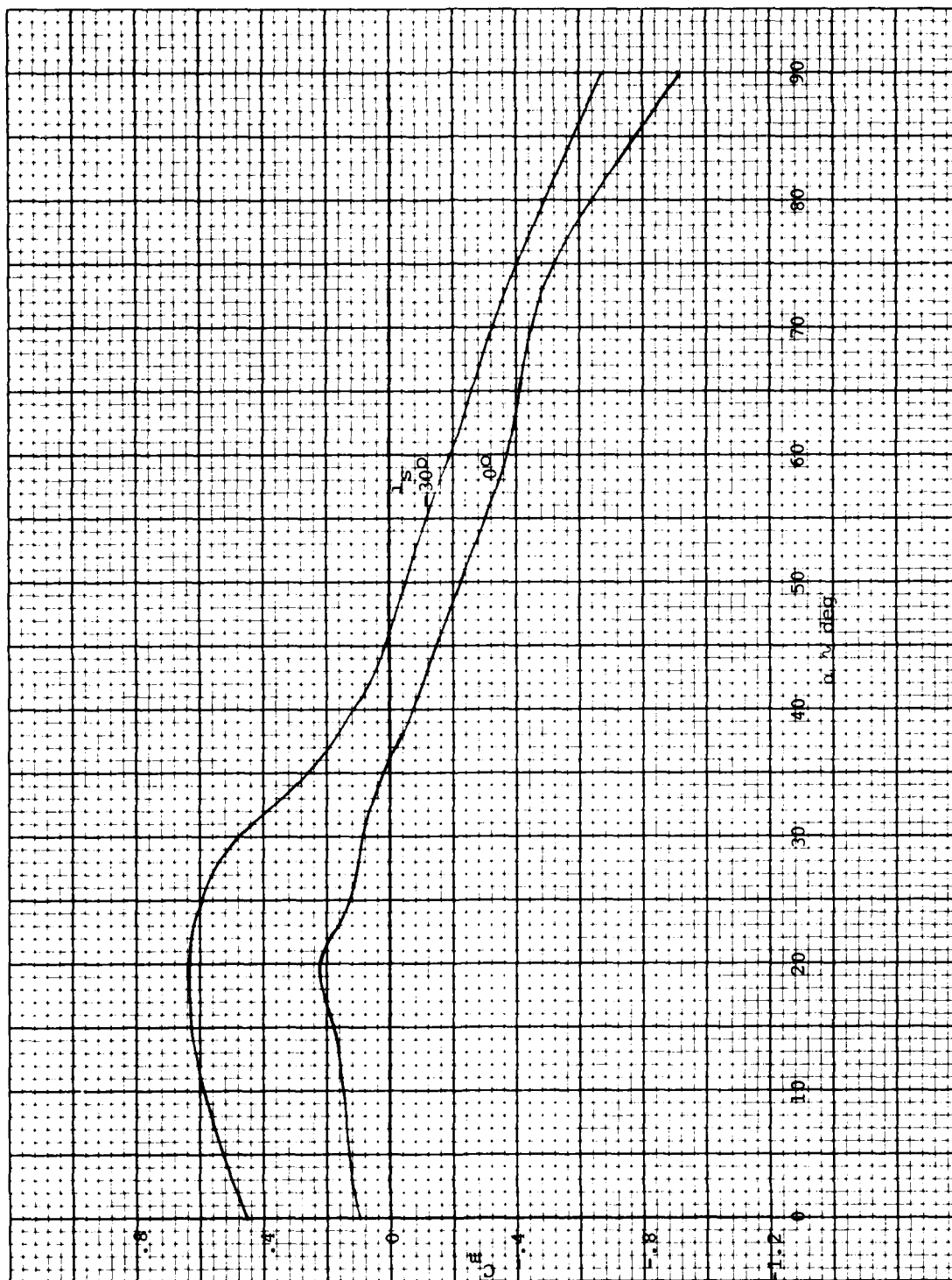
c) -5% static margin

Figure 5. (Continued)
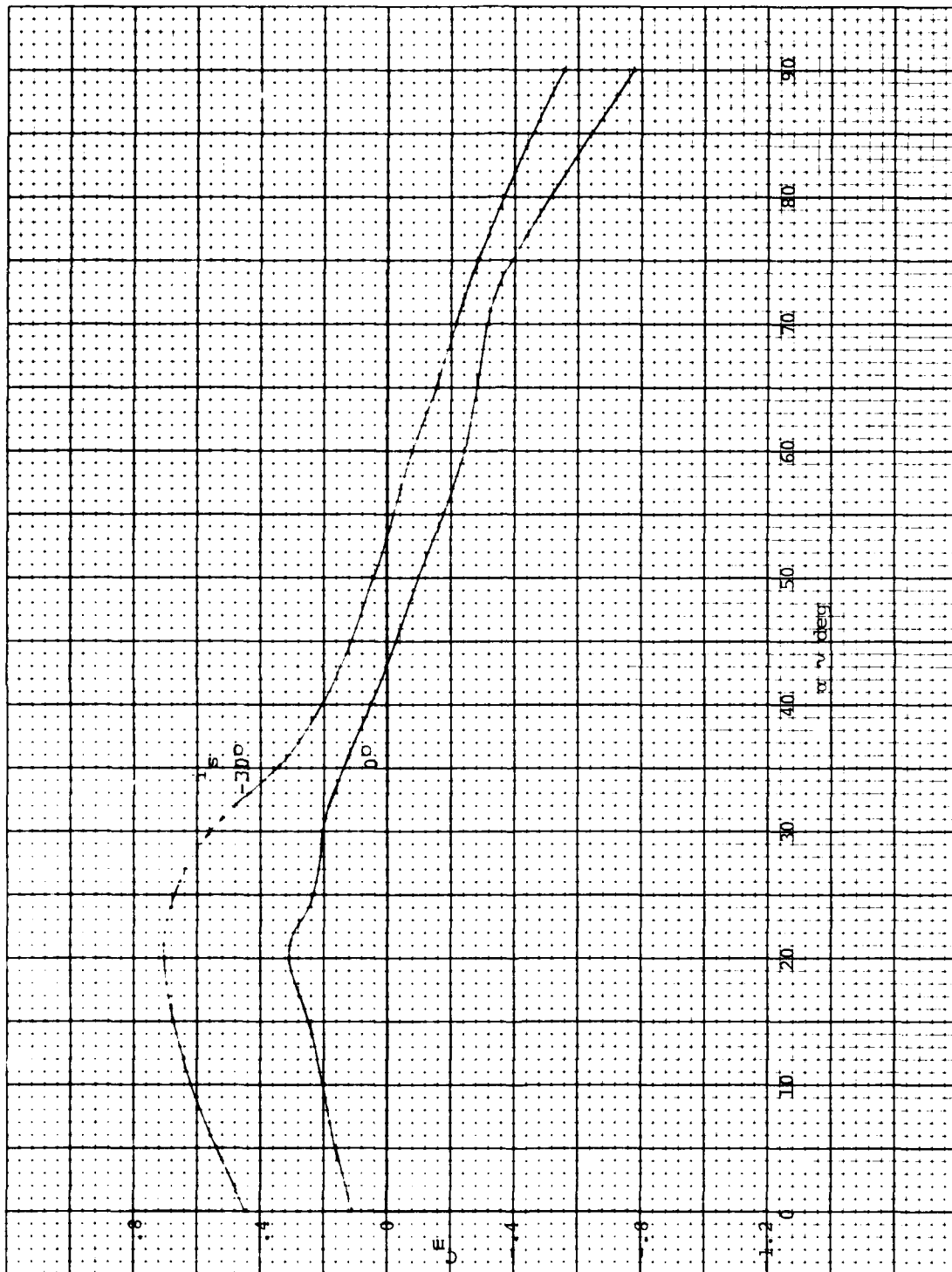
d) -10% static margin

Figure 5. (Concluded)
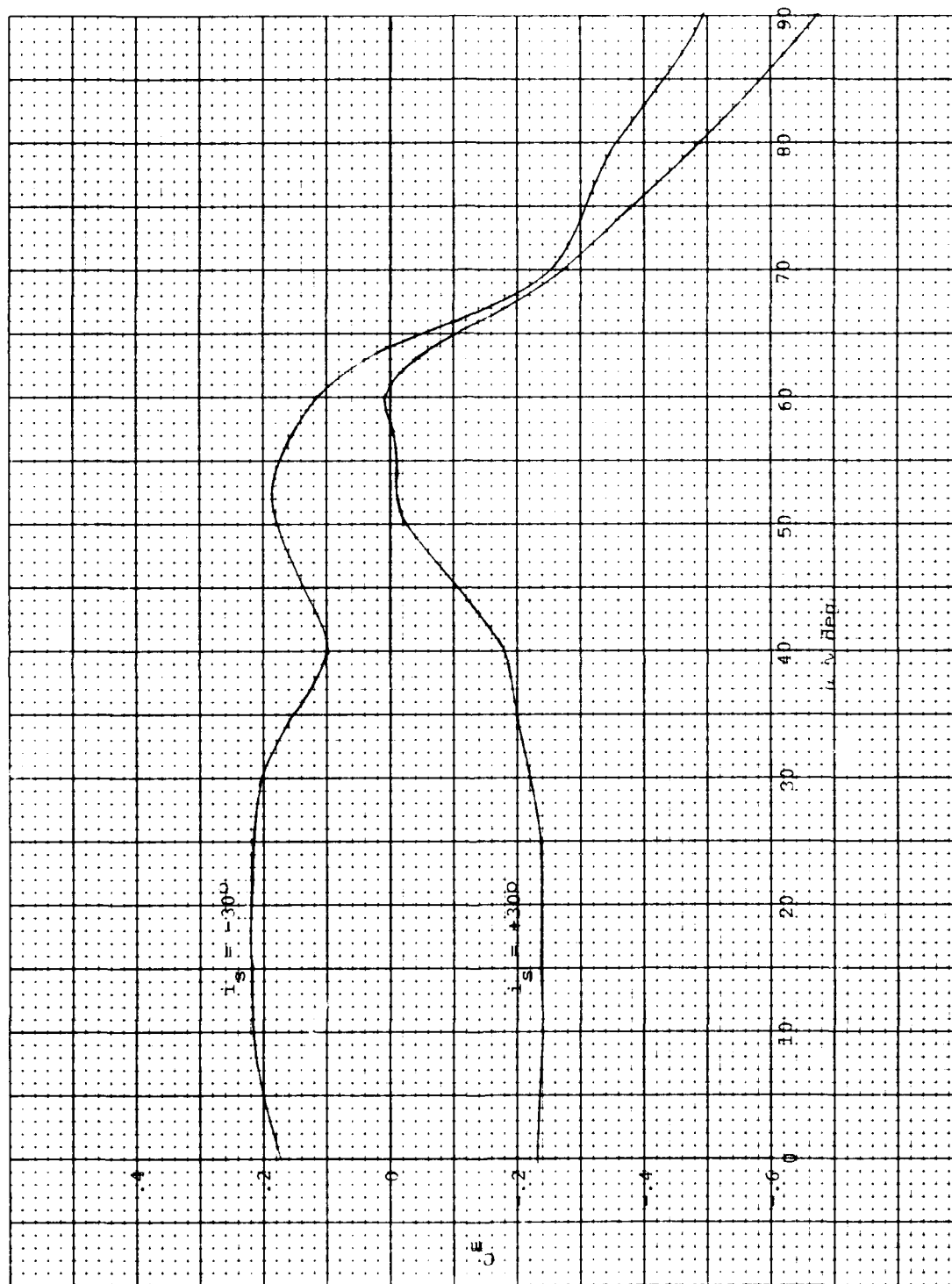
Figure 6. Alternate pitching moment coefficient as a function of angle of attack
and longitudinal control deflection
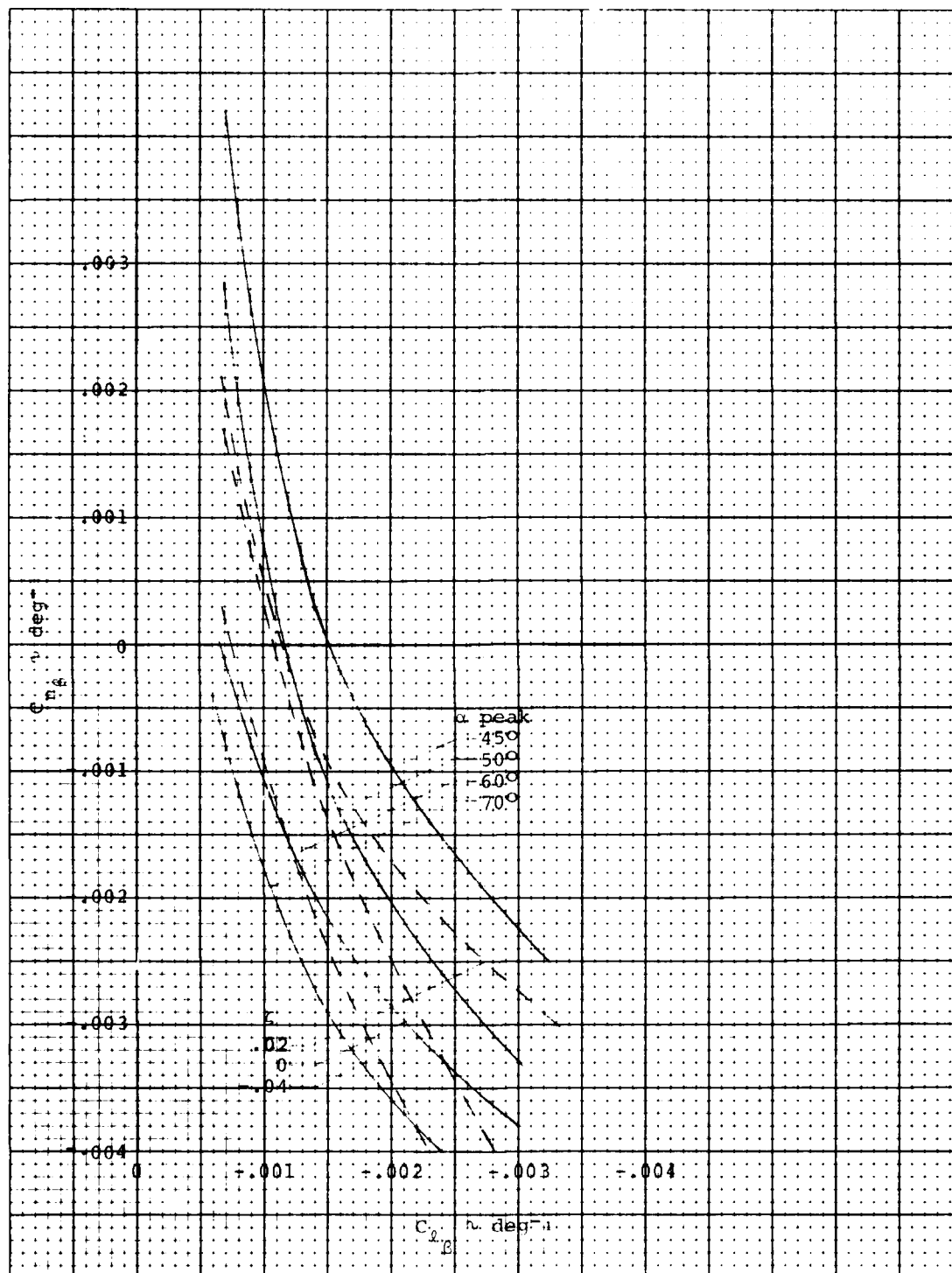
Figure 7. Constant alpha peak and damping ratio curves
as a function of lateral and directional stability
for a 9% static margin airplane with proverse $C_{n_{\delta_a}}$
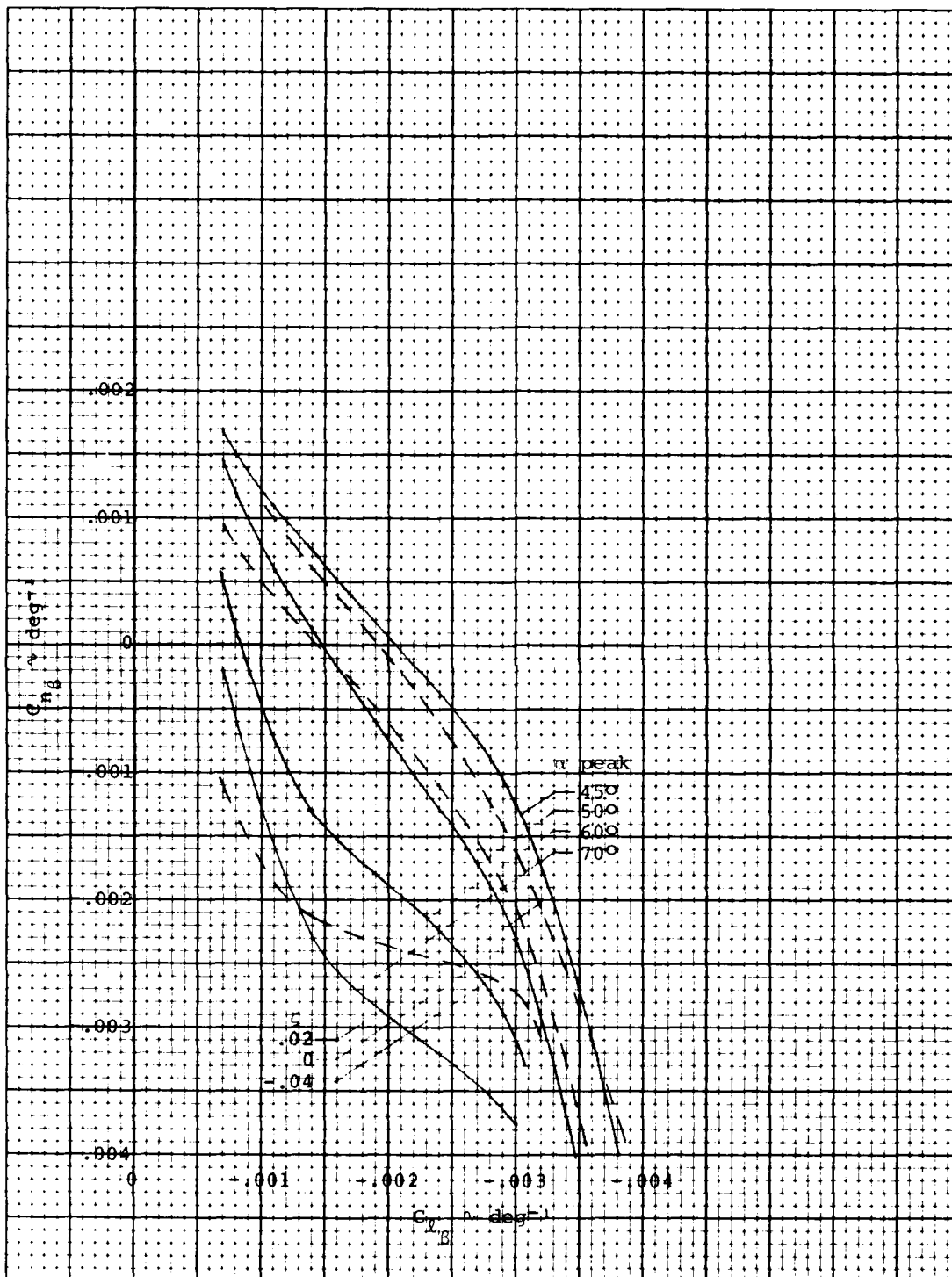
41

Figure 8. Constant alpha peak and damping ratio curves
as a function of lateral and directional stability
for a 9% static margin airplane with neutral $C_{n_{\delta_a}}$
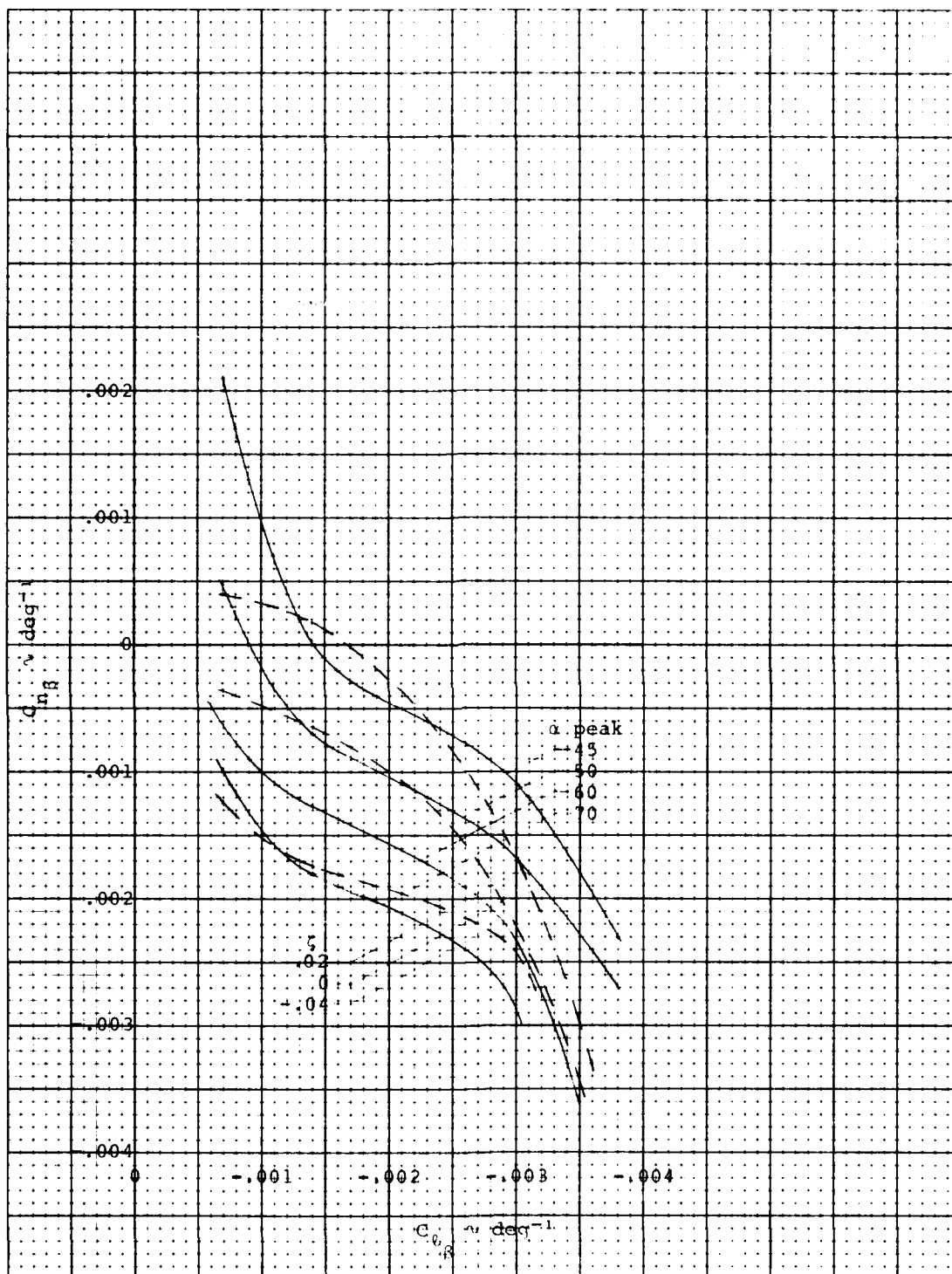
Figure 9. Constant alpha peak and damping ratio curves
as a function of lateral and directional stability
for 9° static margin airplane with adverse C_{n_δ}

43
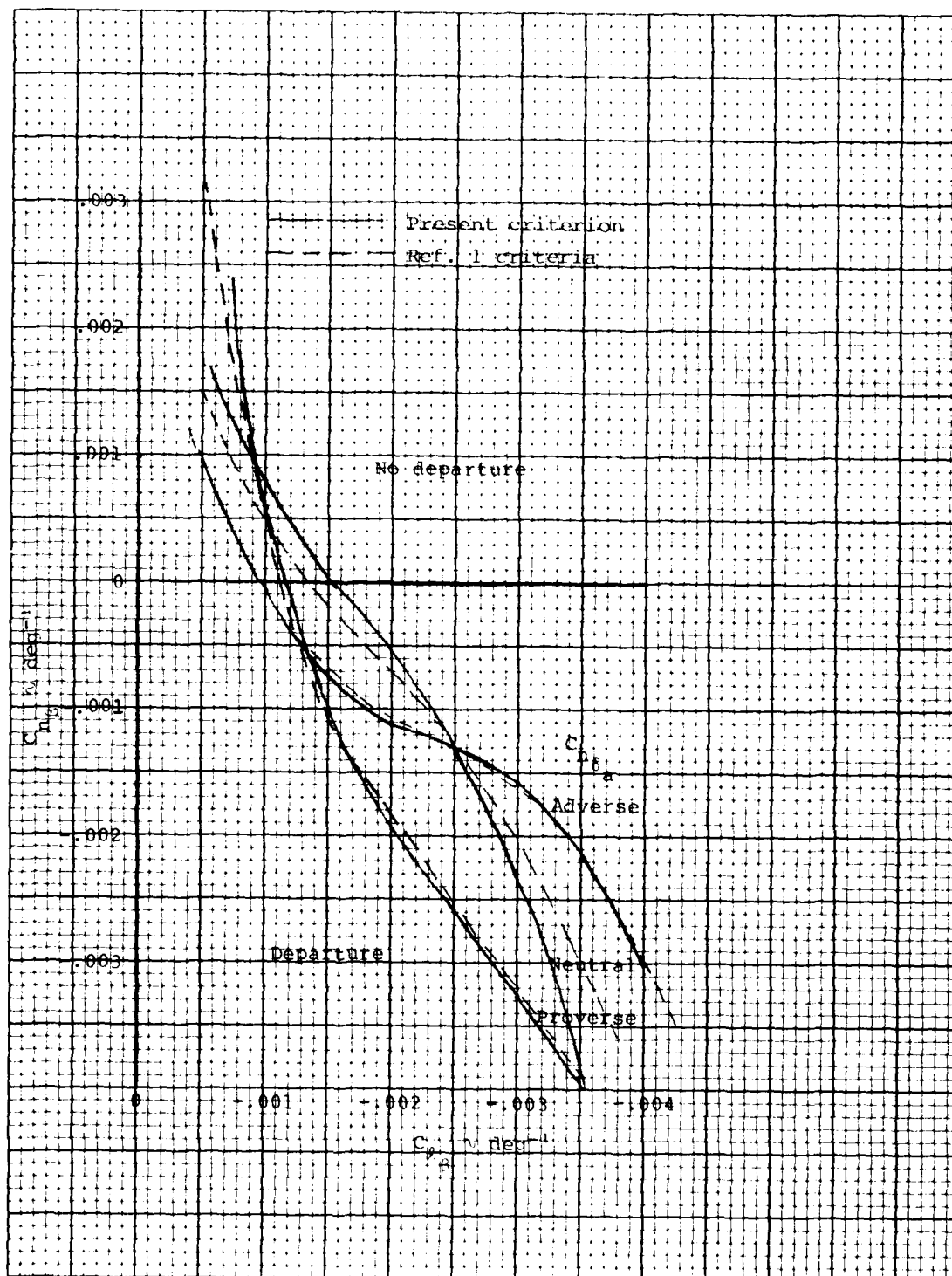
Figure 10. Comparison of departure boundaries based on
Reference 1 criteria and last peak angle-of-attack
criterion for 9° static margin airplane.

44
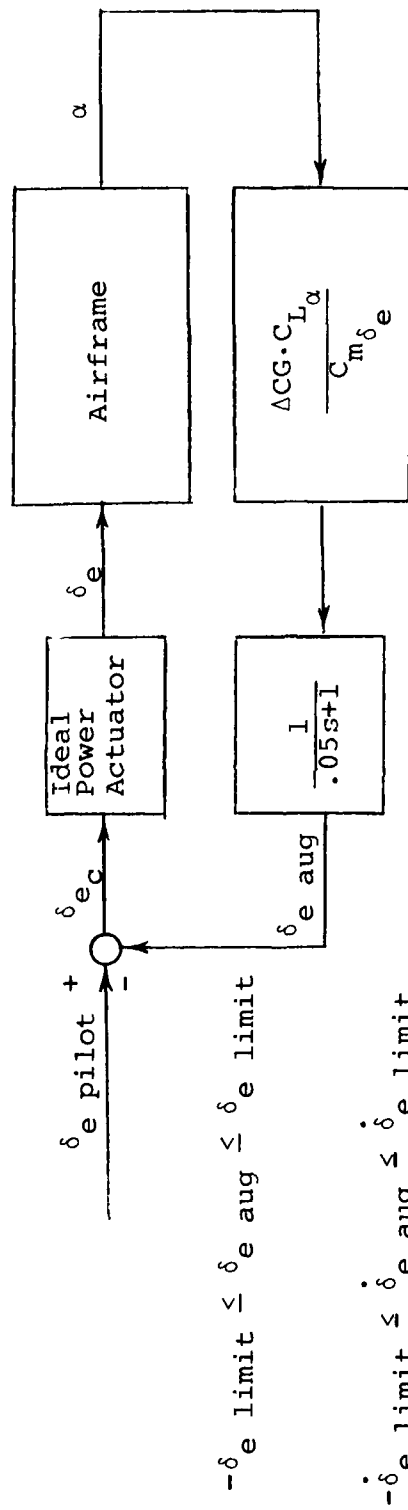
Figure 11. Simple feedback augmentation block diagram
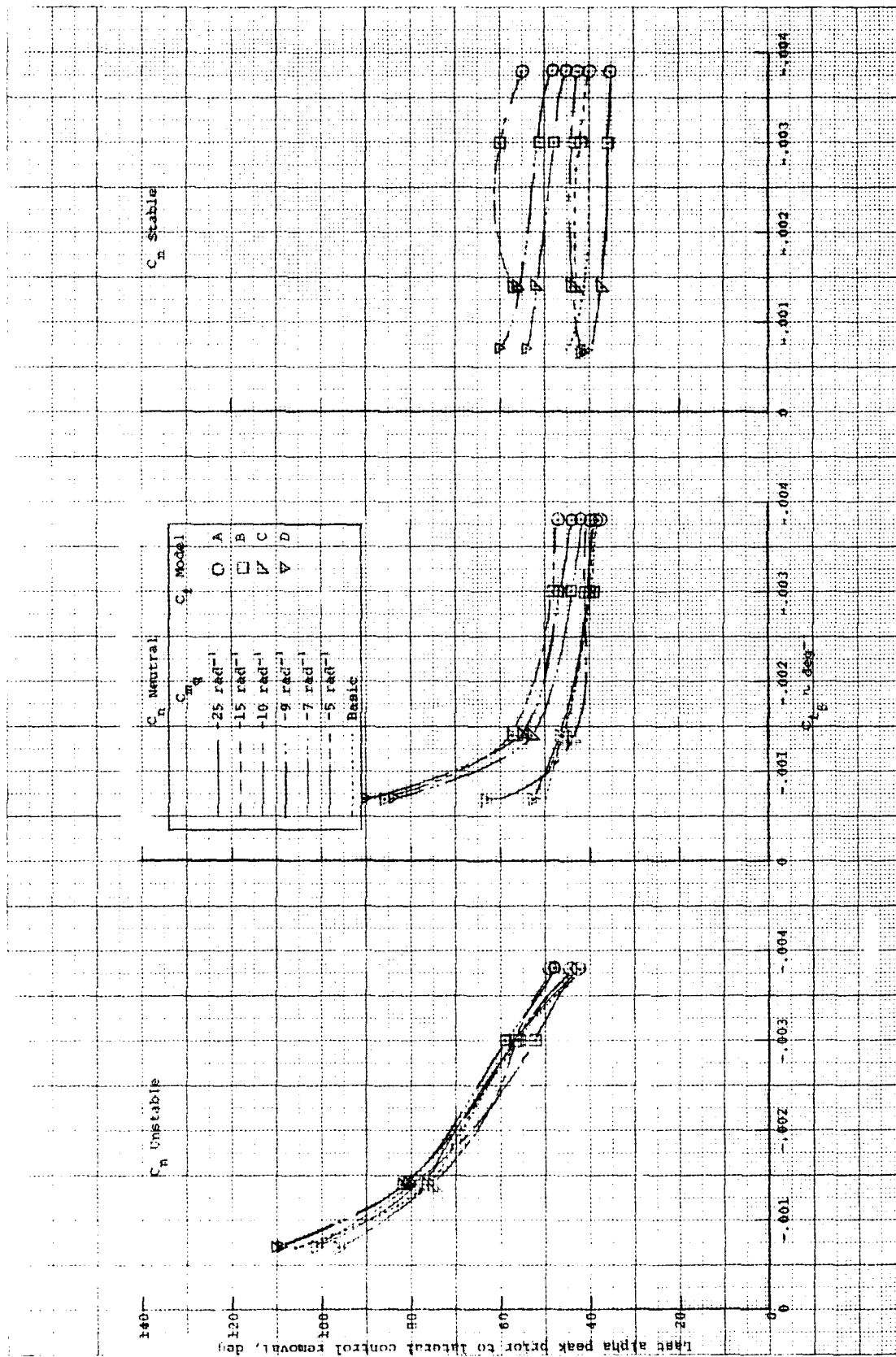
$-\delta_e \text{ limit} \leq \delta_e \text{ aug} \leq \delta_e \text{ limit}$

$-\dot{\delta}_e \text{ limit} \leq \dot{\delta}_e \text{ aug} \leq \dot{\delta}_e \text{ limit}$

45

a) Last alpha peak prior to lateral control removal as a function of the aerodynamic models

Figure 12. Influence of C_{m_q} on design charts for determining departure and uncoordinated roll reversal susceptibility for a 9% static margin airplane having adverse $C_{n_{\delta_a}}$
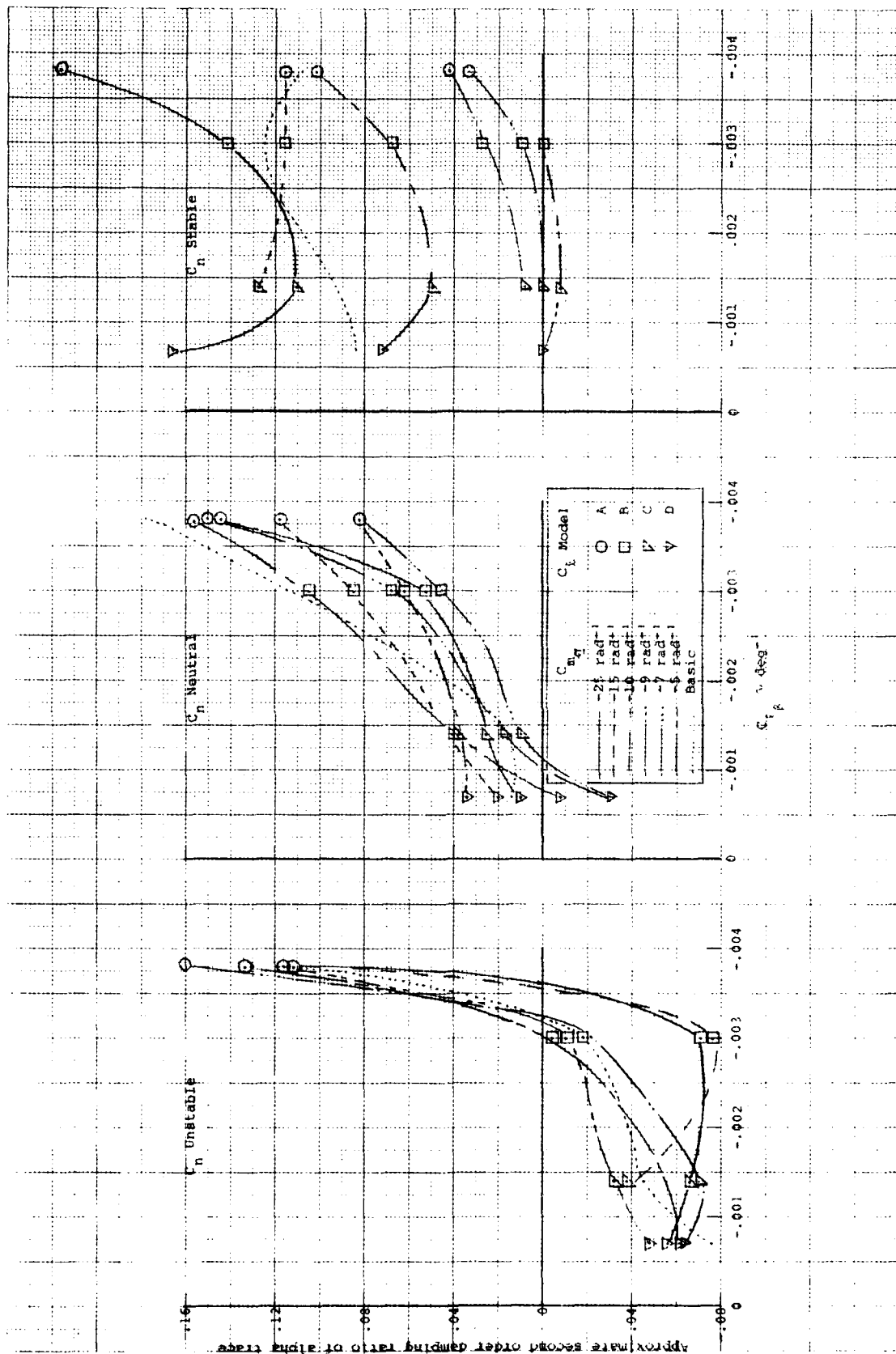
b) Approximate second order damping ratio of alpha trace as a function of the aerodynamic models

Figure 12. (Continued)
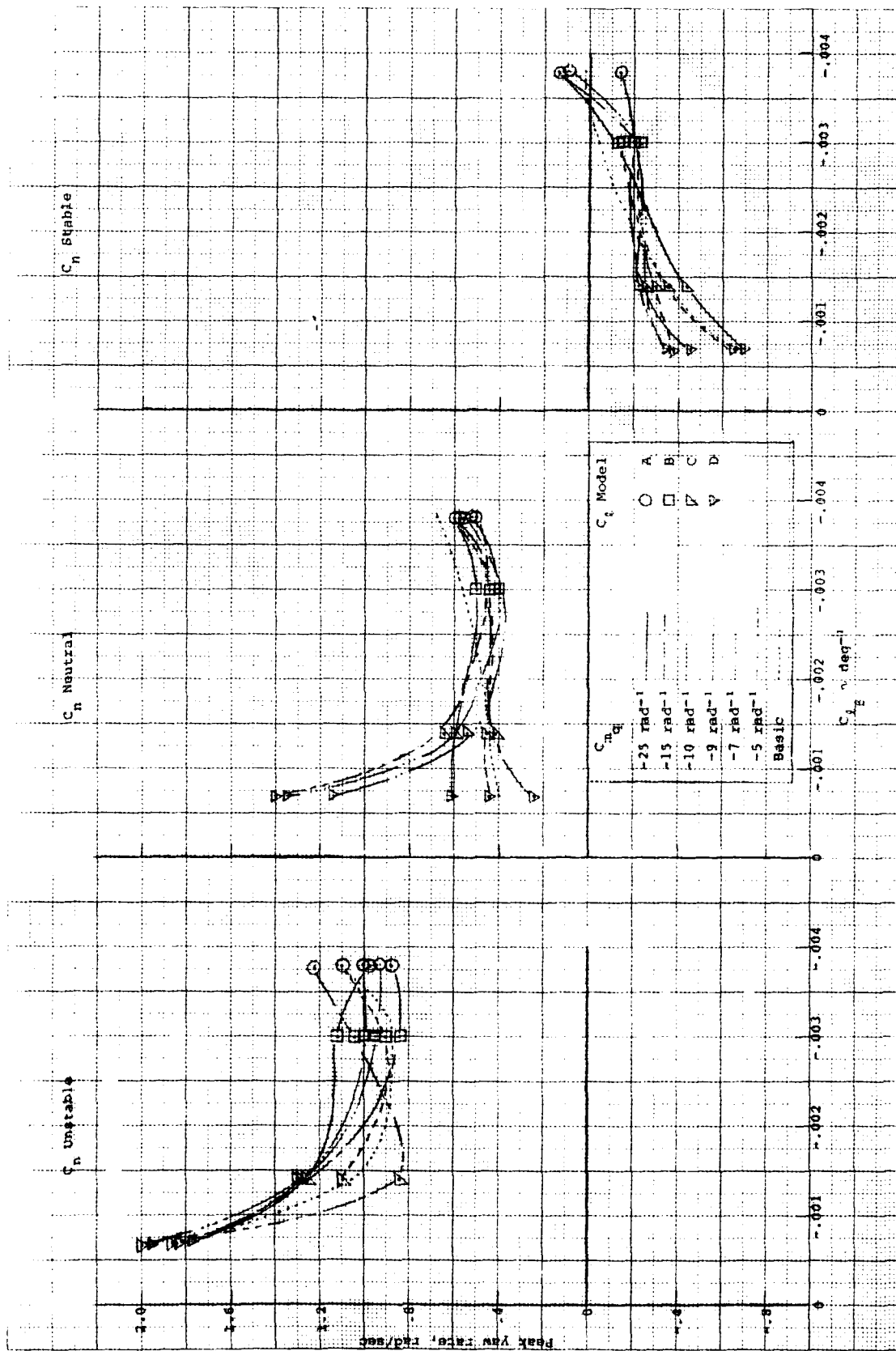
c) Peak yaw rate as a function of the aerodynamic models

Figure 12. (Continued)
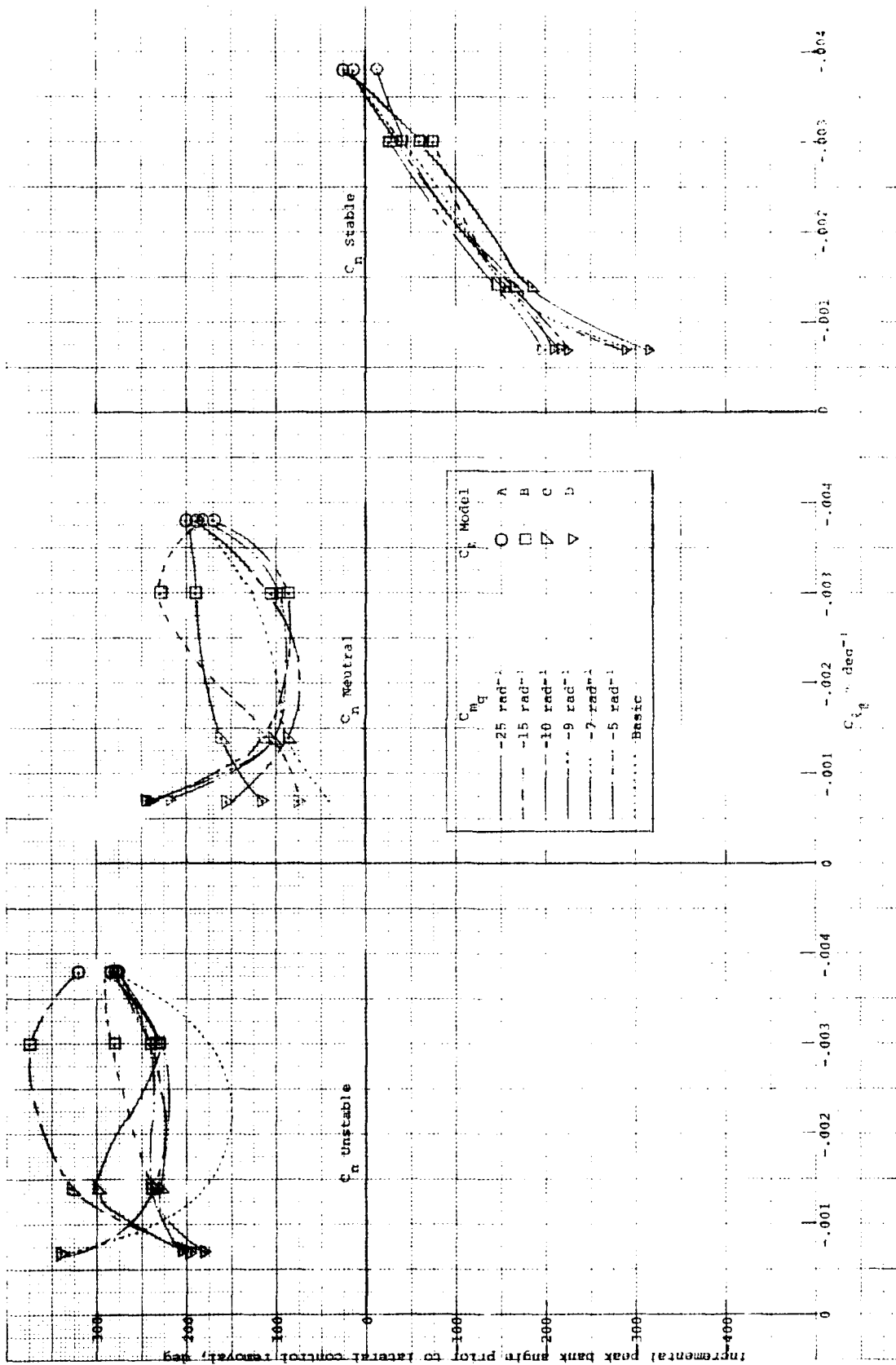
d) Incremental peak bank angle prior to lateral control removal as a function of the aerodynamic models

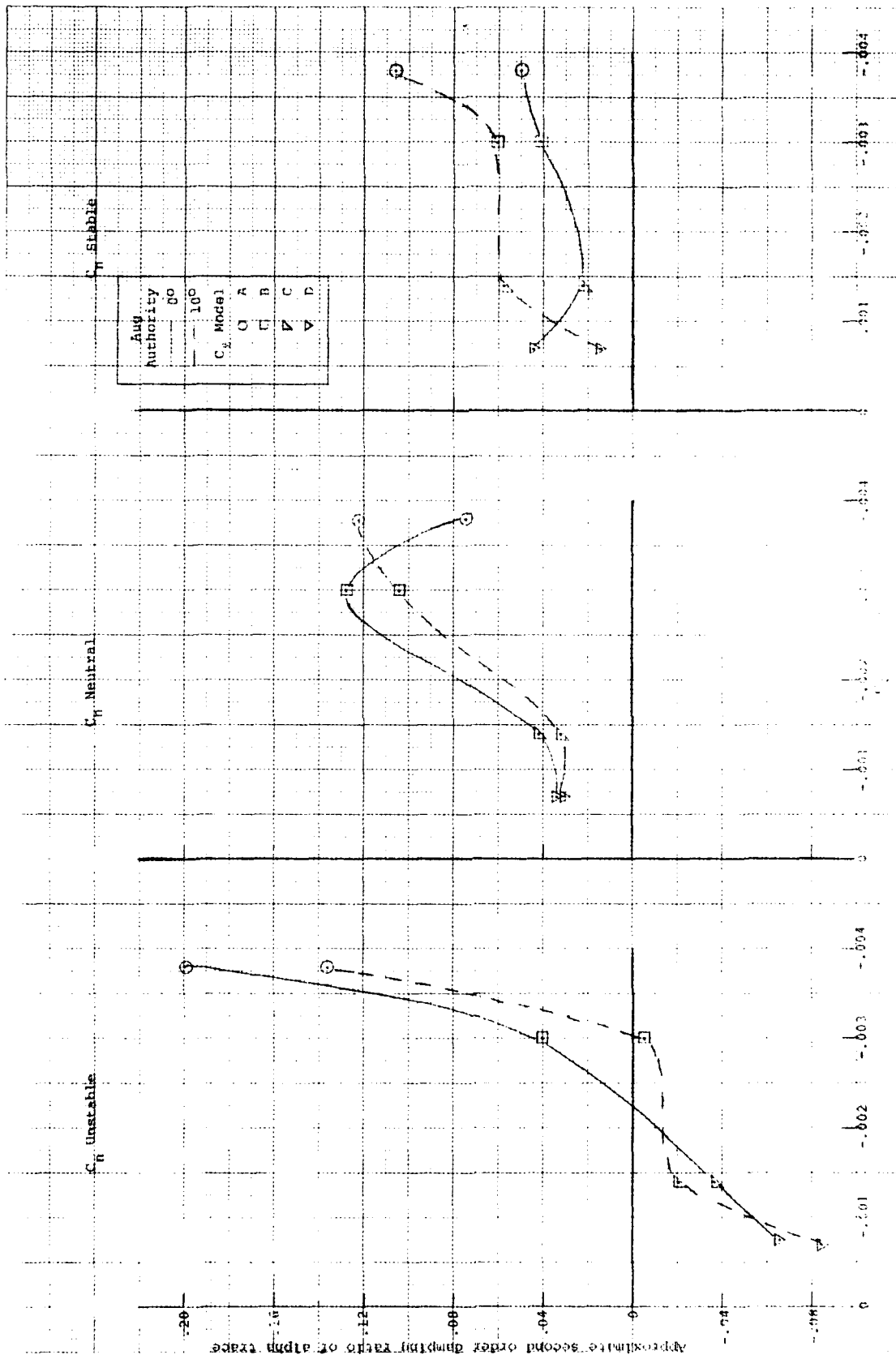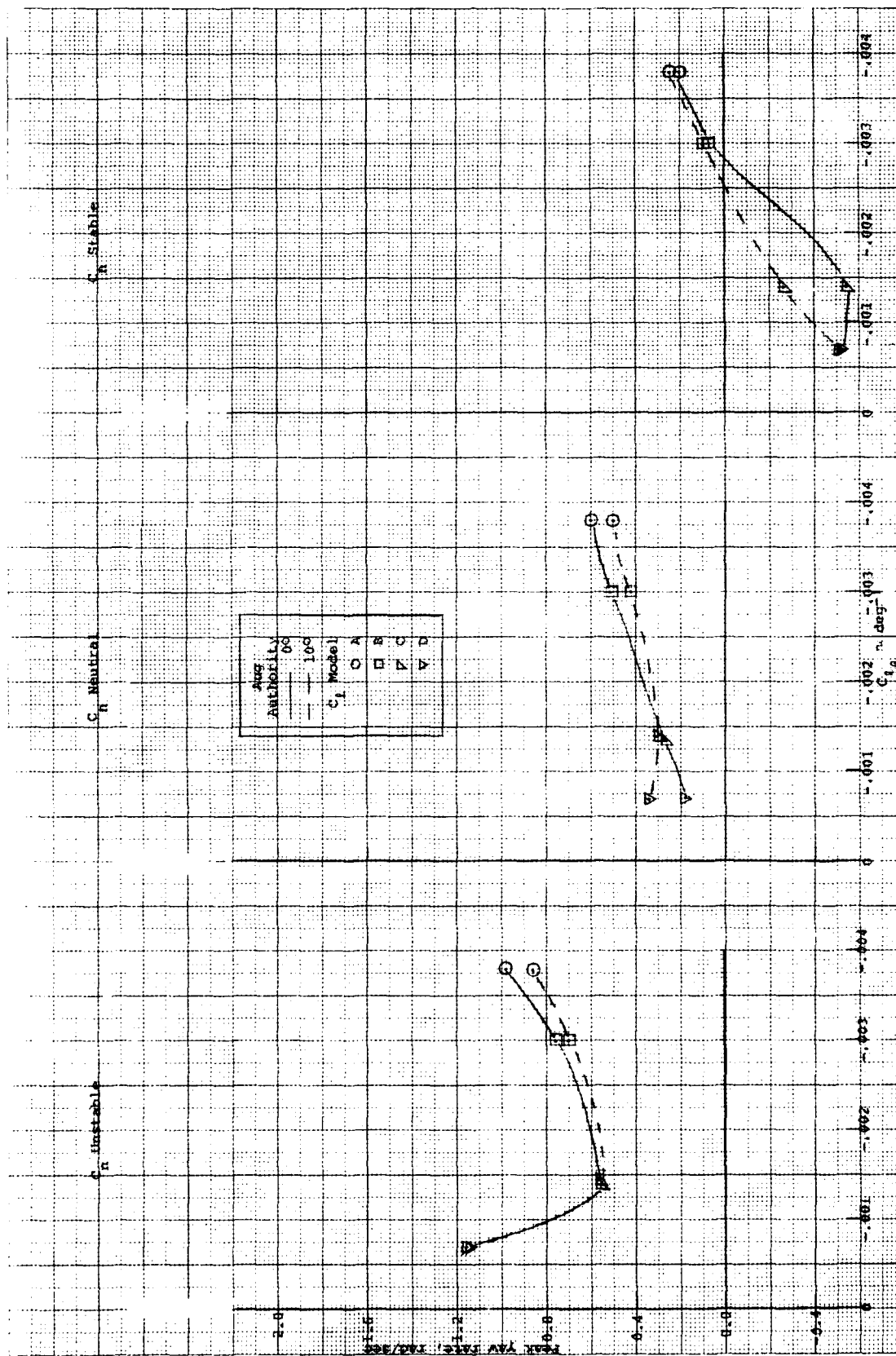Figure 12.   (concluded)
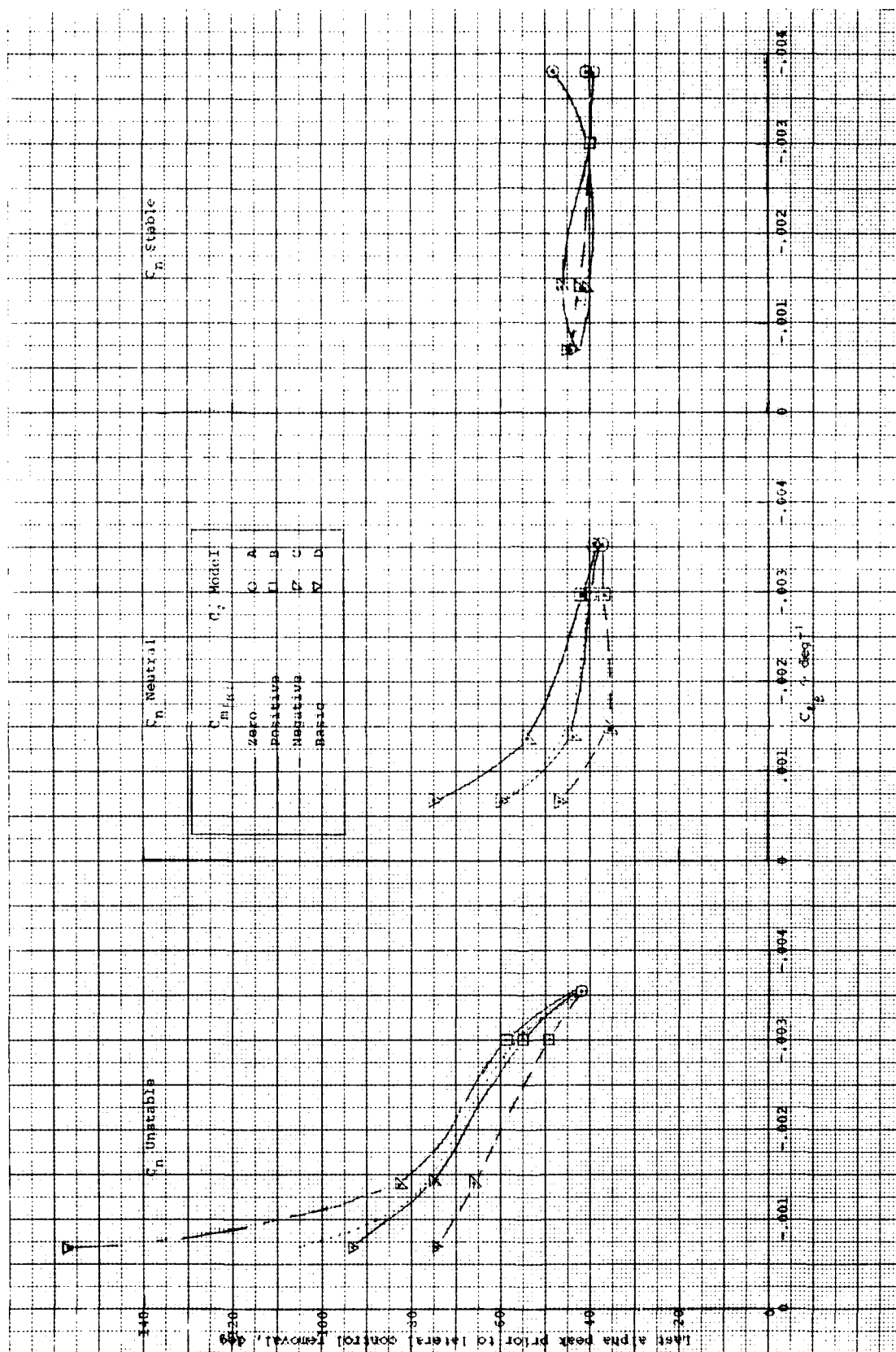
a) Last alpha peak prior to lateral control removal as a function of the aerodynamic models

Figure 13. Influence of $C_{m_{1/4}}$ on design charts for determining departure and uncoordinated roll reversal susceptibility for a 9% static margin airplane by adverse $C_{n_{\delta a}}$

Figure 14. Continued.

51
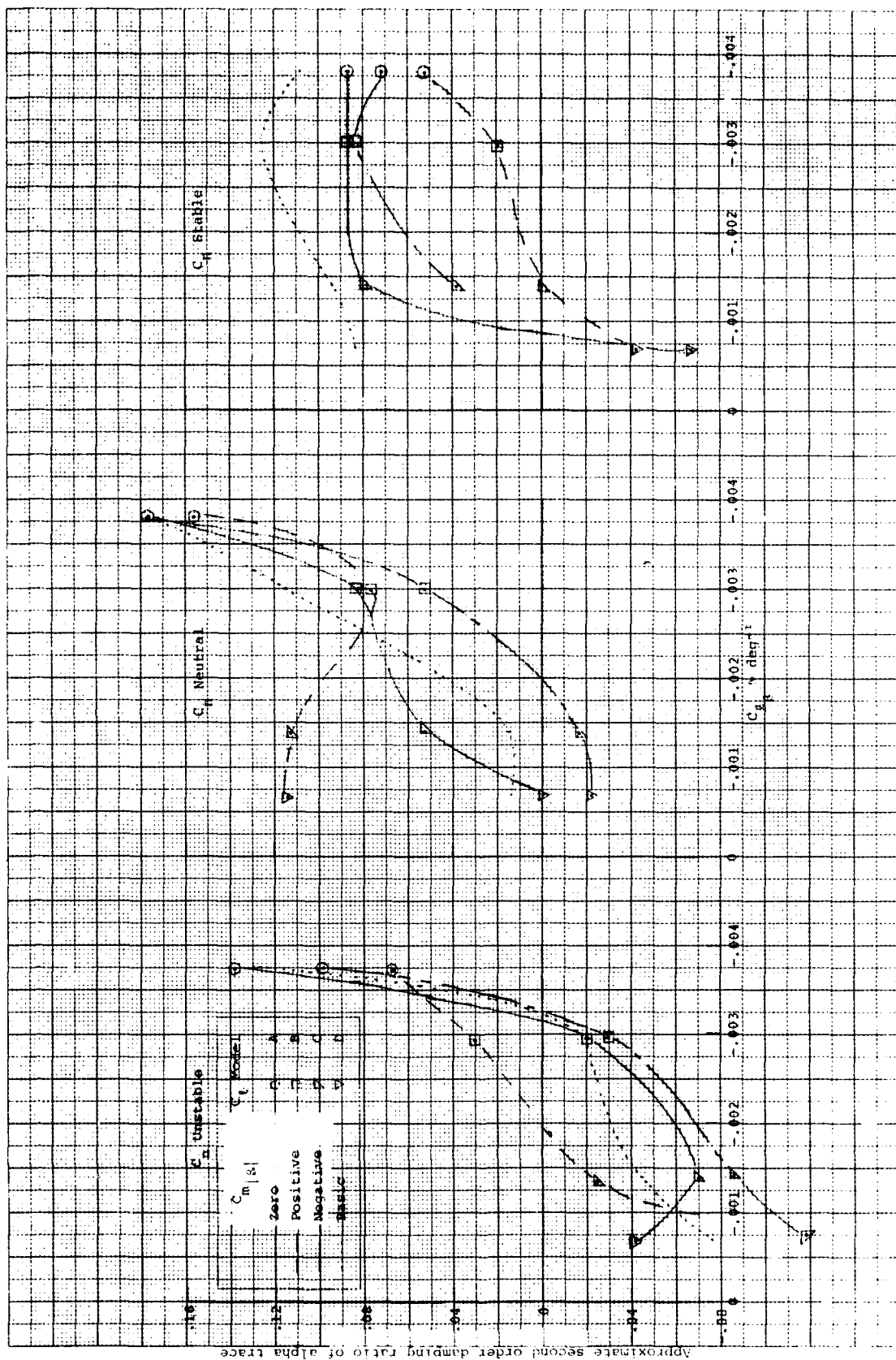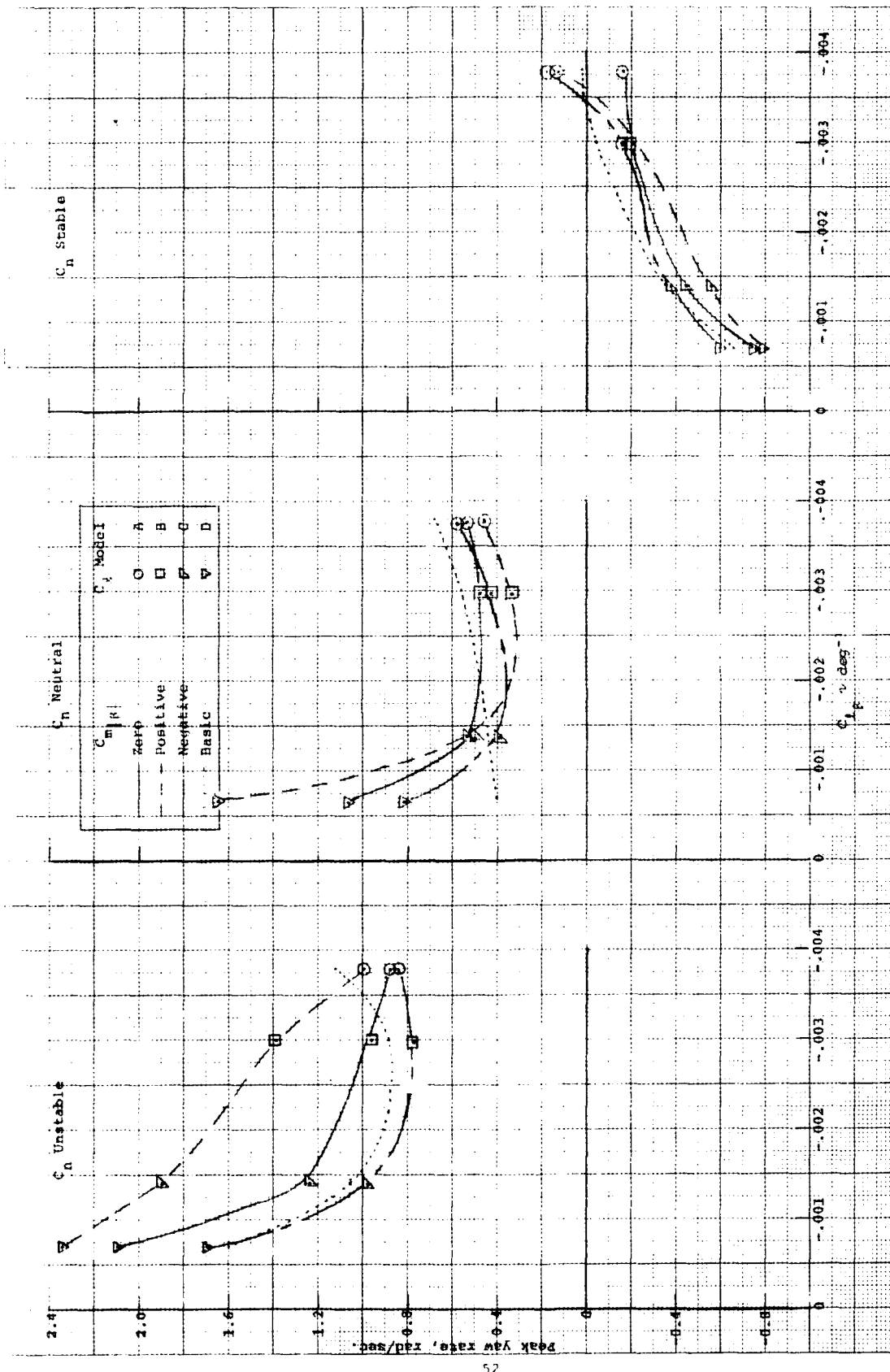
c) Peak yaw rate as a function of the aerodynamic models

Figure 13. (Continued)
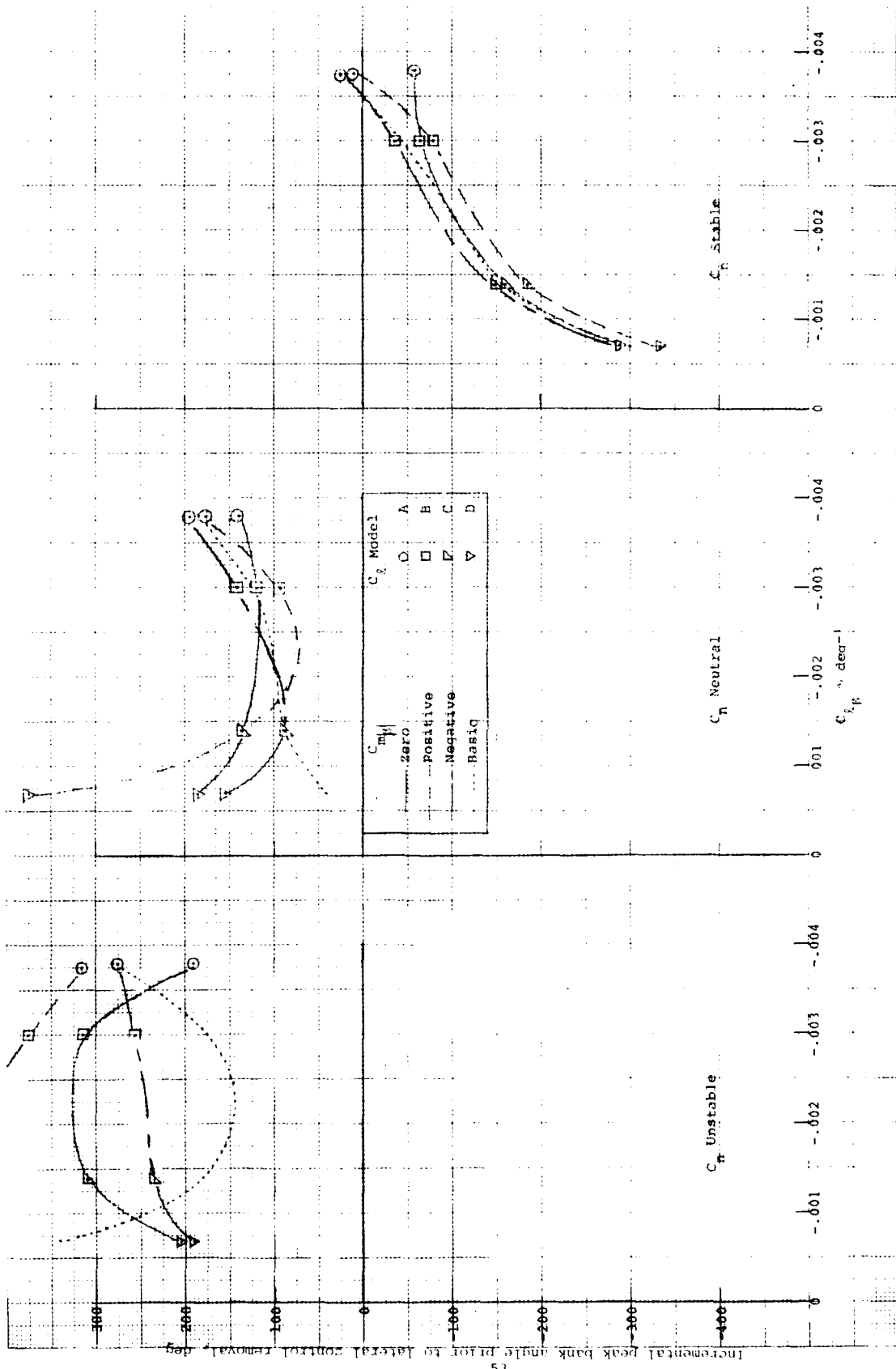
d) Incremental peak bank angle prior to lateral control removal as a function of the aerodynamic models

Figure 13. (Concluded)
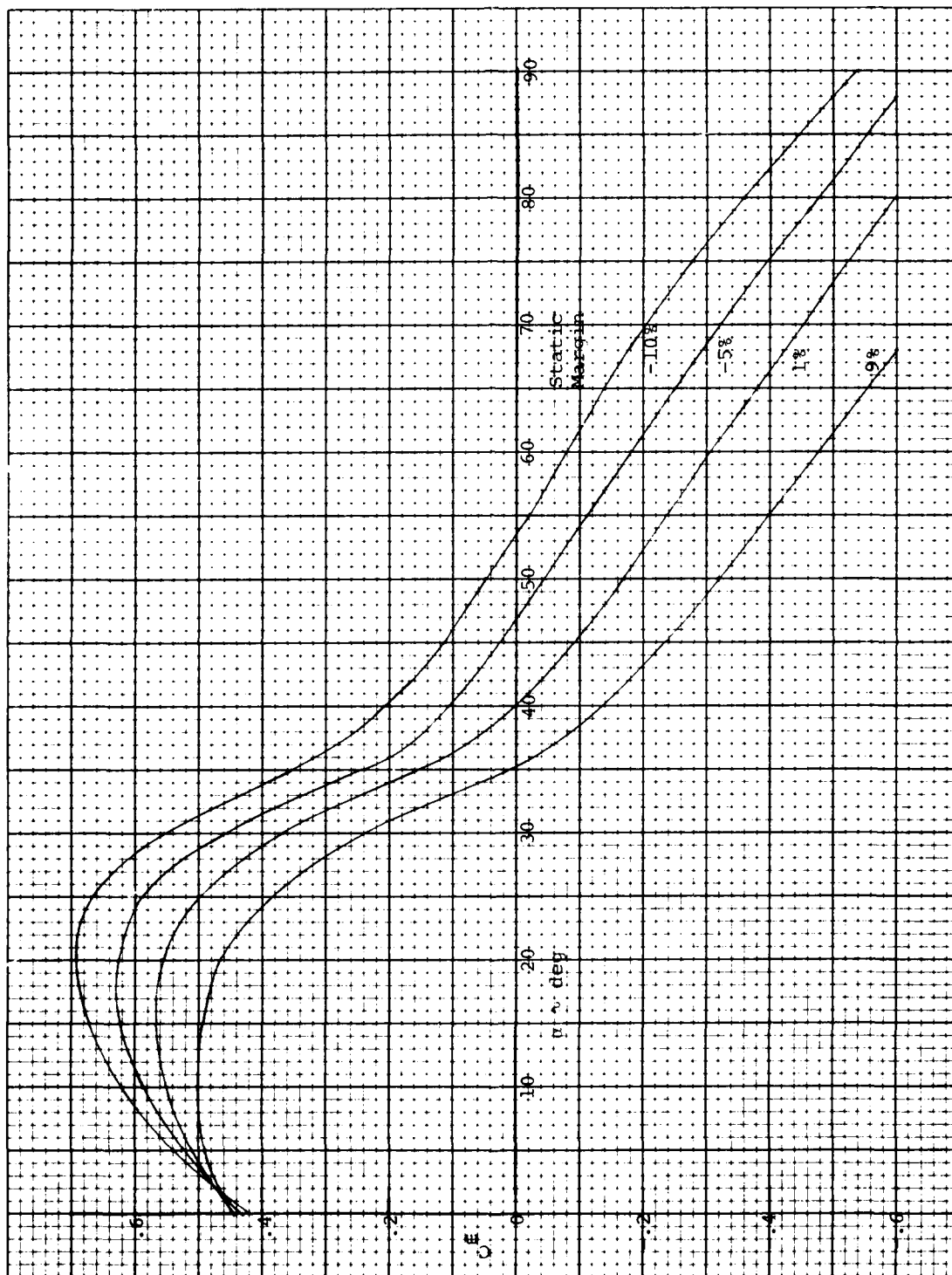
Figure 14. Pitching moment coefficients as a function of angle of attack for various static margins. $i_s = -30$ deg, $\beta = 0$ deg
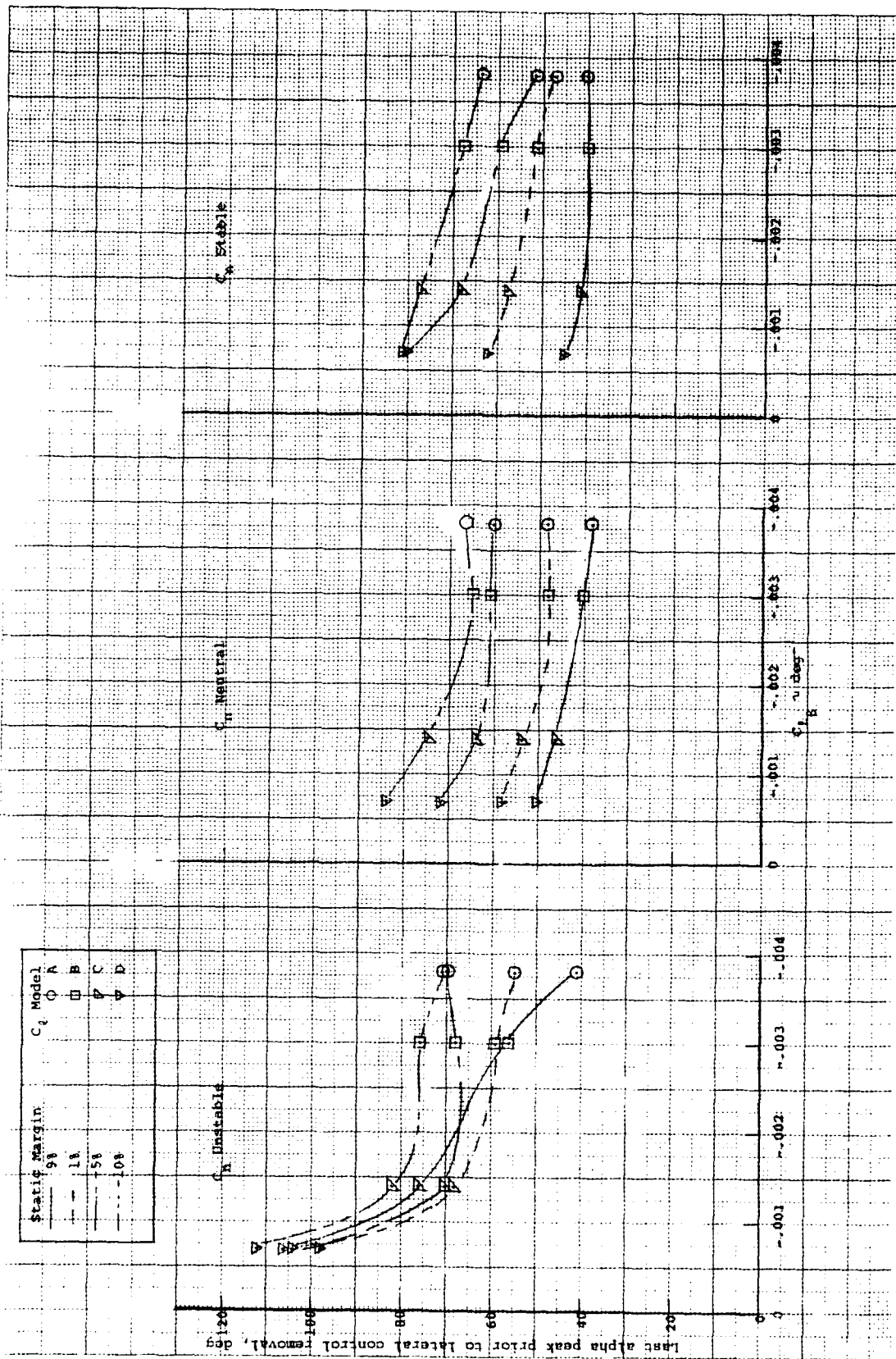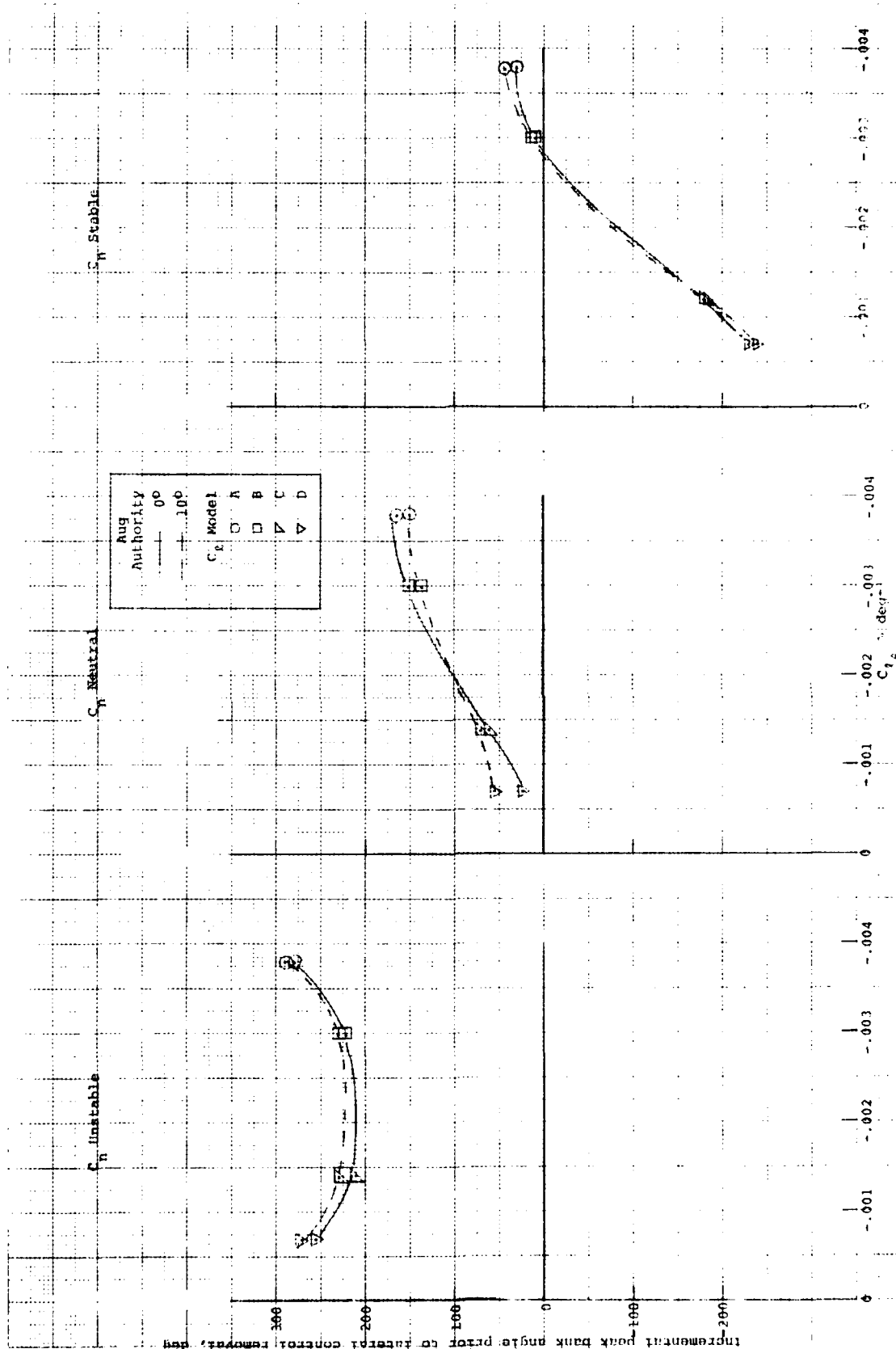
54

a) Last alpha peak prior to lateral control removal as a function of the aerodynamic models

Figure 15. Influence of static margin on design charts for determining departure and uncoordinated roll reversal susceptibility for an airplane having adverse $C_{n_{\delta_a}}$

55

b) Approximate second order damping ratio of alpha trace as a function of the aerodynamic models
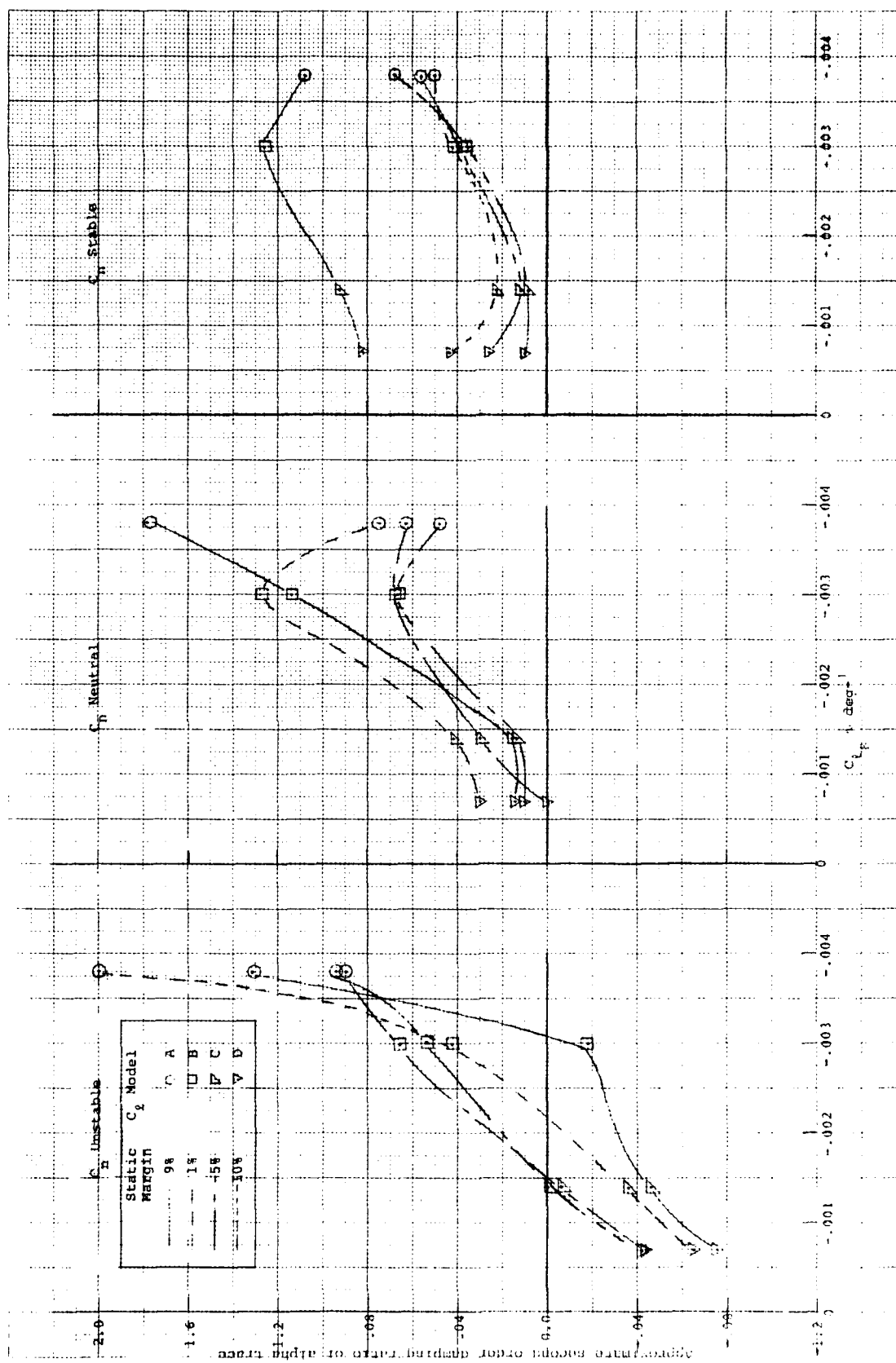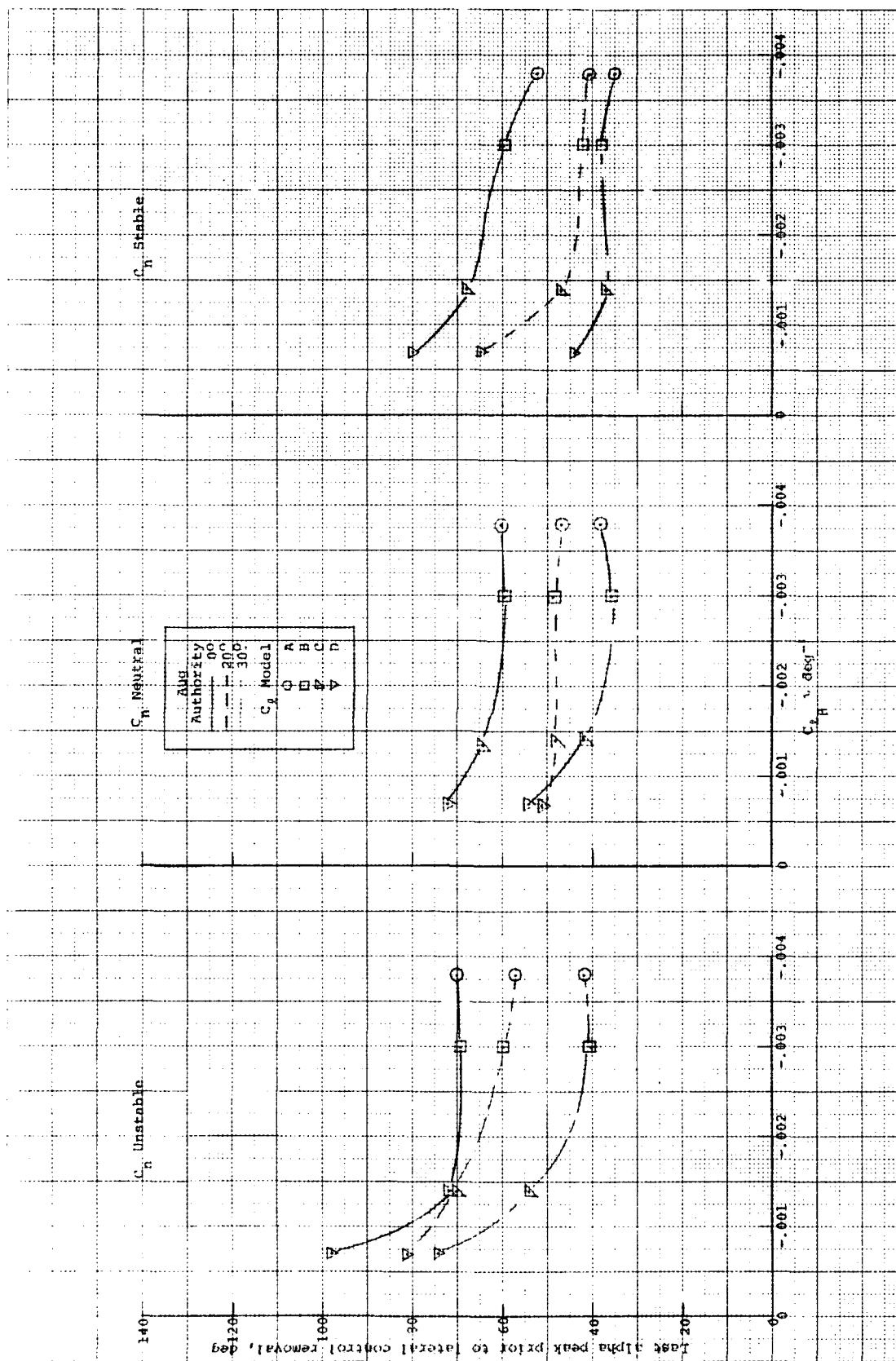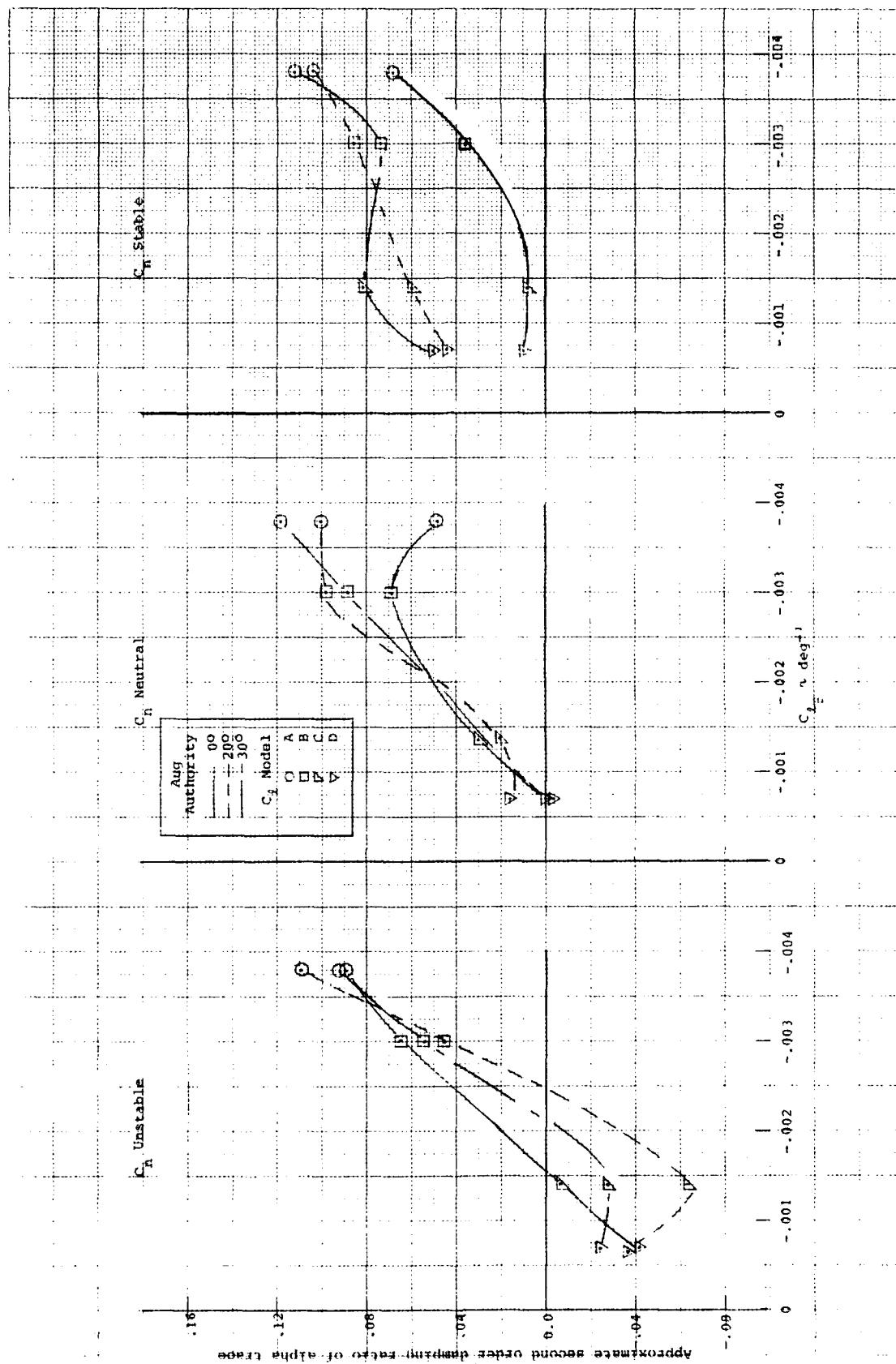
Figure 15. (Continued)
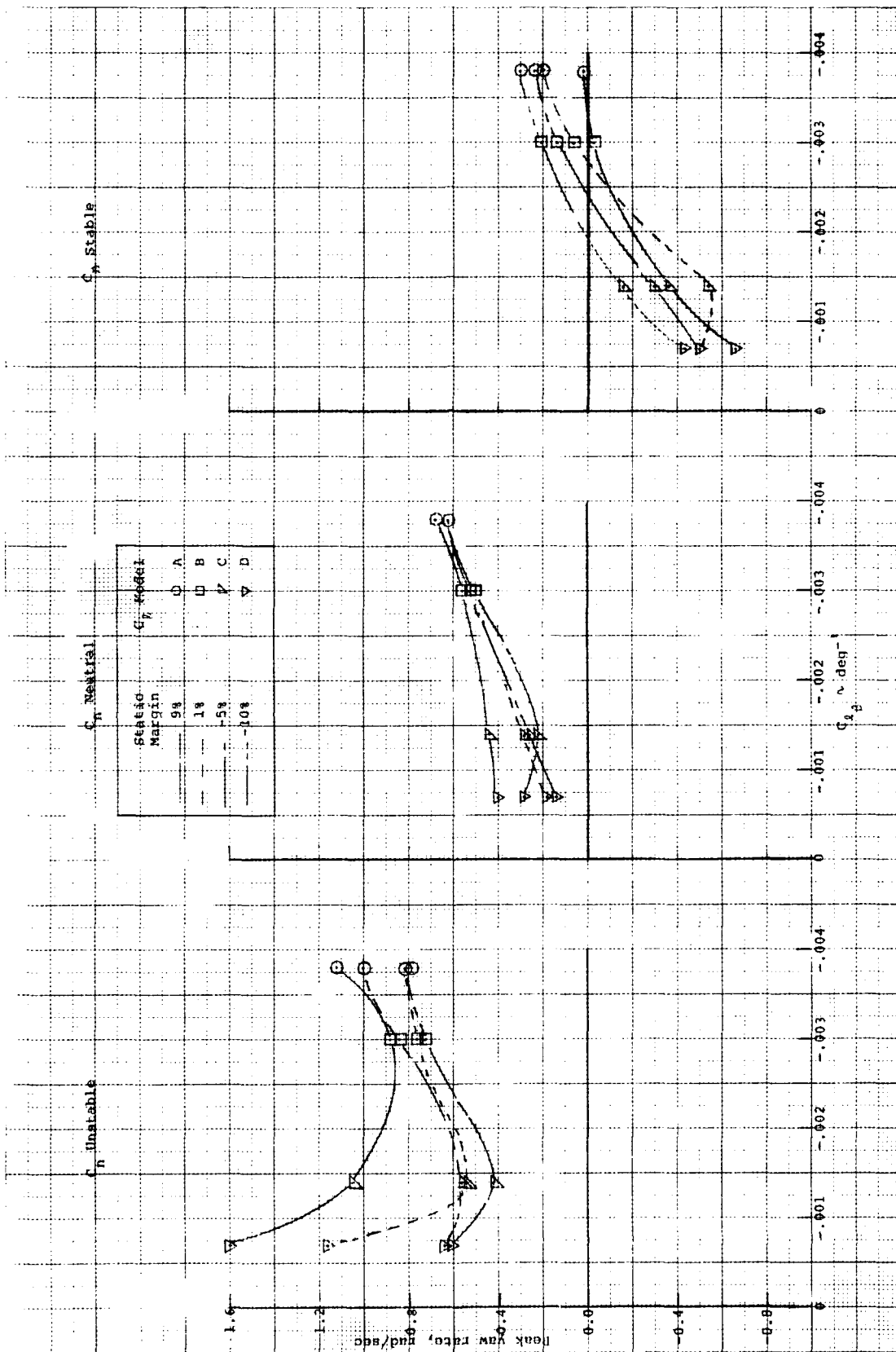
c) Peak yaw rate as a function of the aerodynamic models
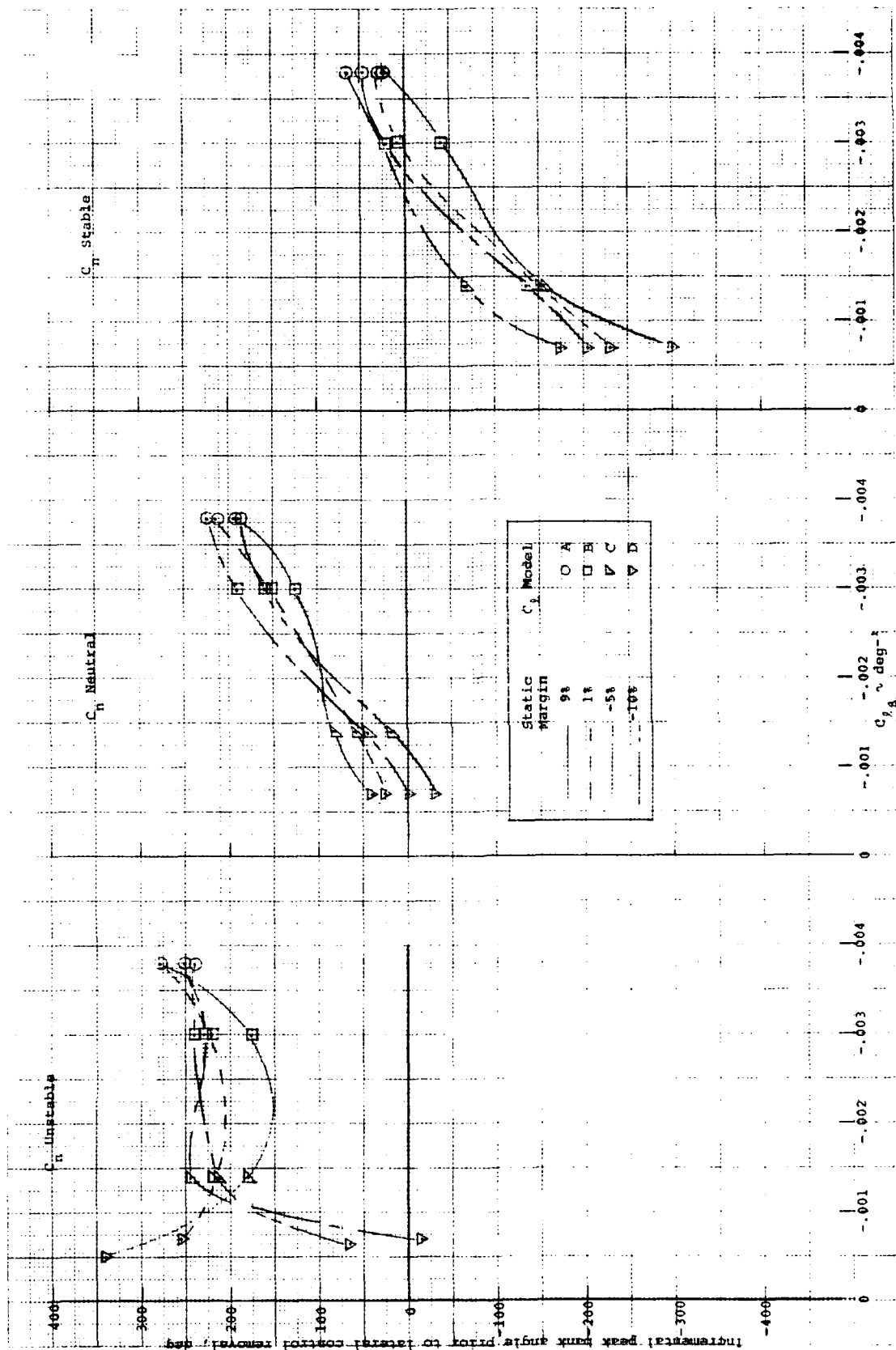
Figure 15. (Continued)

d) Incremental peak bank angle prior to lateral control removal as a function of the aerodynamic models

Figure 15. (Concluded)

58
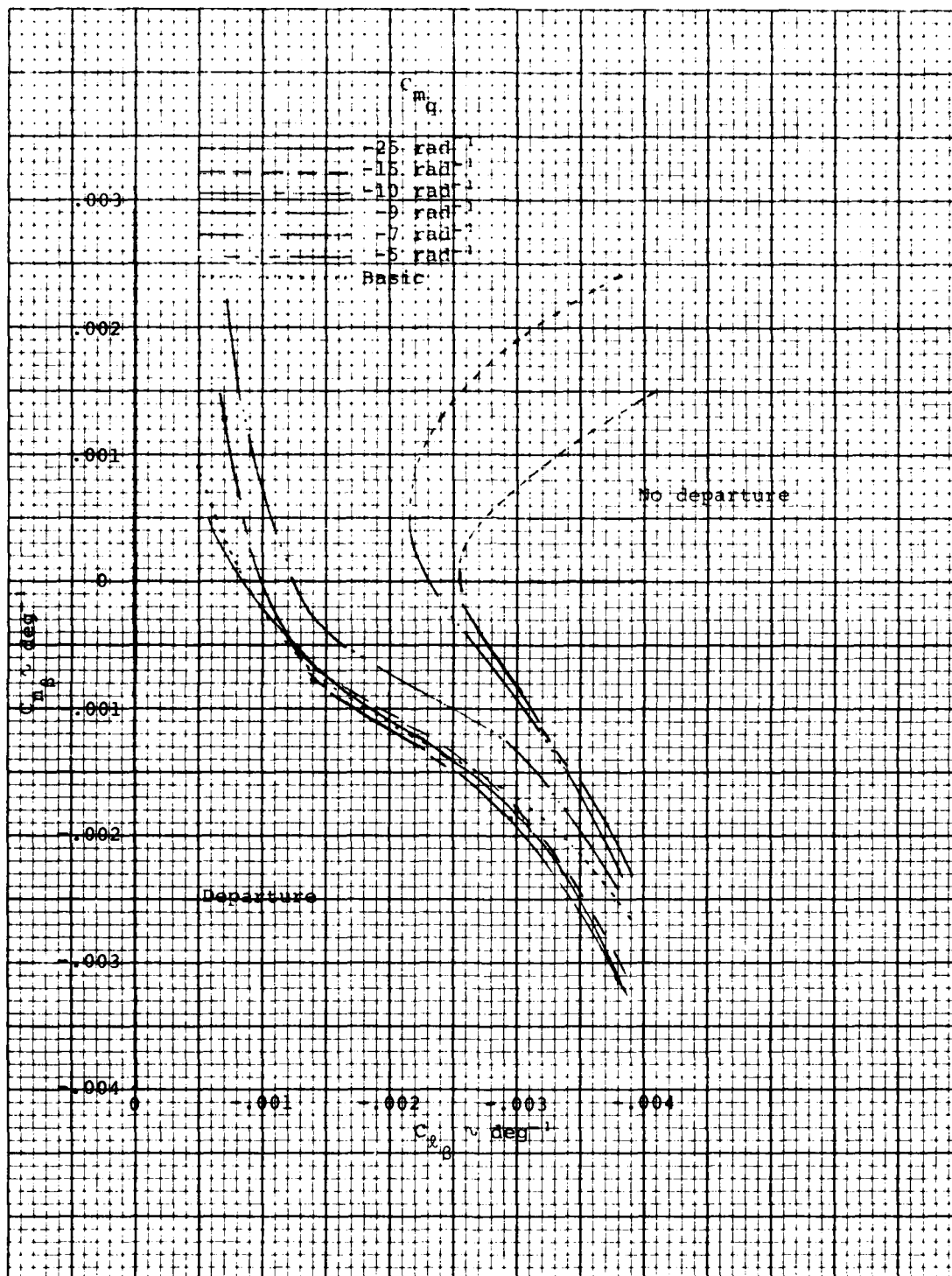
Figure 16. Influence of C_{m_α} on departure boundaries for a
9% static margin airplane having adverse $C_{n_{\delta_a}}$

59
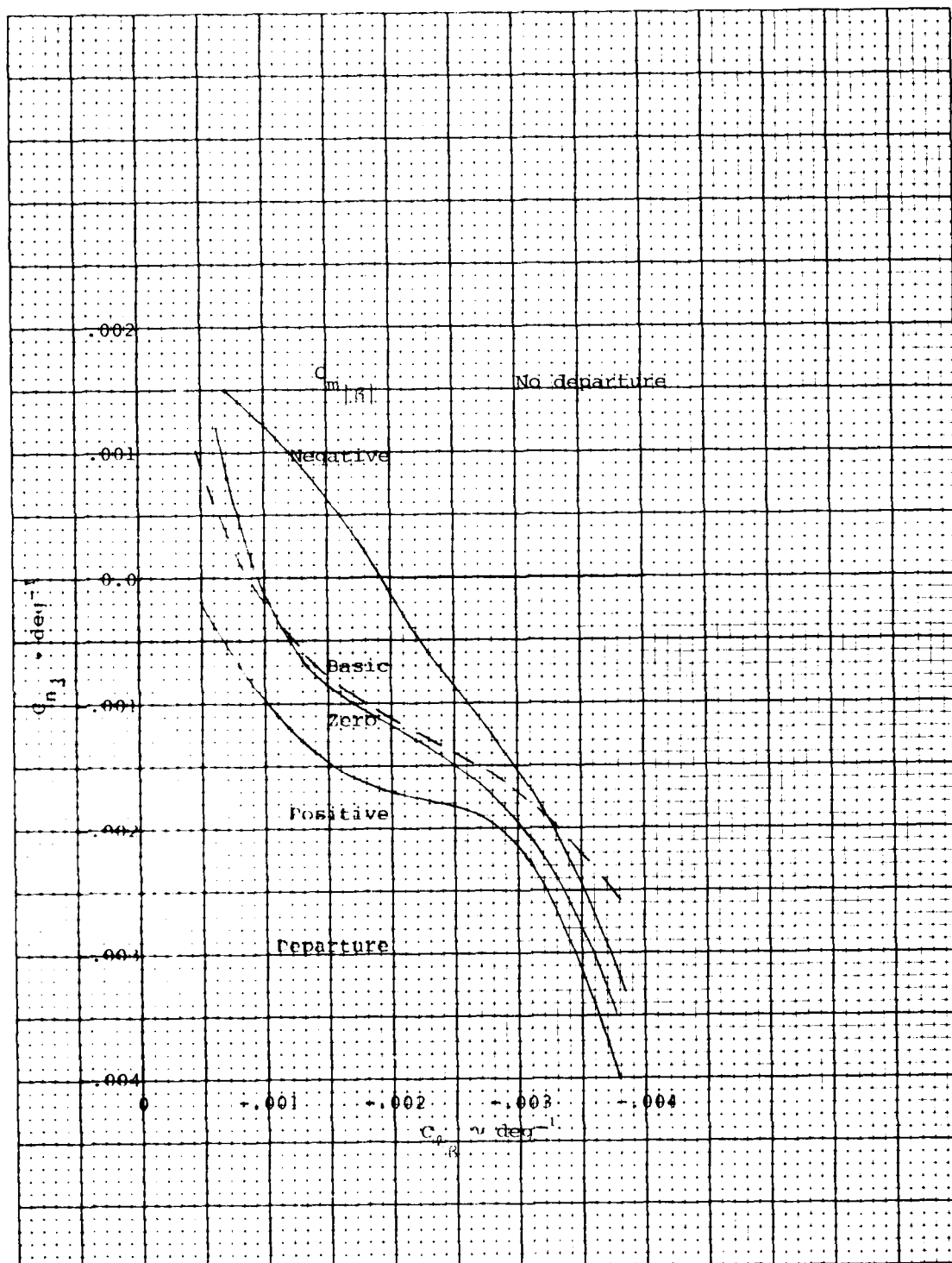
Figure 17. Influence of $C_{m_{|\beta|}}$ on departure boundaries
for a 9° static margin airplane having adverse $C_{n_{\delta_a}}$
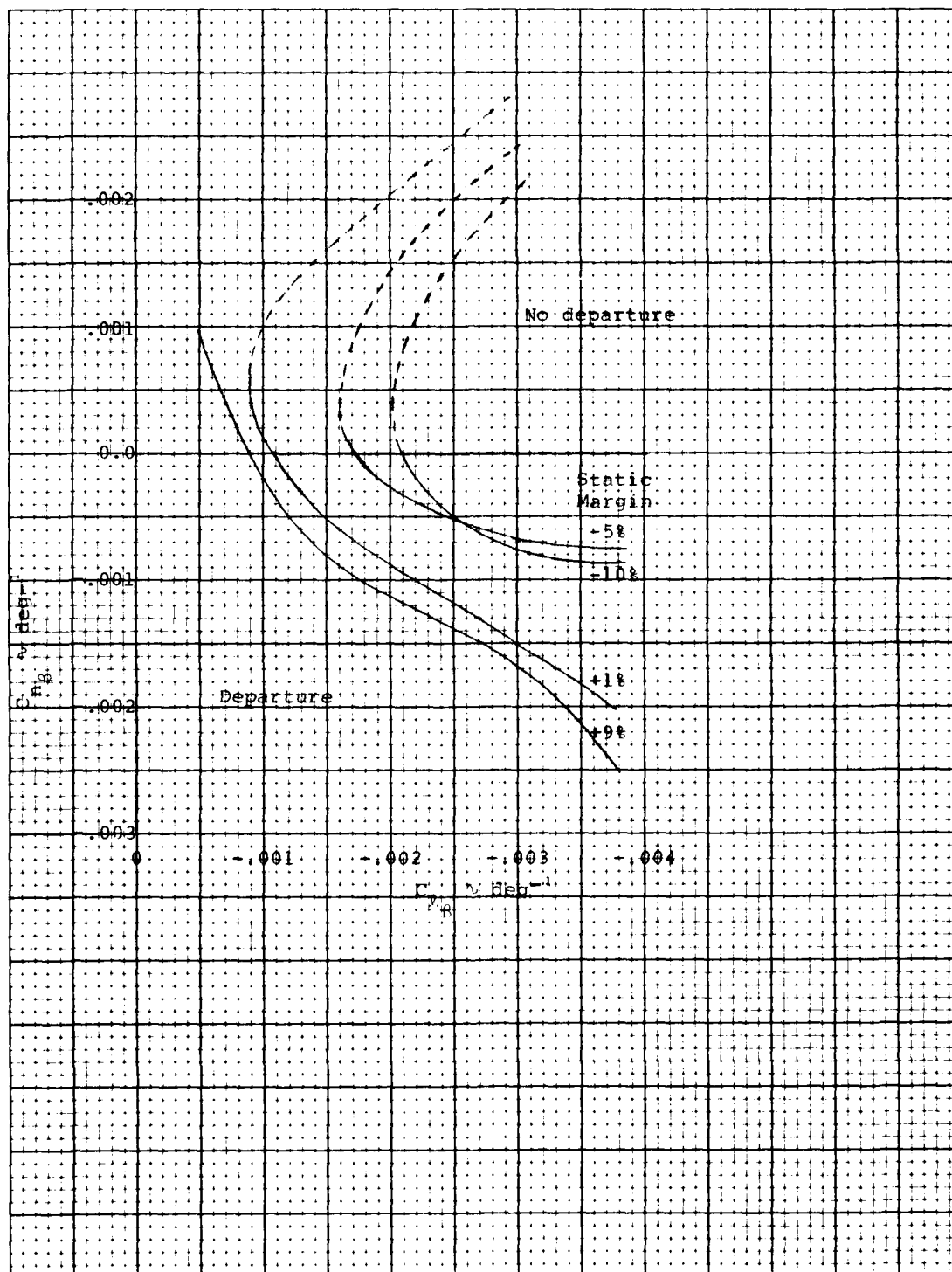
Figure 18. Influence of static margin on departure boundaries for unaugmented airplane having adverse $C_{n_{\delta_a}}$
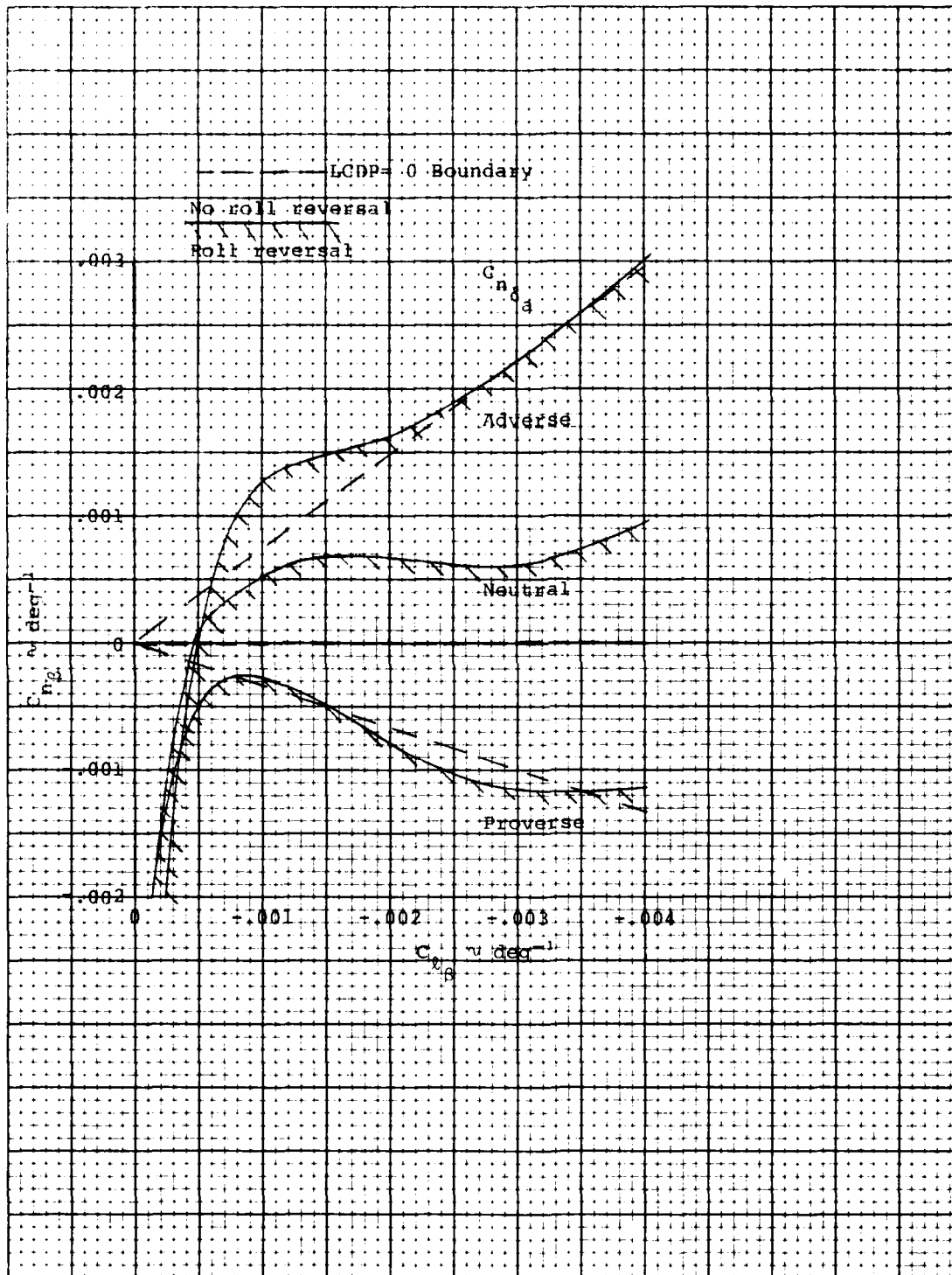
Figure 19. Comparison of uncoordinated roll reversal boundaries
(Reference 1) and lateral control departure boundaries
(Reference 4) for different levels of $C_{n_{\delta_a}}$
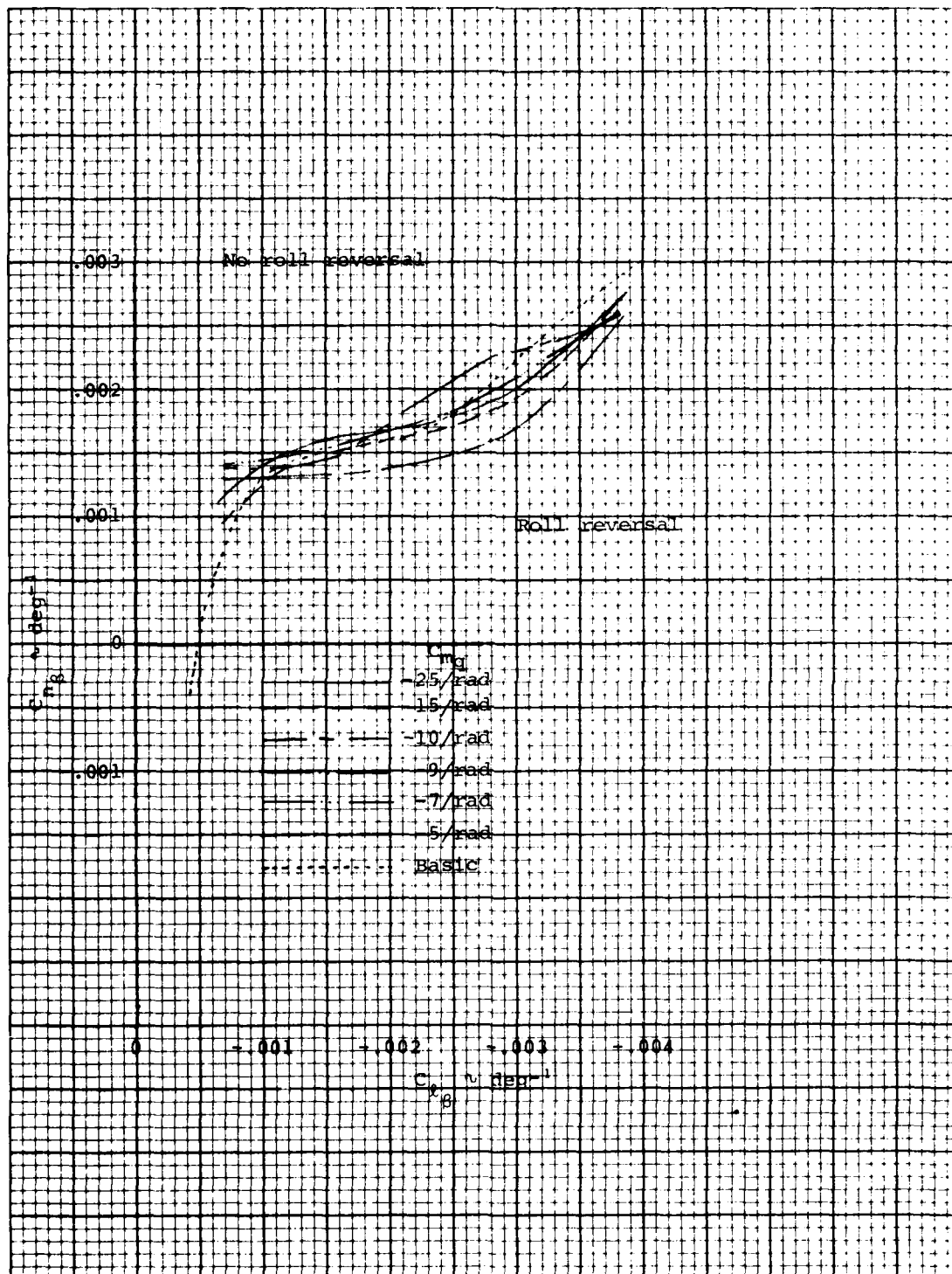
Figure 20. Influence of C_{m_q} on uncoordinated roll reversal boundaries for a 9% static margin airplane having adverse $C_{n_{\delta_a}}$

63
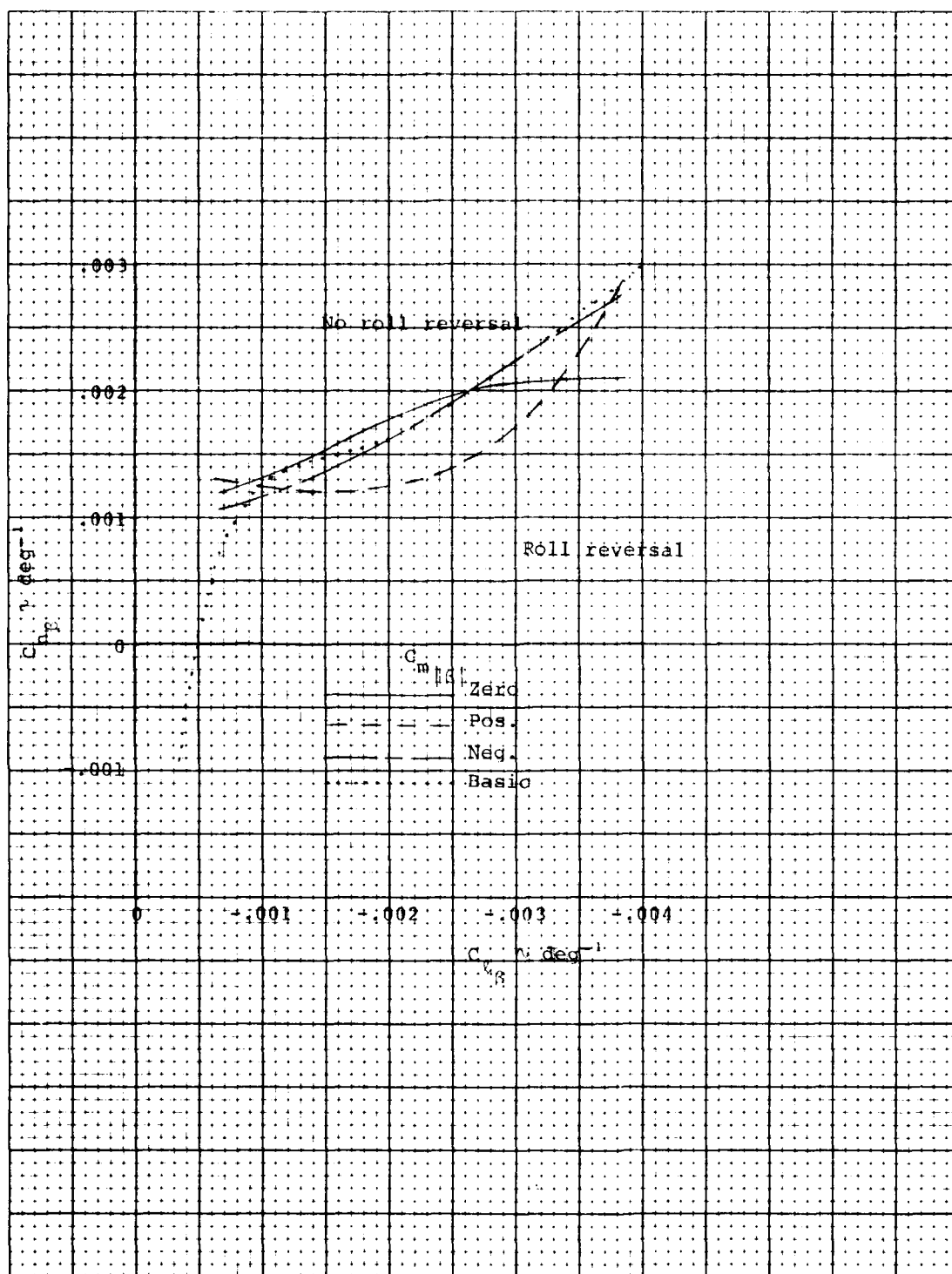
Figure 21. Influence of $C_{m_{|\rho|}}$ on uncoordinated roll reversal boundaries for a 9% static margin airplane having adverse $C_{n_{\delta_a}}$

64
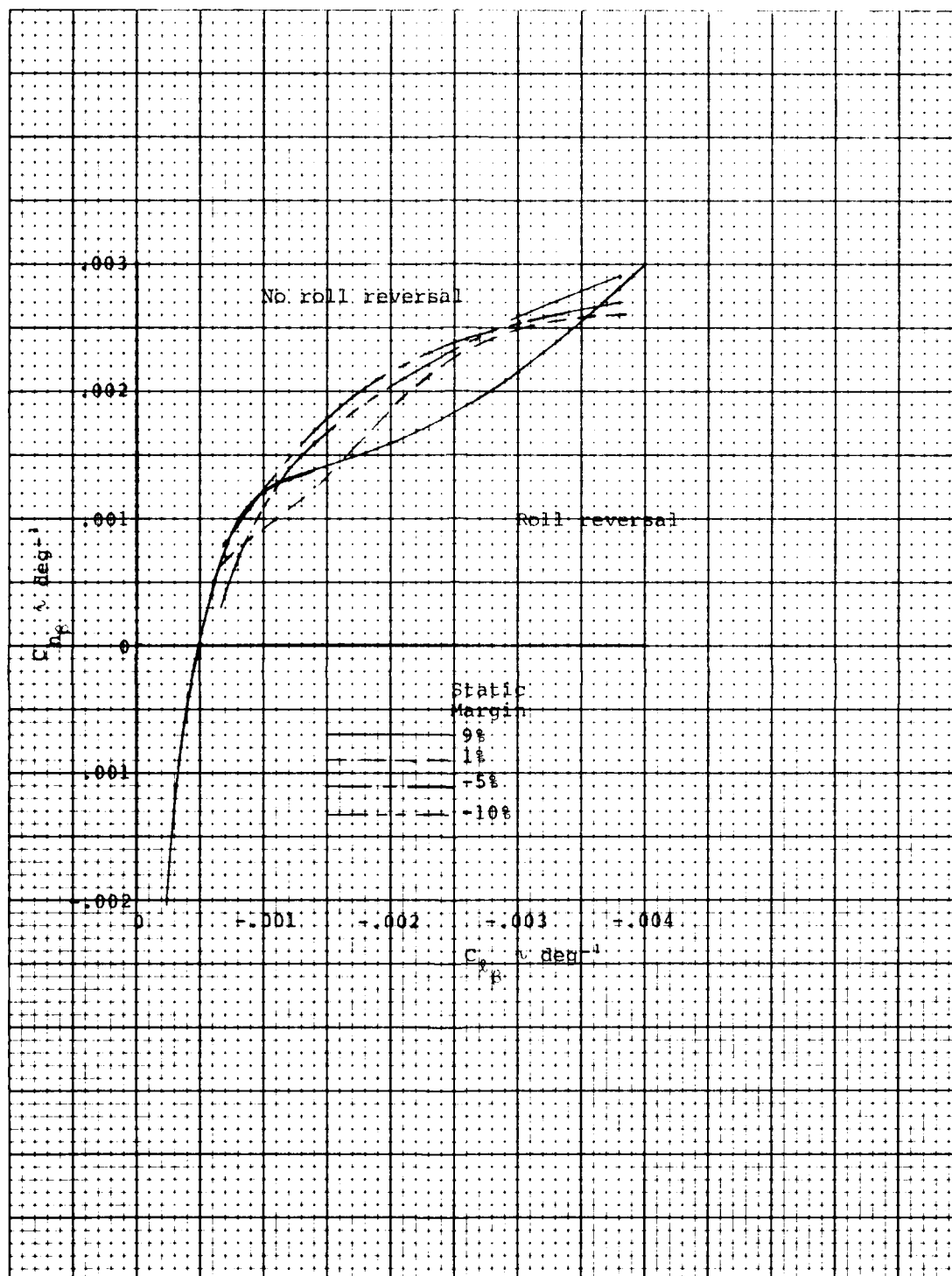
Figure 22. Influence of static margin on uncoordinated roll reversal boundaries for an airplane having adverse $C_{n_{\delta_a}}$

65
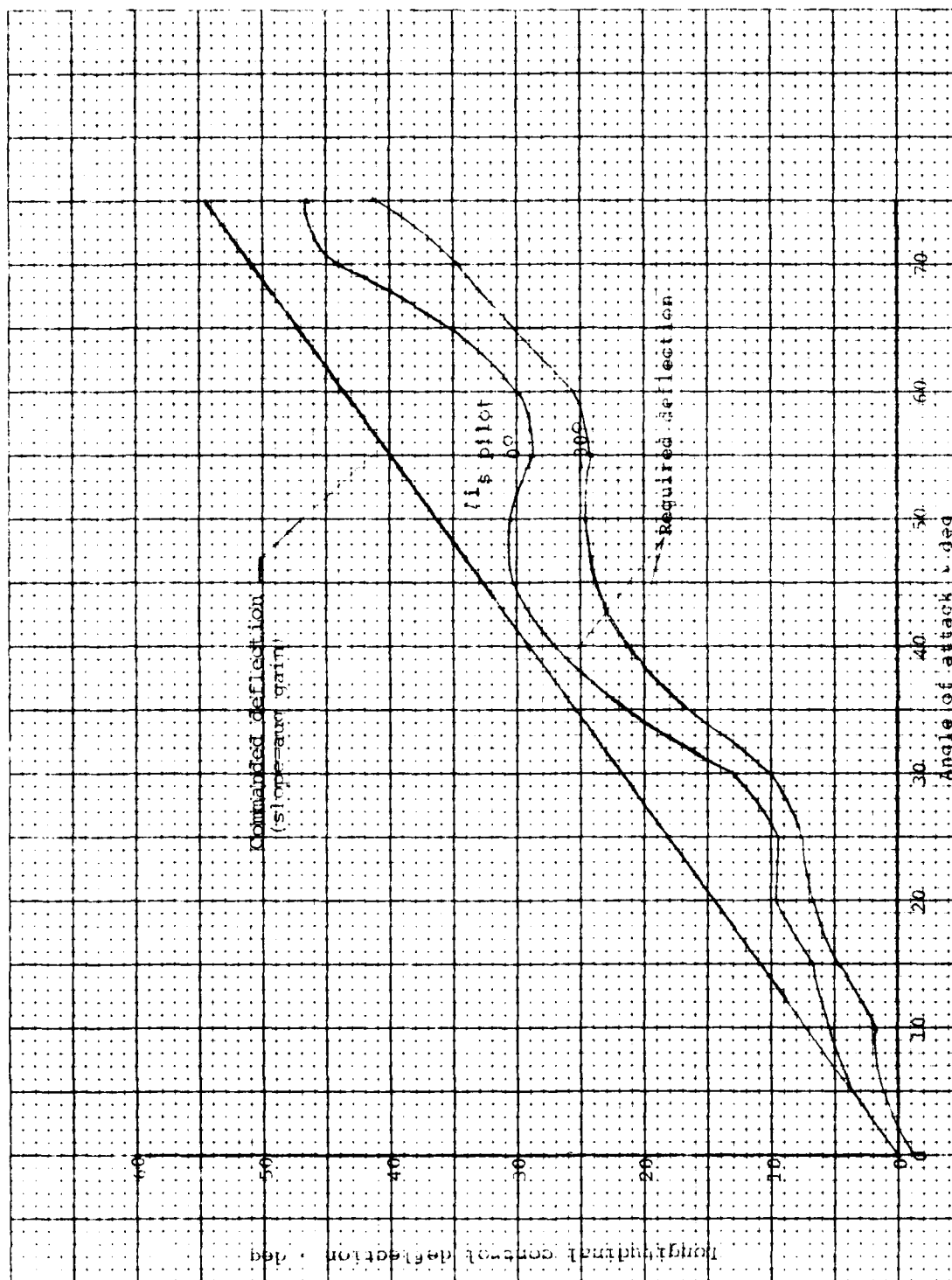
Figure 23. Longitudinal control deflection commanded by augmentation system compared with the deflection required to statically match the $9°$ static margin airplane pitching moment curve for pilot control input of 0 and -30 degrees
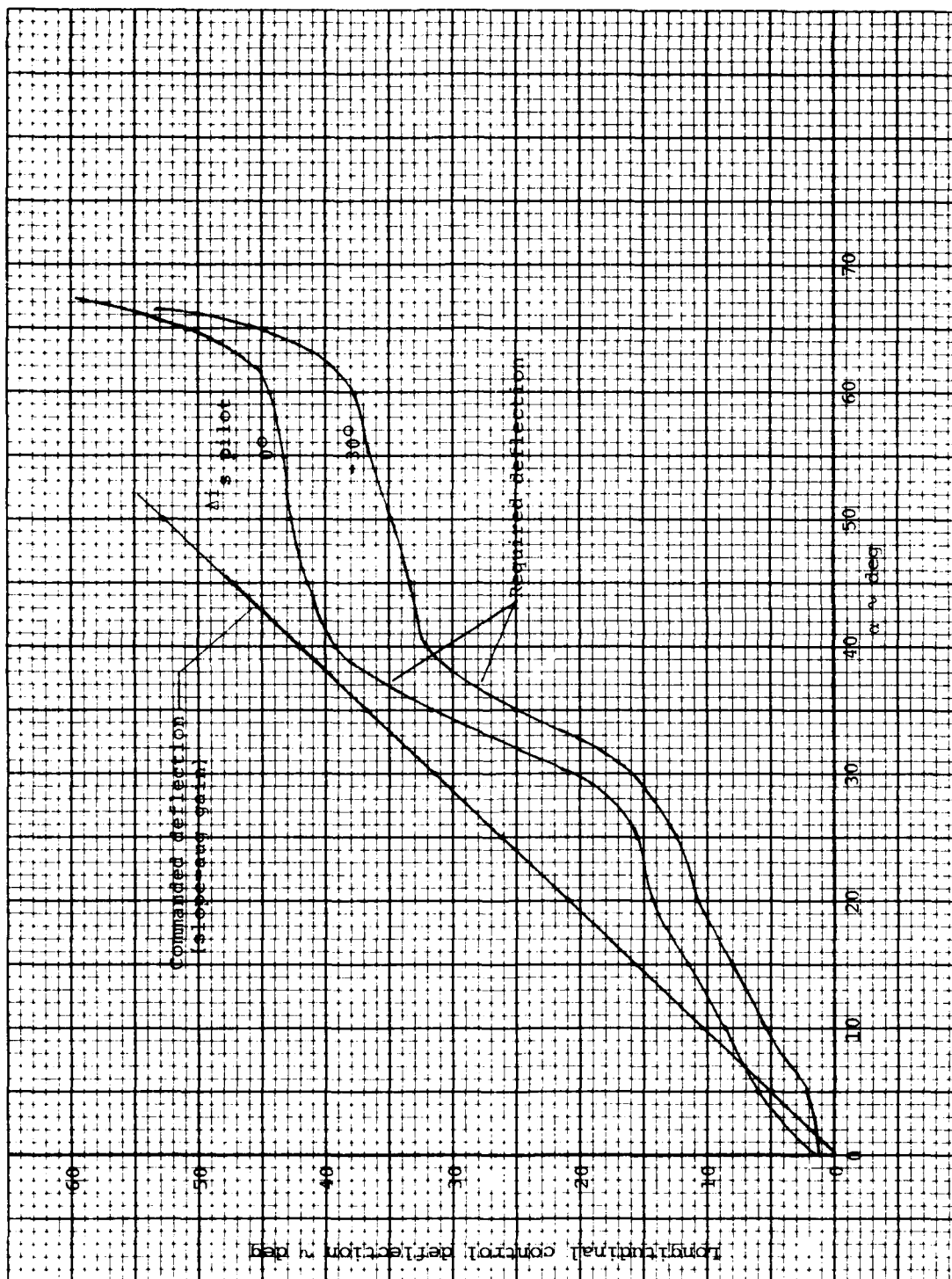
a) $1°$ static margin

b) -5% static margin

Figure 23. (Continued)

67
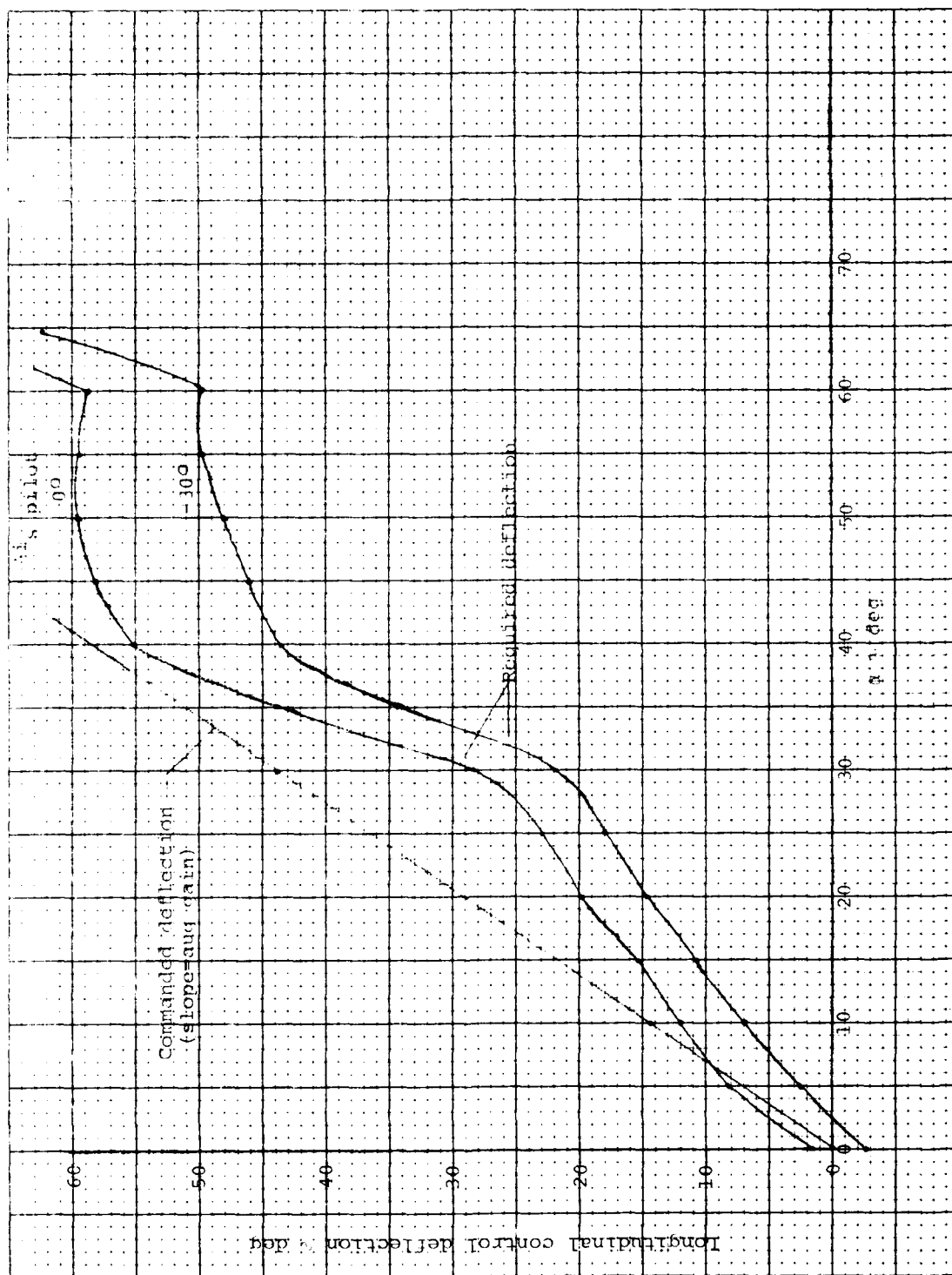
c) -10% static margin

Figure 23. (Concluded)
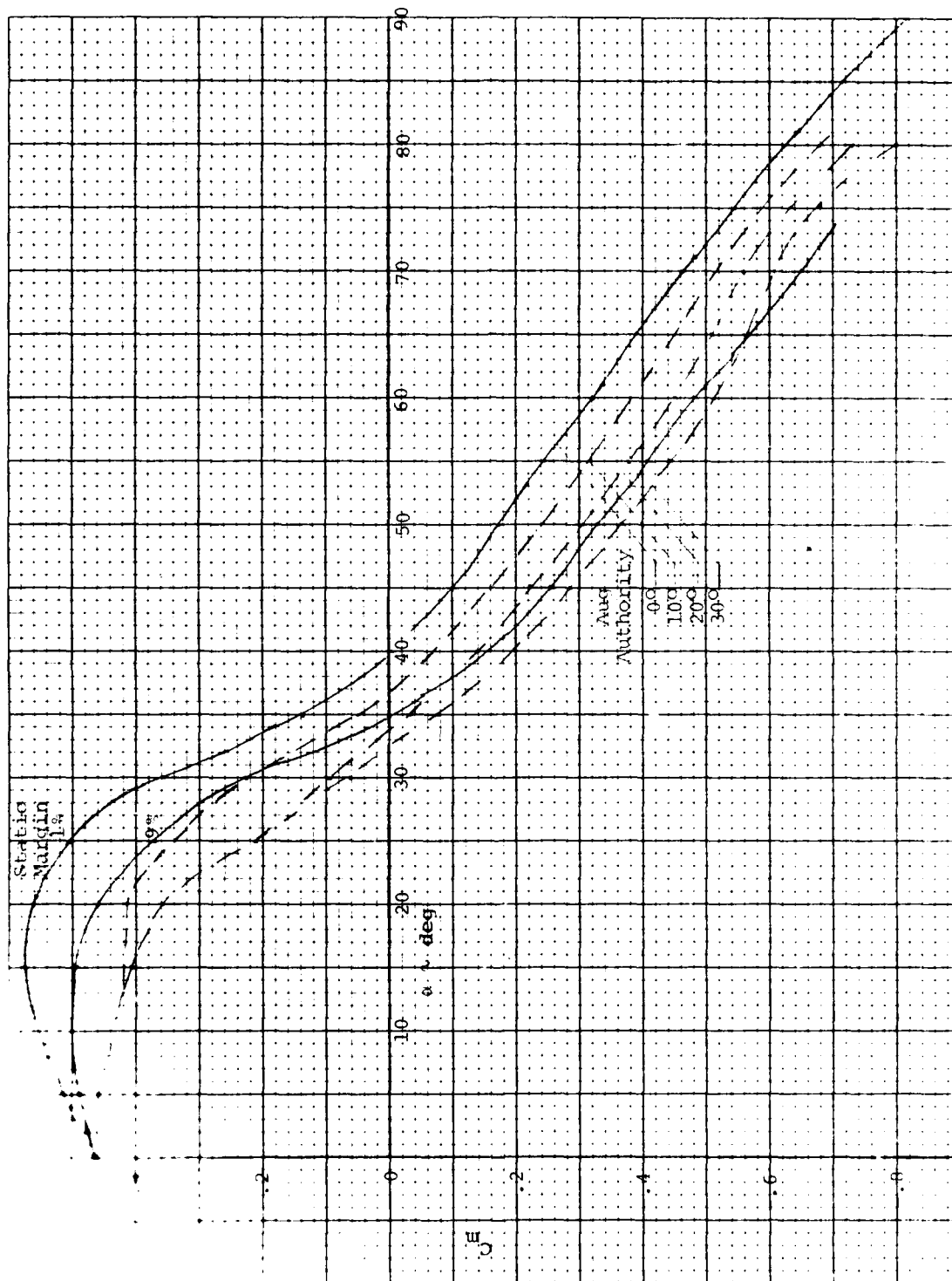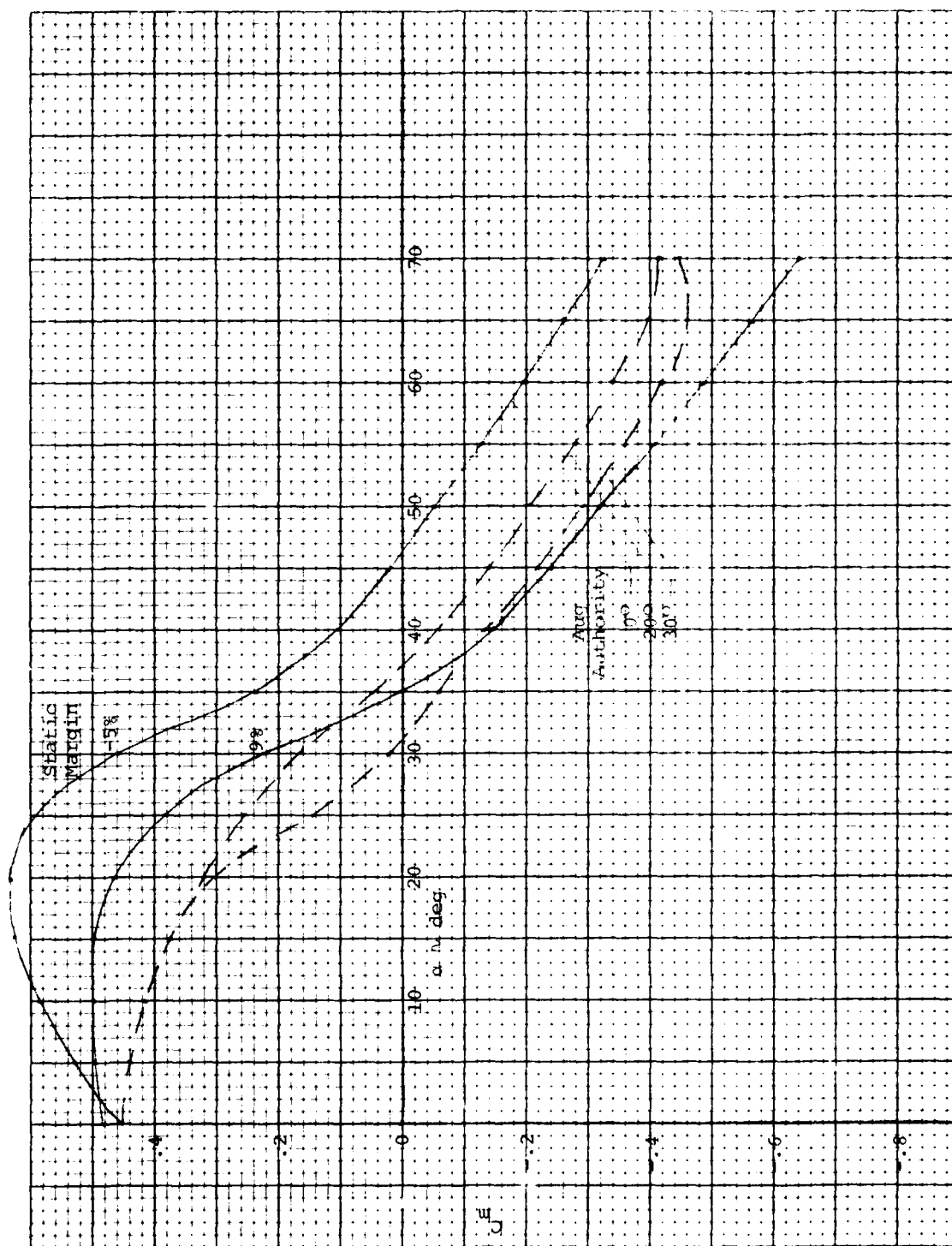
b) -5% static margin

Figure 24. (Continued)
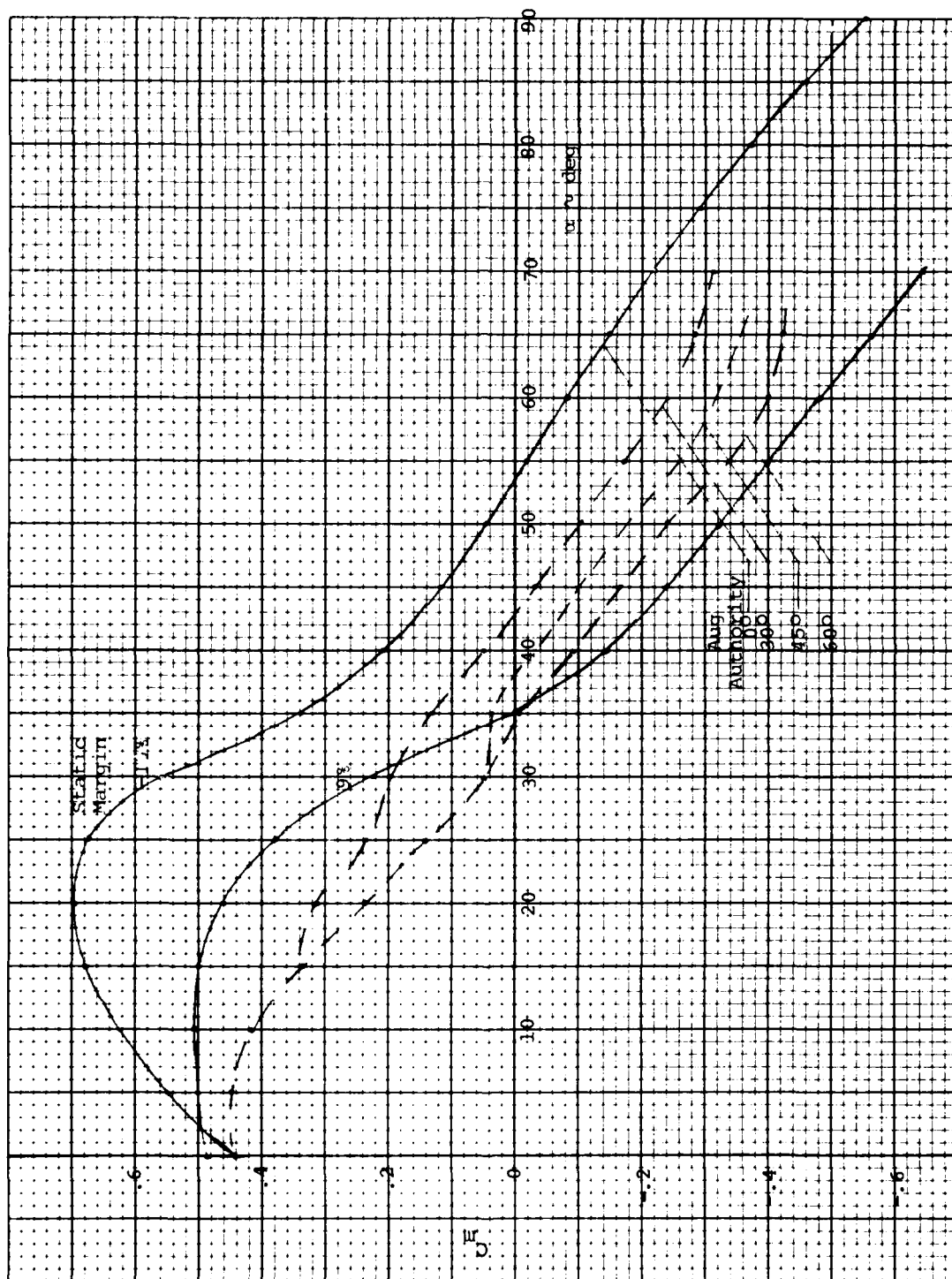
c) -10% static margin

Figure 24. (Concluded)
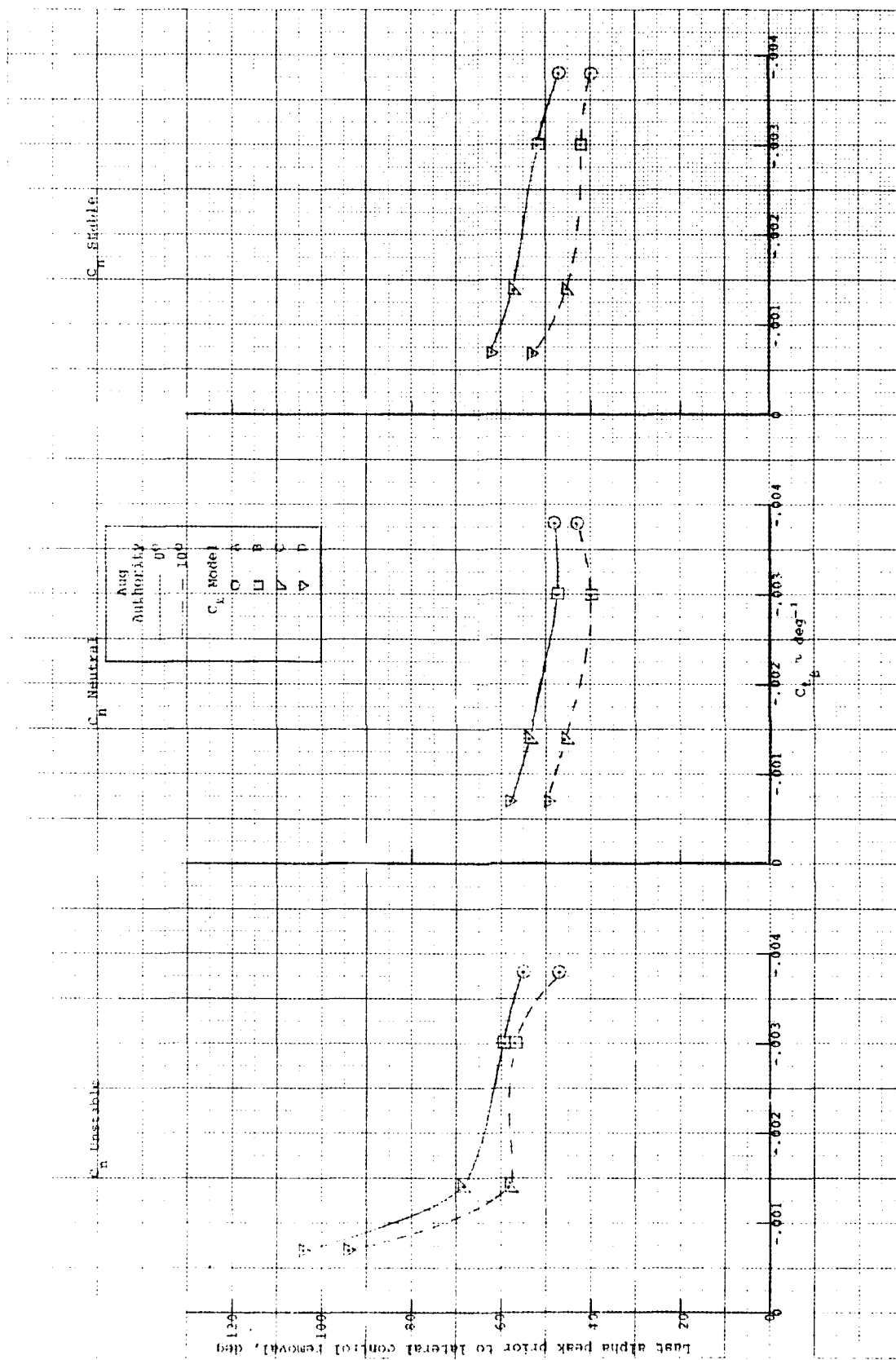
a) Last alpha peak prior to lateral control removal as a function of the aerodynamic models

Figure 25. Effect of control authority on design charts for determining departure and uncoordinated roll reversal susceptibility for a 12 static margin airplane having adverse C_n

Approximate second order damping ratio of alpha trace

c) Peak yaw rate as a function of the aerodynamic models

Figure 25. (Continued)

74

d) Incremental peak bank angle prior to lateral control removal as a function of the minor.

Figure 25. (Concluded)

a) Last alpha peak prior to lateral control removal as a function of the aerodynamic models

Figure 26. Effect of control authority on design charts for determining departure and uncoordinated roll reversal susceptibility for a -5° static margin airplane having adverse $C_{n_{\delta_a}}$

b) Approximate second order damping ratio of alpha trace as a function of the aerodynamic models

Figure 26. (Continued)

77

c) Peak yaw rate as a function of the aerodynamic models

Figure 26. (Continued)

78
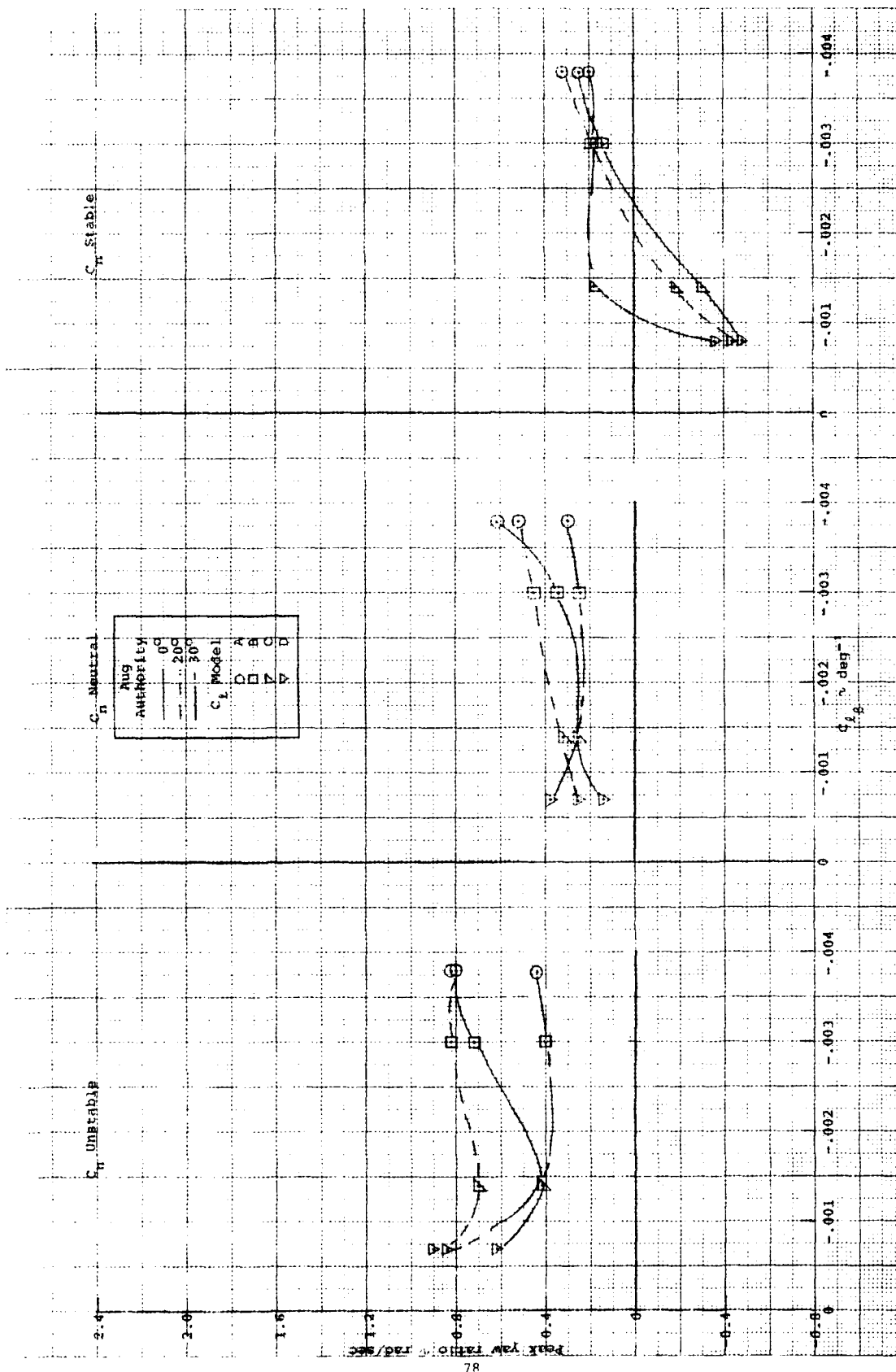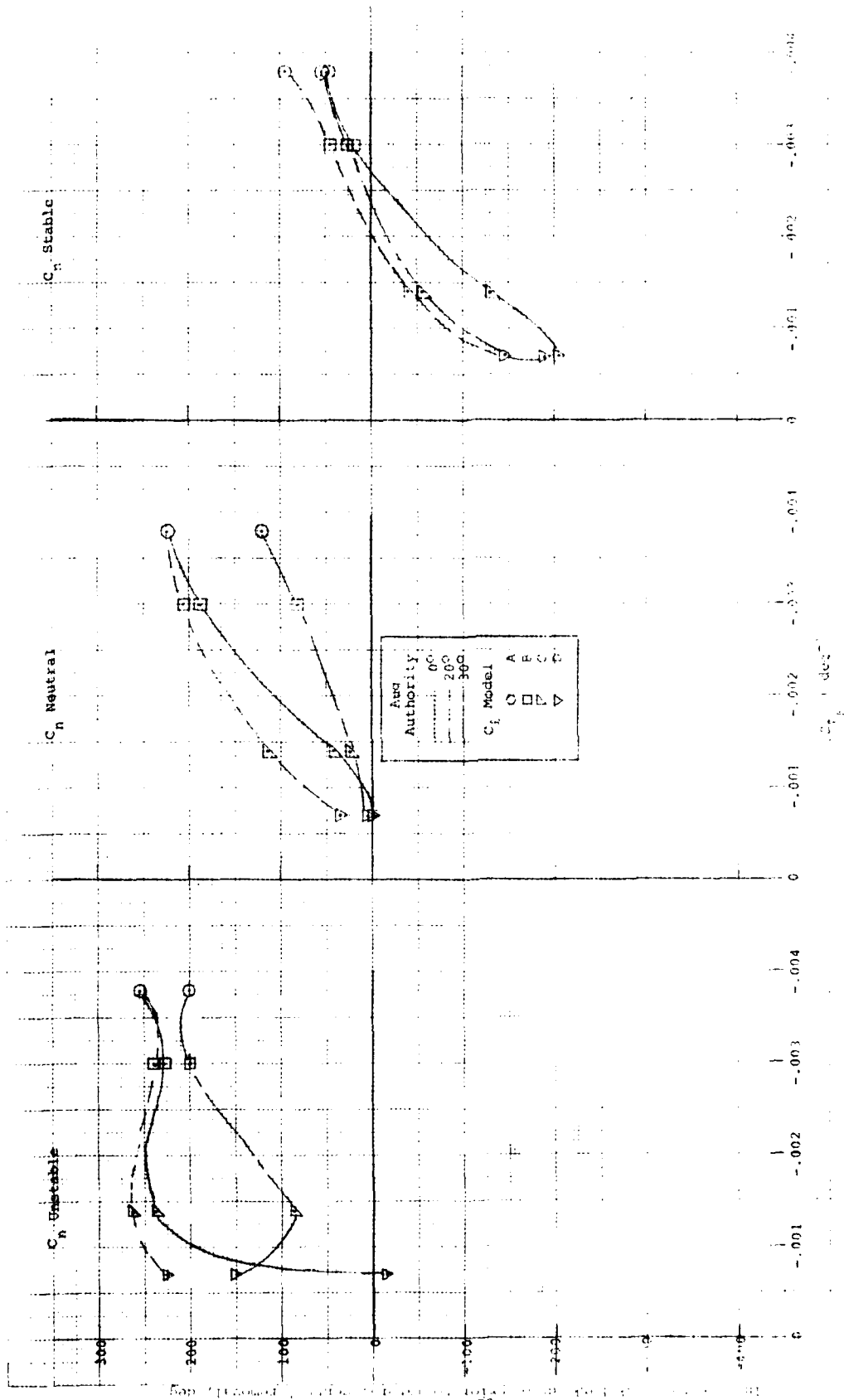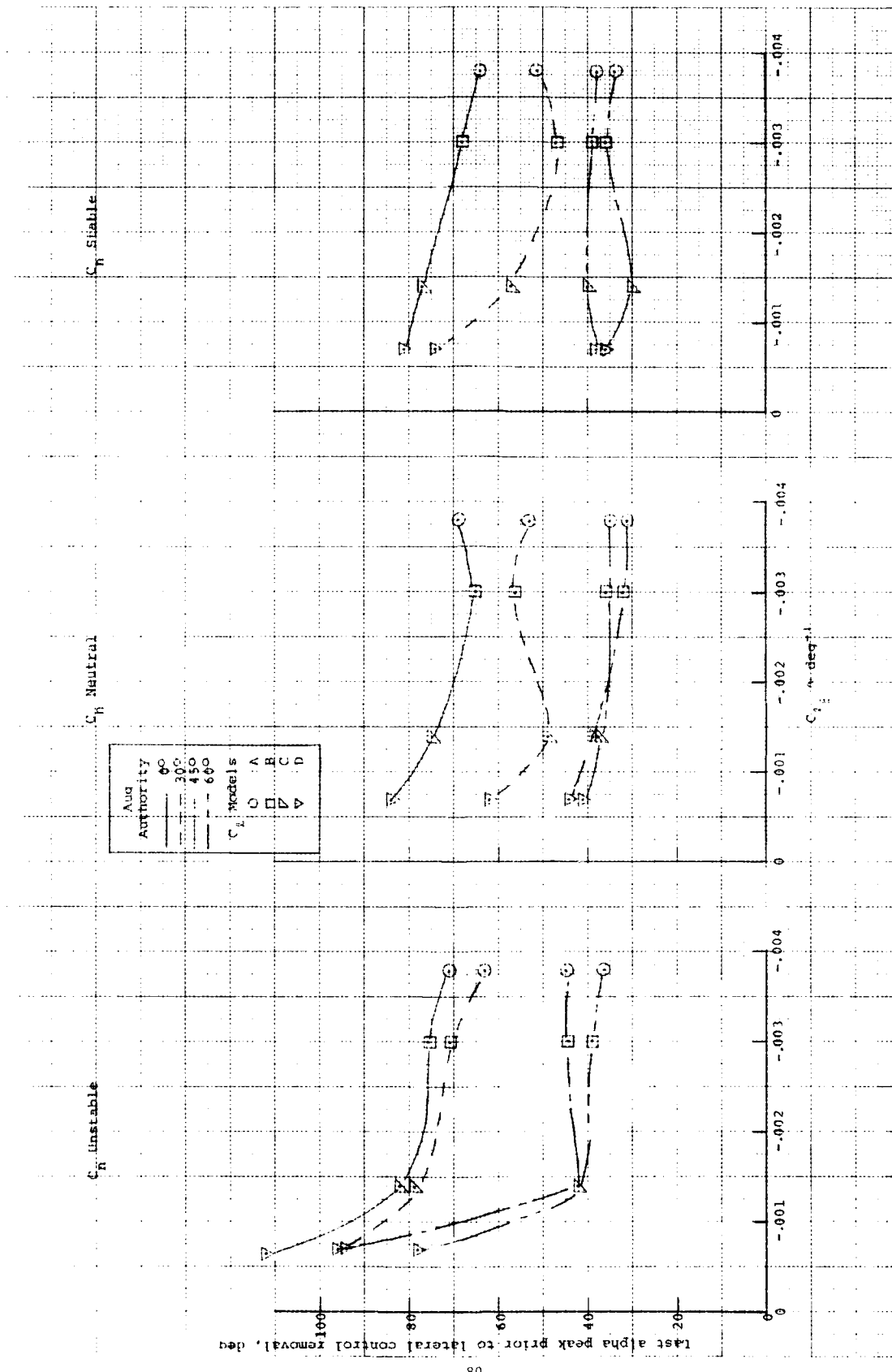
a) Last alpha peak prior to lateral control removal as a function of the aerodynamic models

Figure 27. Effect of control authority on design charts for determining departure and uncoordinated roll reversal susceptibility for a -10% static margin airplane having adverse C_{n_β}

b) Approximate second order damping ratio of alpha trace as a function of the second derivative of yawing moment coefficient. (Continued)

Figure of the graph axes and legend:

Vertical axis: Approximate second order damping ratio of alpha trace (.16, .12, .08, .04, 0, -.04, -.08)

Horizontal axes: C_{n_β}, deg^{-1}

Three panels labeled: C_n Unstable, C_n Neutral, C_n Stable

Legend:
Aug Authority
0°
30°
45°
60°

C_ℓ Models:
A ○
B □
C △
D ▽

Figure 22. Rear yaw rate as a function of the aerodynamic damping. (Continued)

d) Incremental peak bank angle prior to lateral control removal as a function of the aerodynamic models

Figure 27. (Concluded)

83
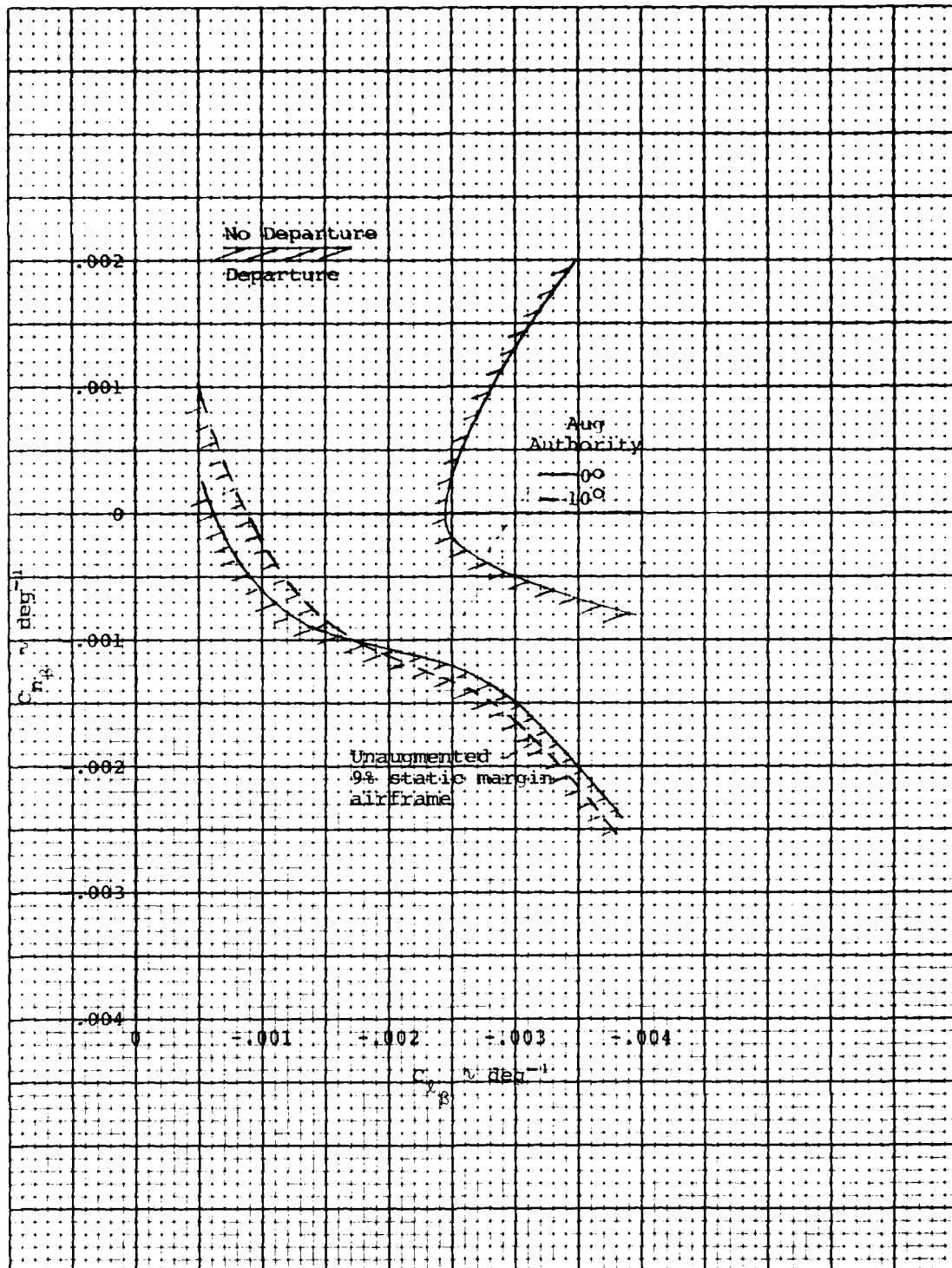
Figure 28.   Influence of augmentation authority on departure
boundaries for a 1% static margin airplane having adverse
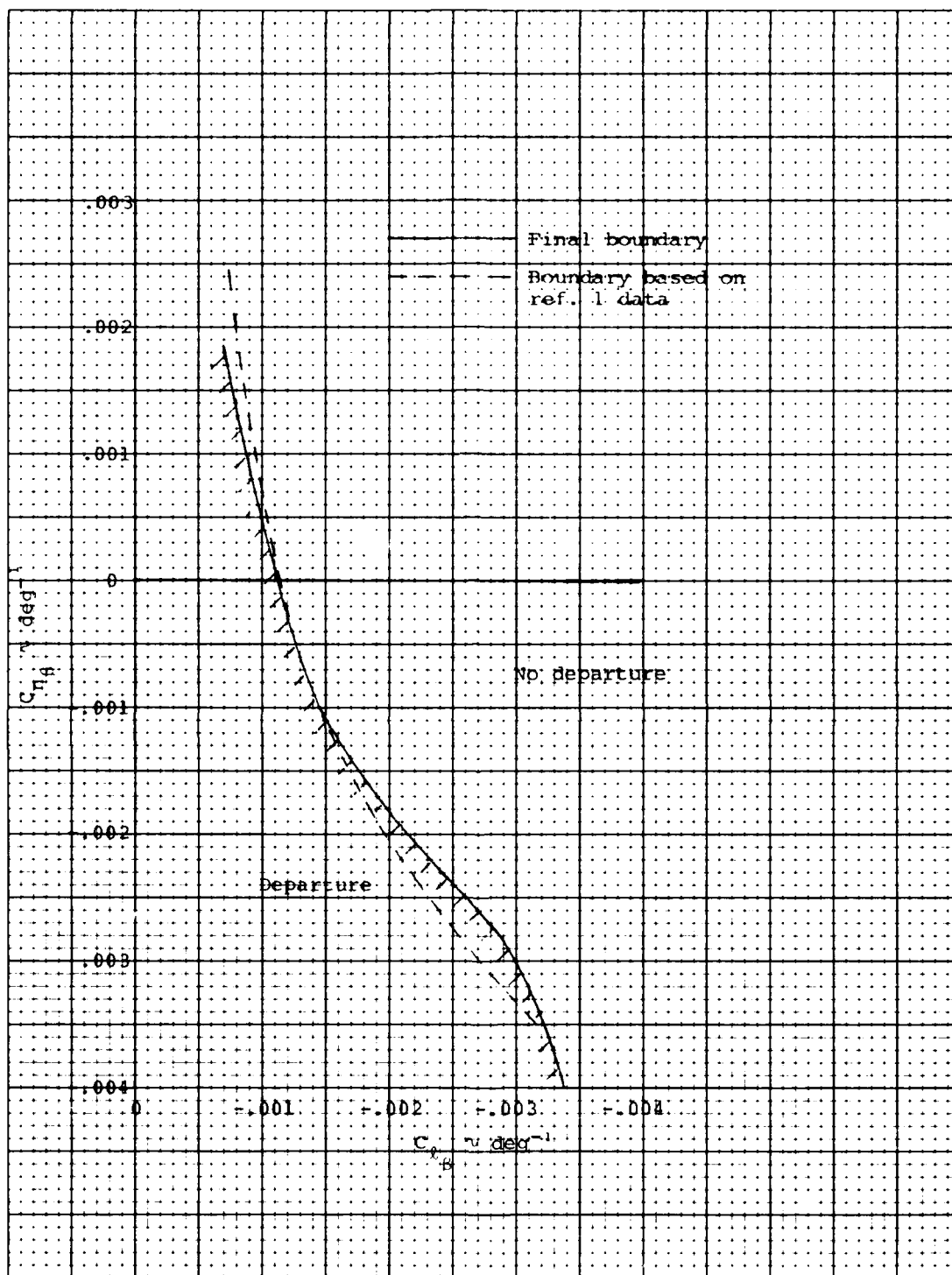$C_{n_{\delta_a}}$

84
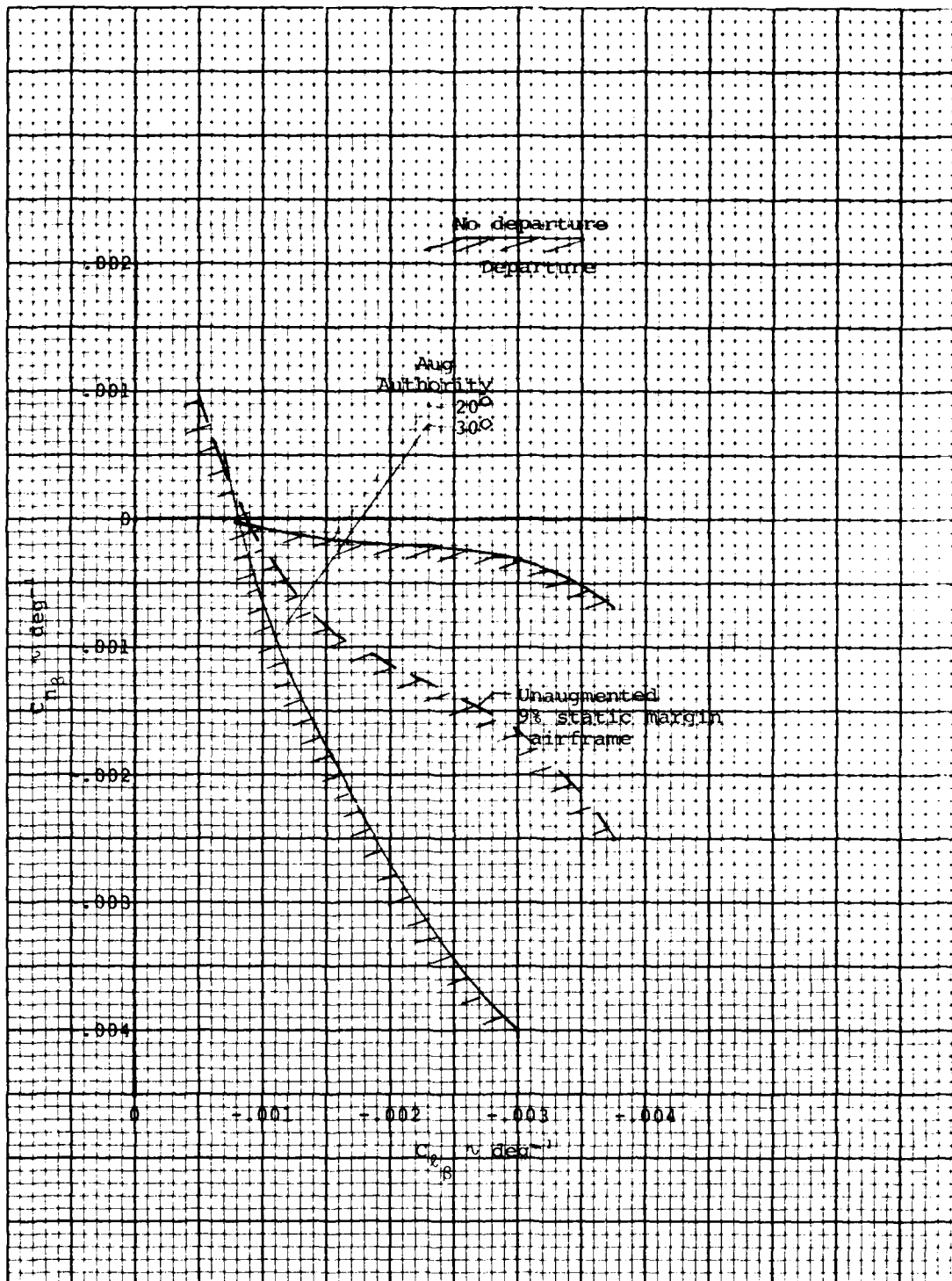
Figure 29. Influence of augmentation authority on departure boundaries for a -5% static margin airplane having adverse $C_{n_{\delta a}}$
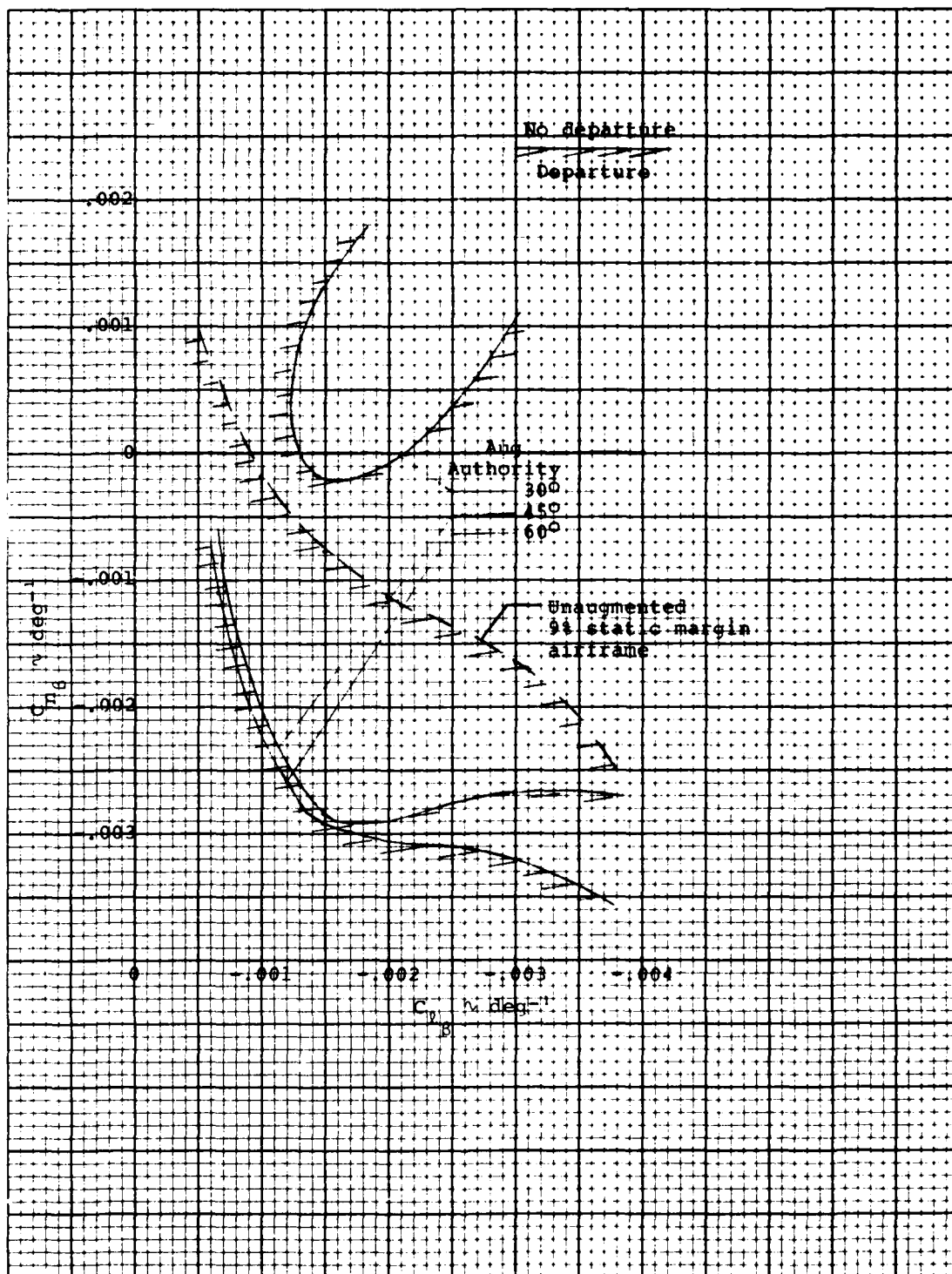
Figure 30. Influence of augmentation authority on departure boundaries for a -10% static margin airplane having adverse $C_{n_{\delta_a}}$
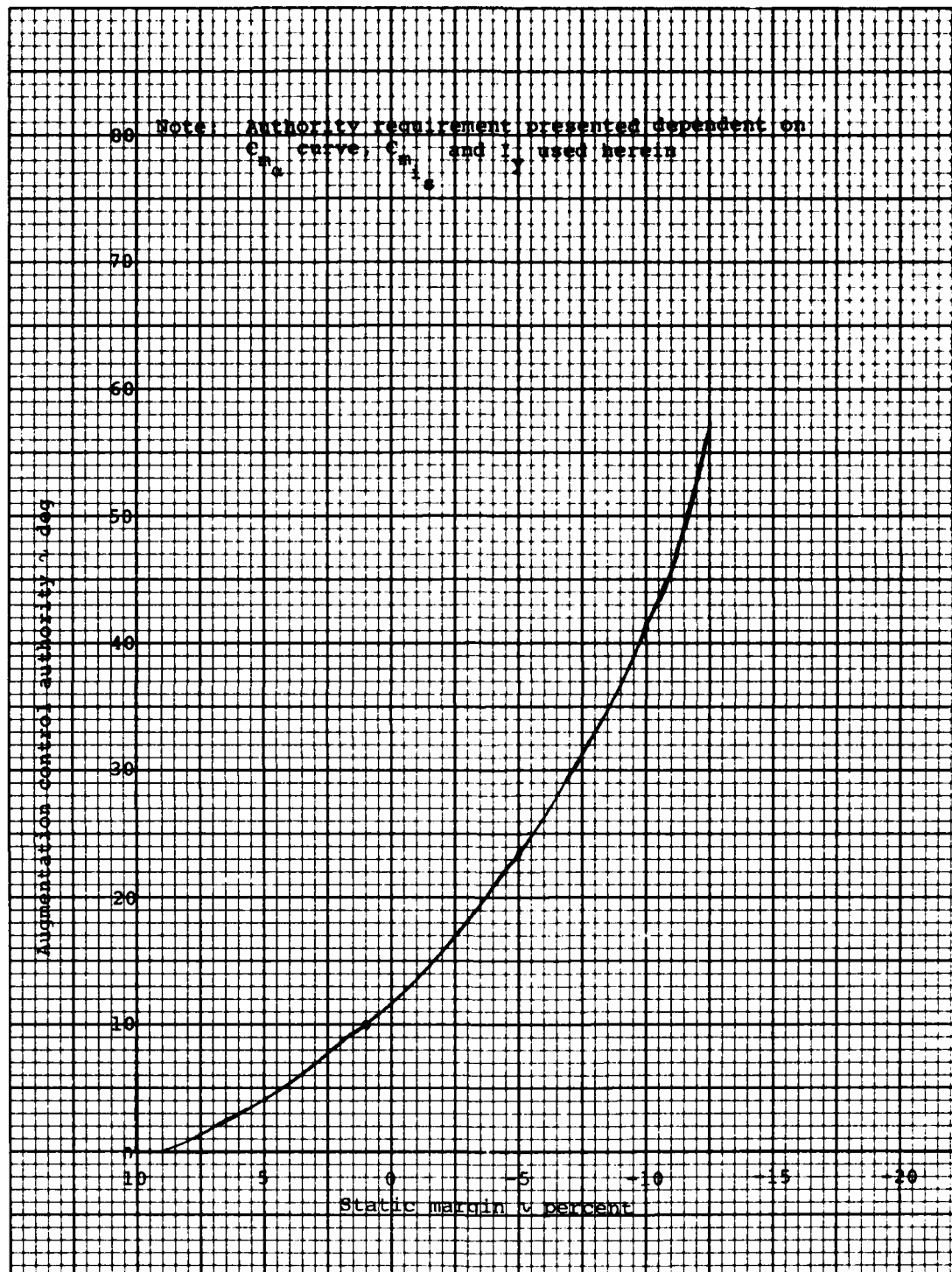
Figure 31. Augmentation system control authority required to maintain applicability of departure boundaries based on a 9% static margin airplane

87
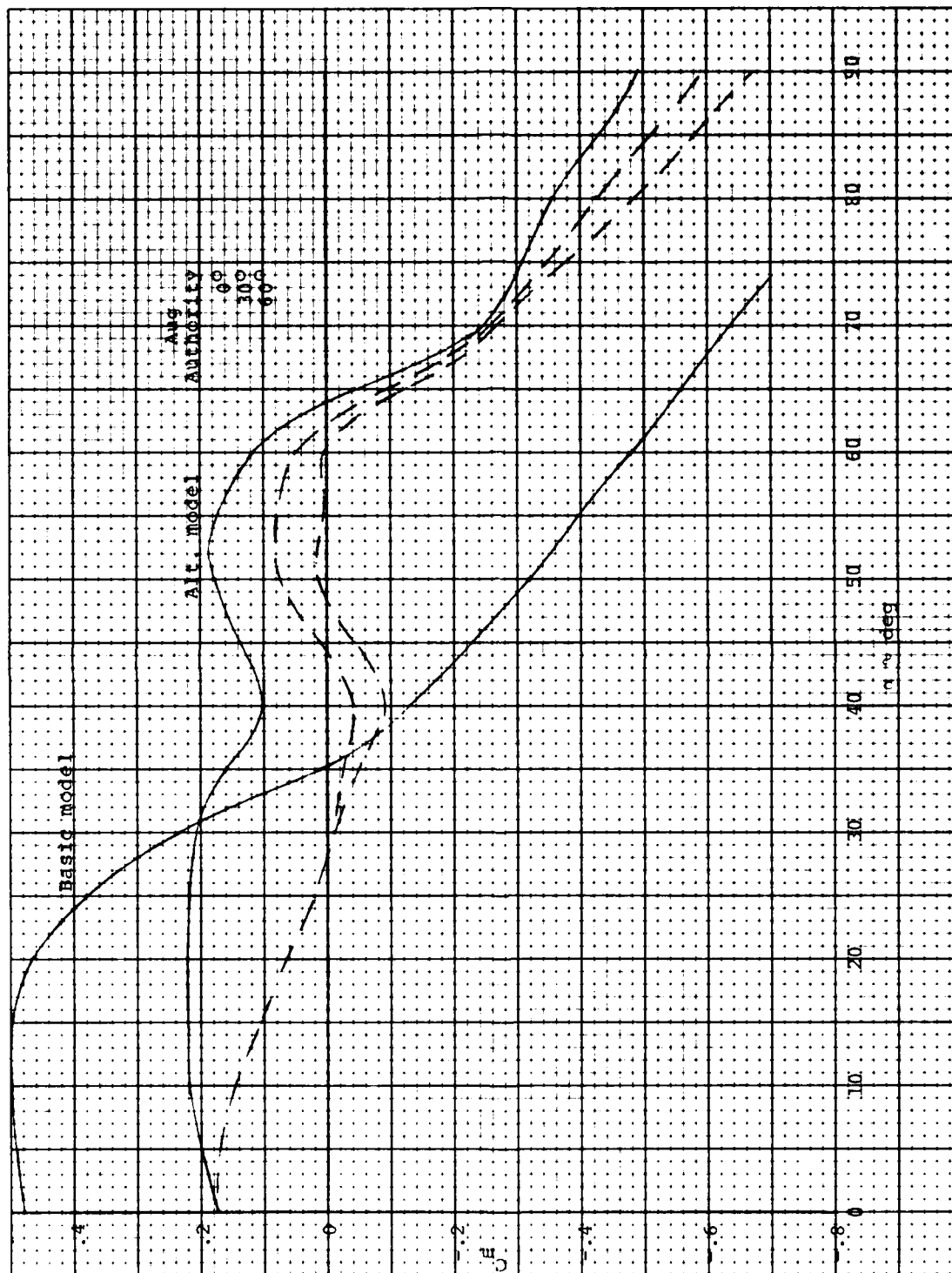
Figure 32. Effective static pitching moment curves for various augmentation authorities for the alternate pitching moment curve. i_s pilot = -30 deg
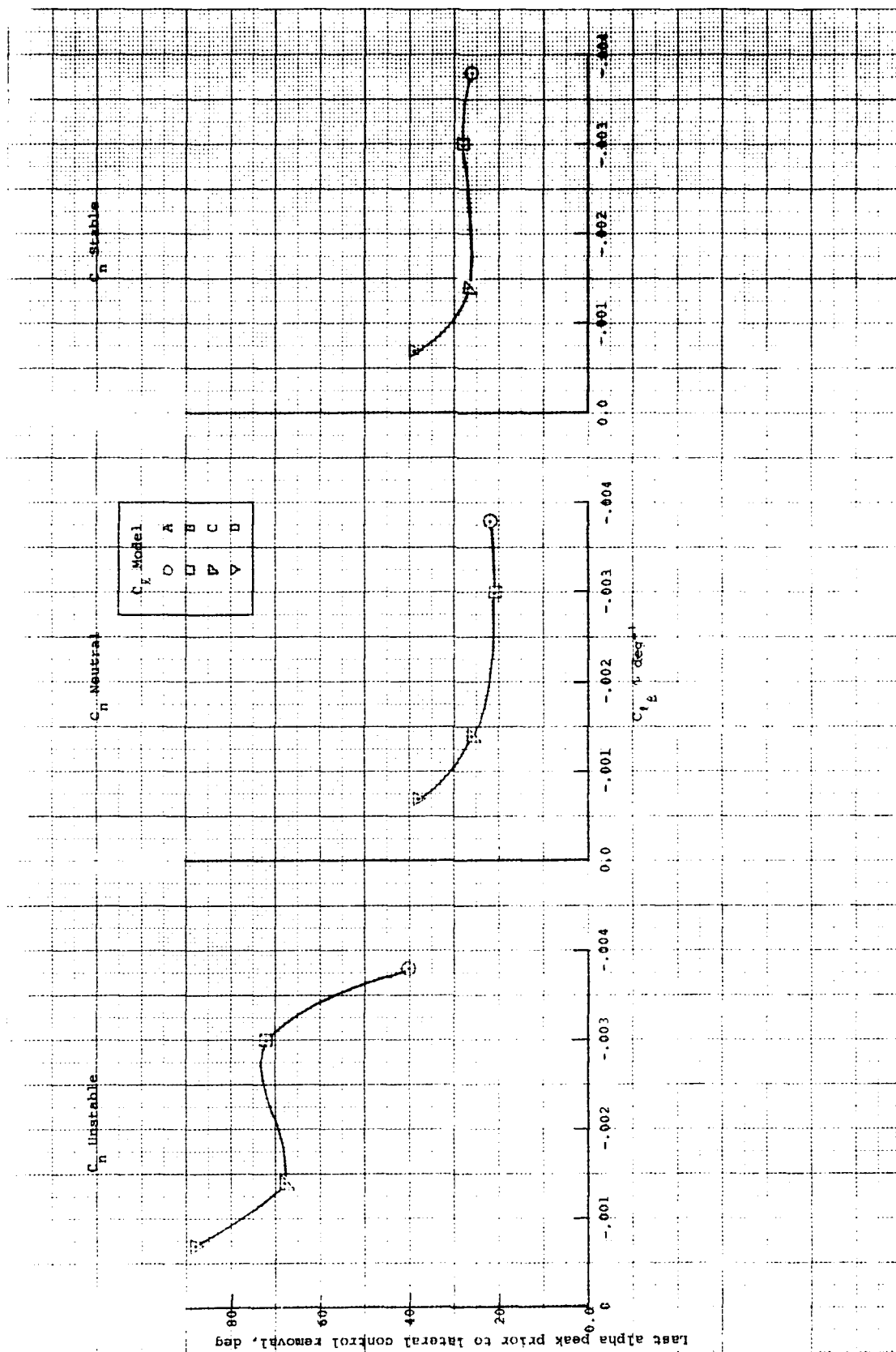
88

Figure 38. Design charts for determining departure and uncoordinated roll reversal susceptibility for the alternate pitching moment coefficient model airplane with full 60 degree augmentation authority

a) Last alpha peak prior to lateral control removal as a function of the aerodynamic models

b) Approximate second order damping ratio of alpha trace as a function of the aerodynamic models

Figure 33. (Continued)
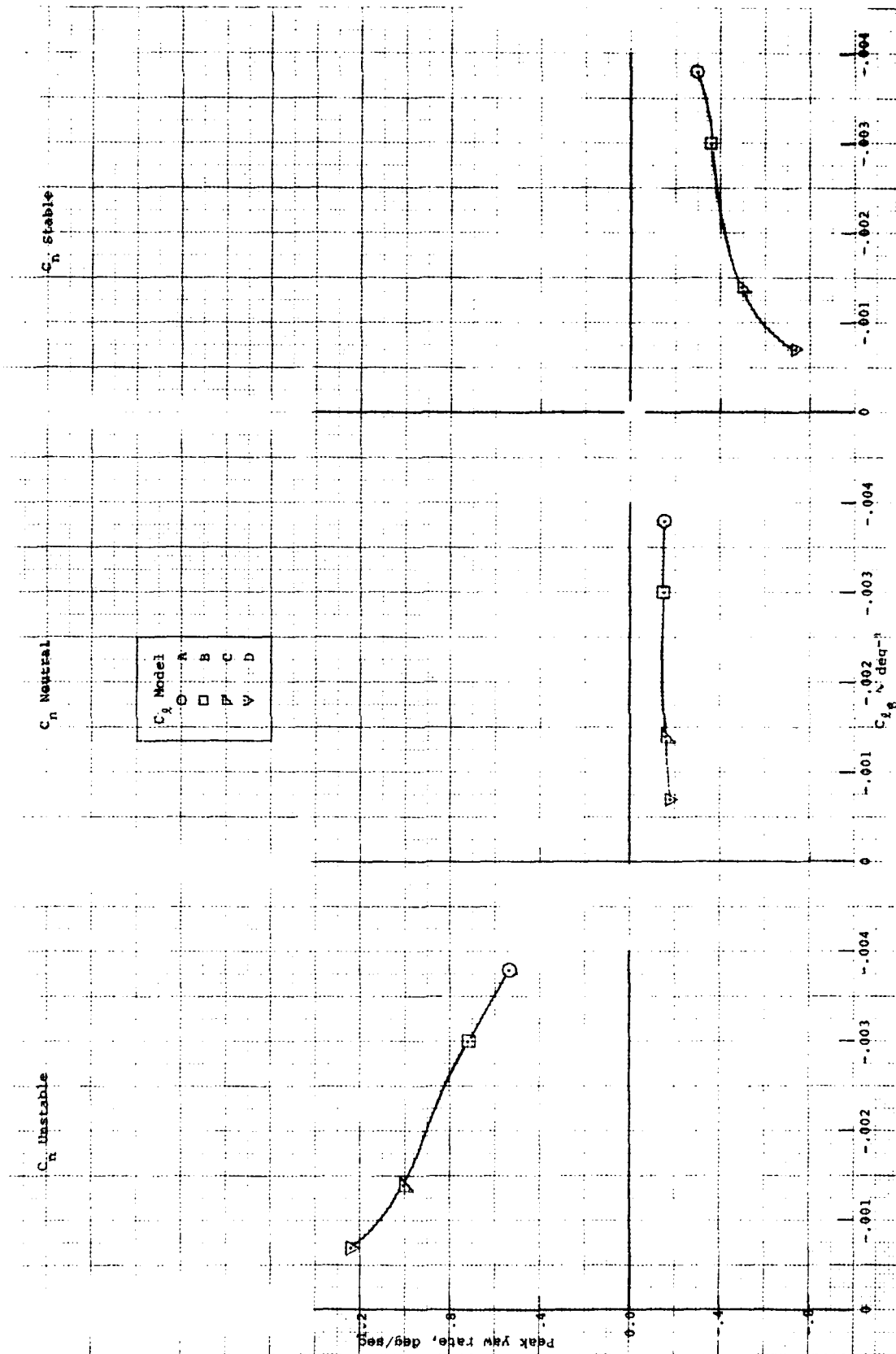
c) Peak yaw rate as a function of the aerodynamic models

Figure 33. (Continued)
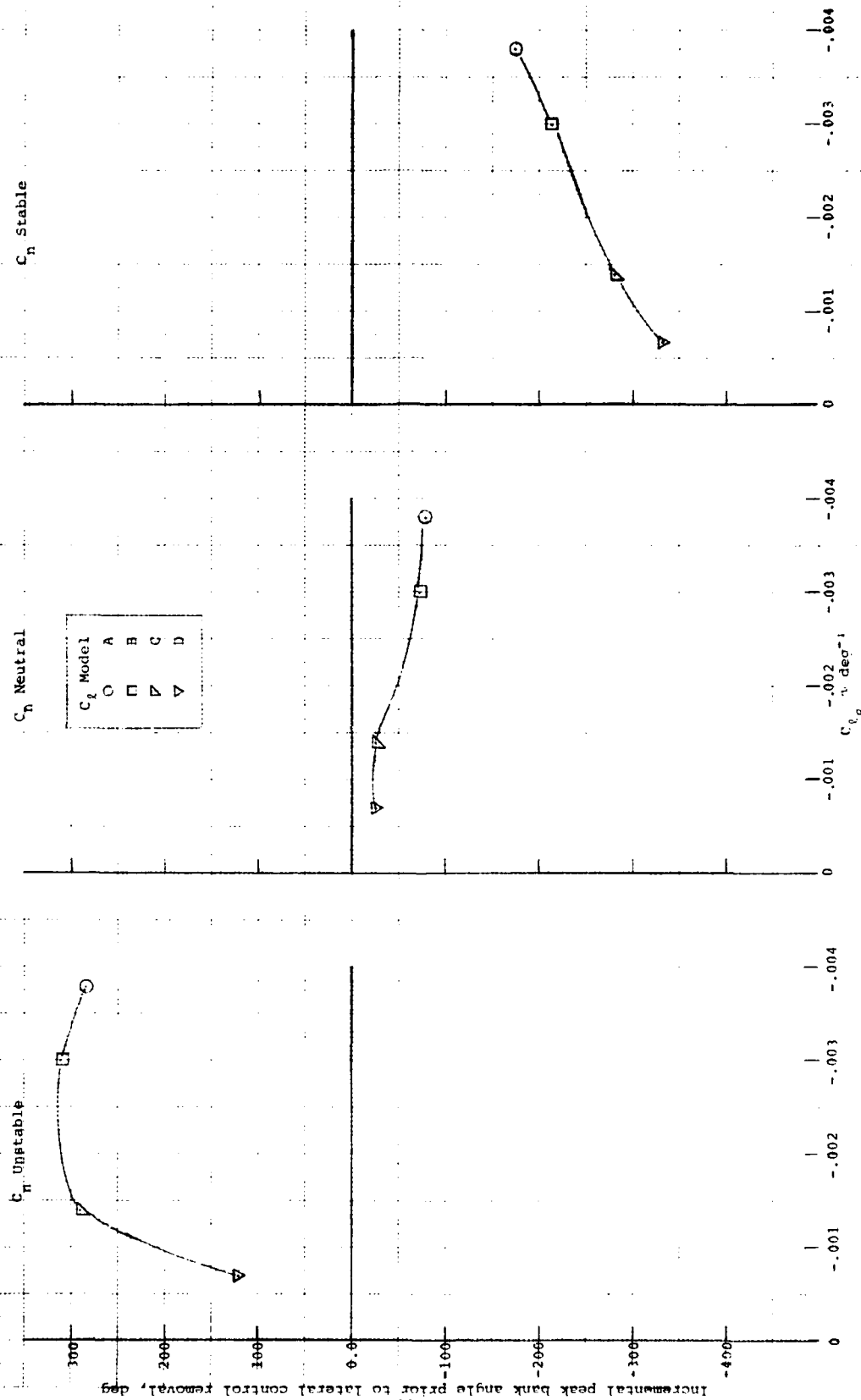
d) Incremental peak bank angle prior to lateral control removal as a function of the aerodynamic models

Figure 31. (Concluded)
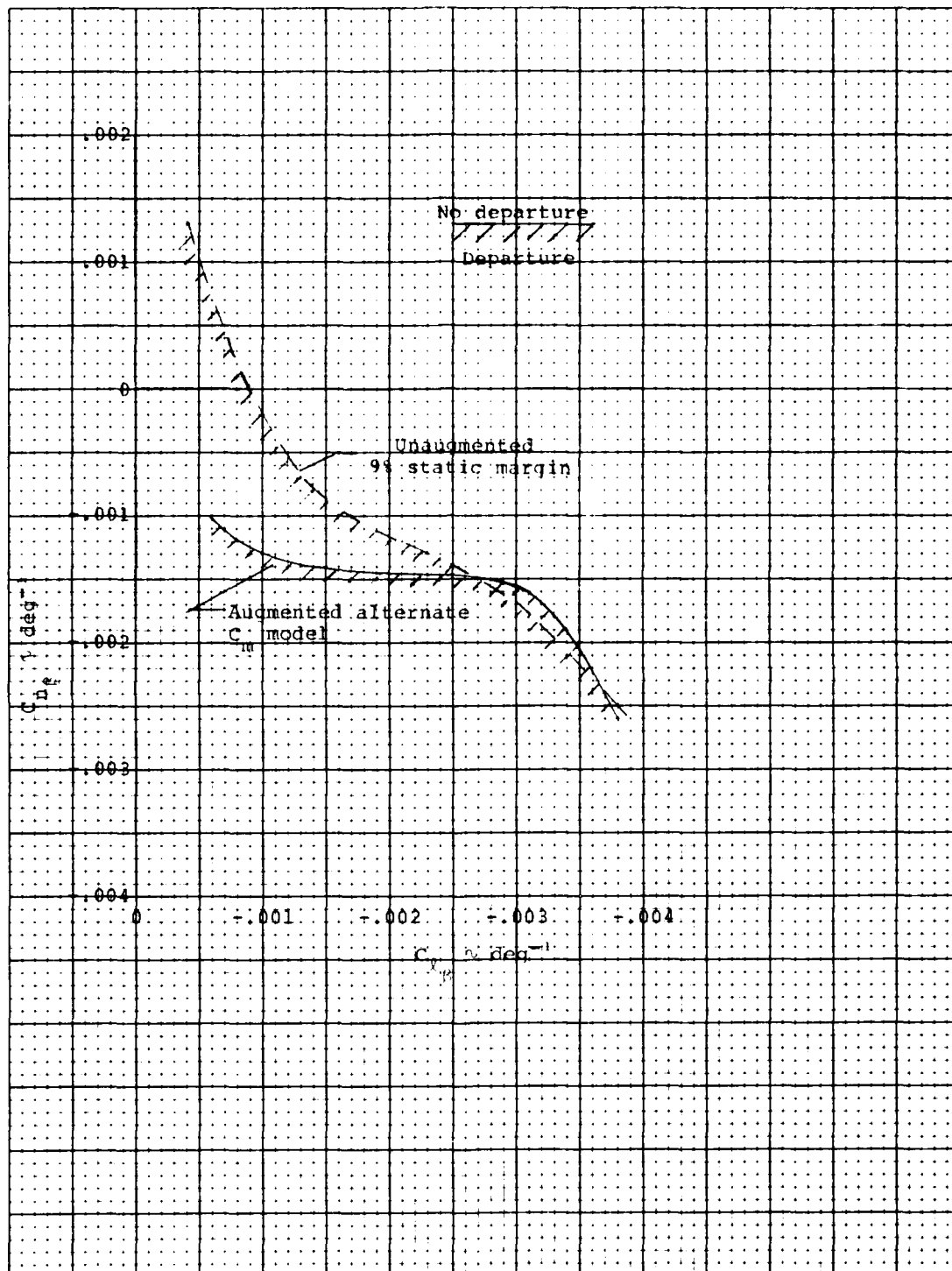
Figure 34.   Departure boundary for the alternate pitching
moment coefficient model airplane with full 60 degree
augmentation authority

Final boundary

Boundary based on ref. 1 data

.003

.002

.001

0

C_{n_β}, deg^{-1}

No departure

.001

.002

Departure

.003

.004

0   –.001   –.002   –.003   –.004

C_{ℓ_β}, deg^{-1}

a) Proverse $C_{n_{\delta_a}}$

Figure 35. Final departure boundaries compared to boundaries
derived using Reference 1 design chart data

94
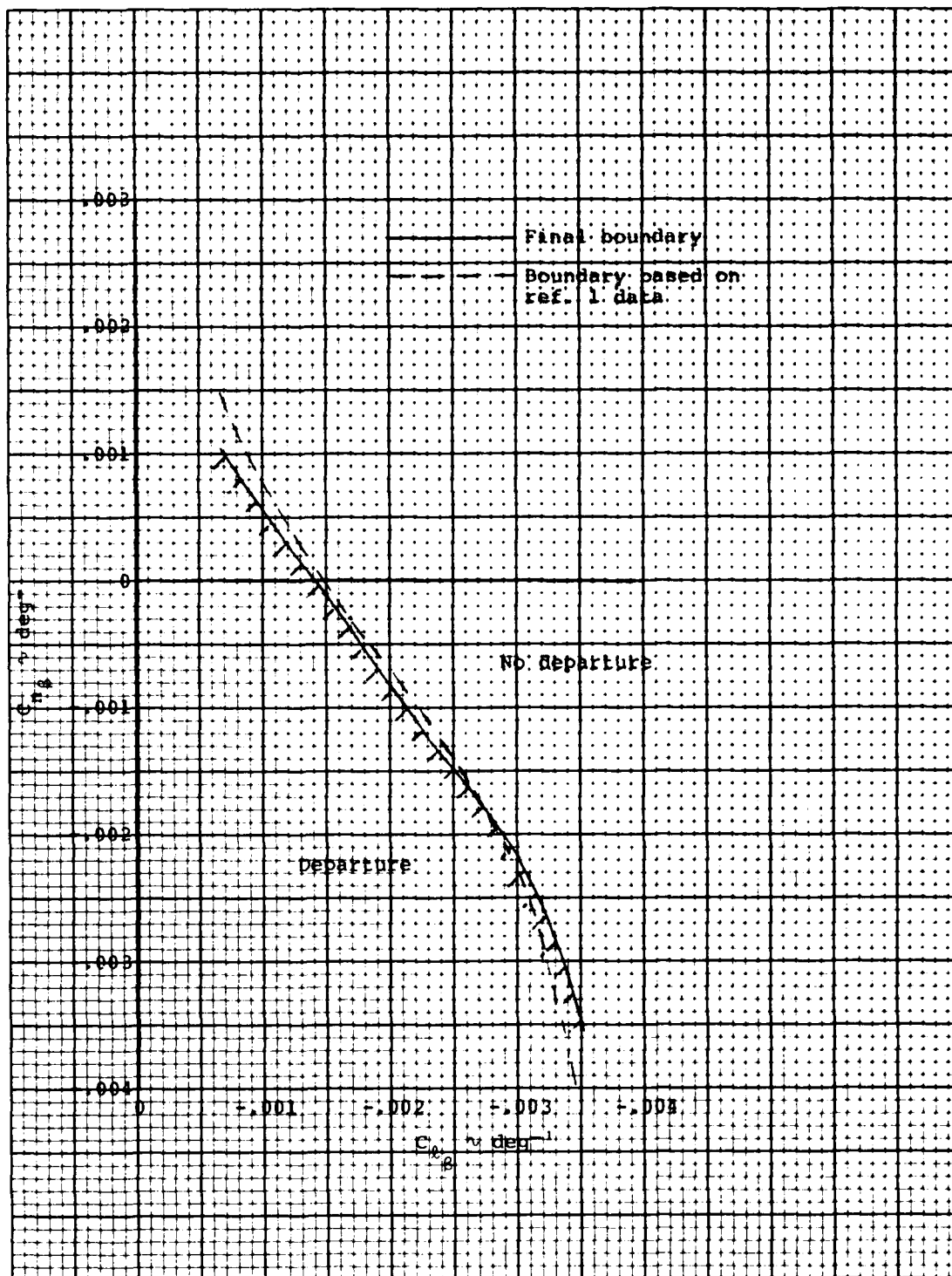
b) Neutral $C_{n_{\delta_\alpha}}$

Figure 35. (Continued)
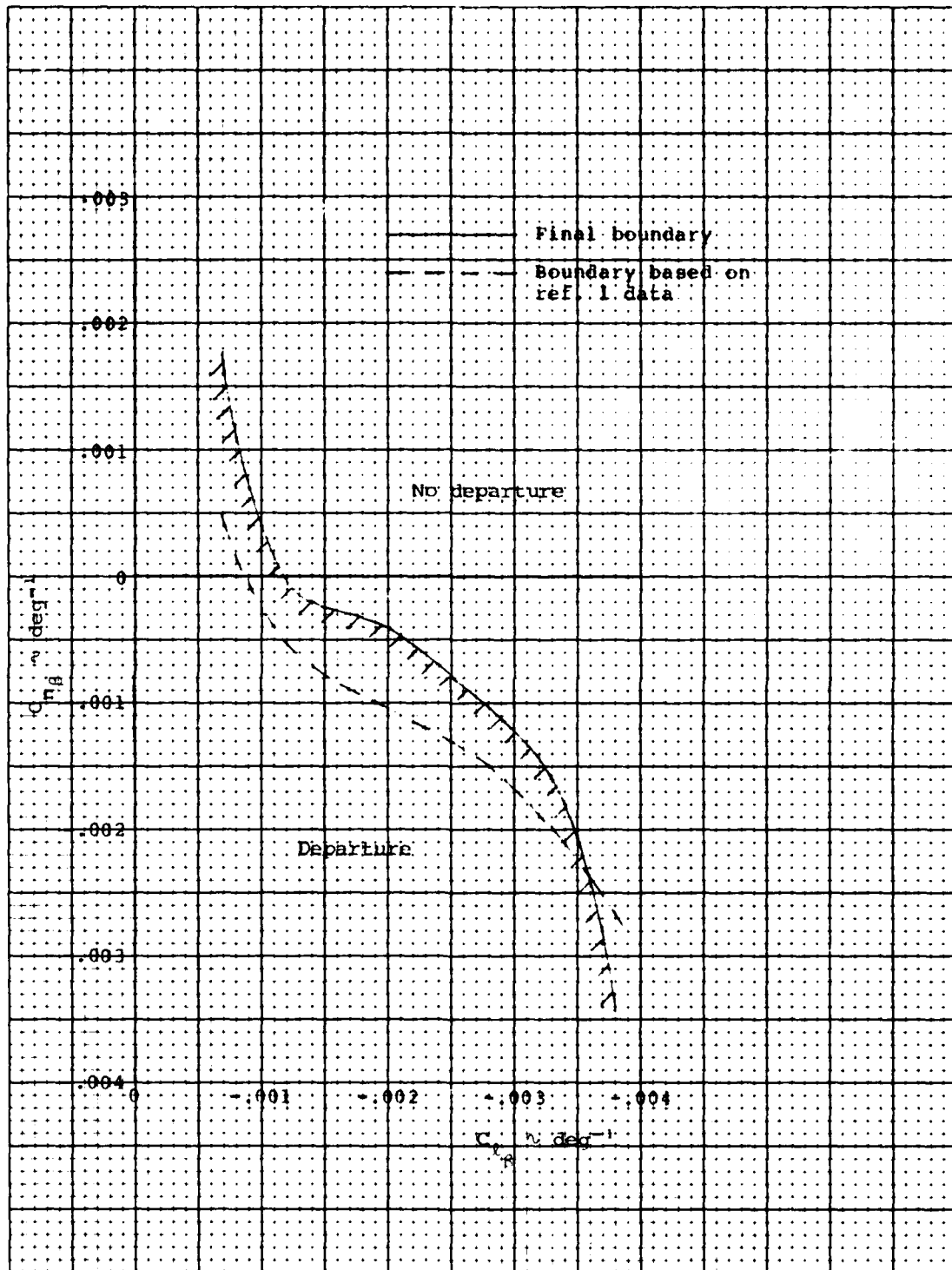
c) Adverse $C_{n_{\delta_a}}$

Figure 35.   (Concluded)

96
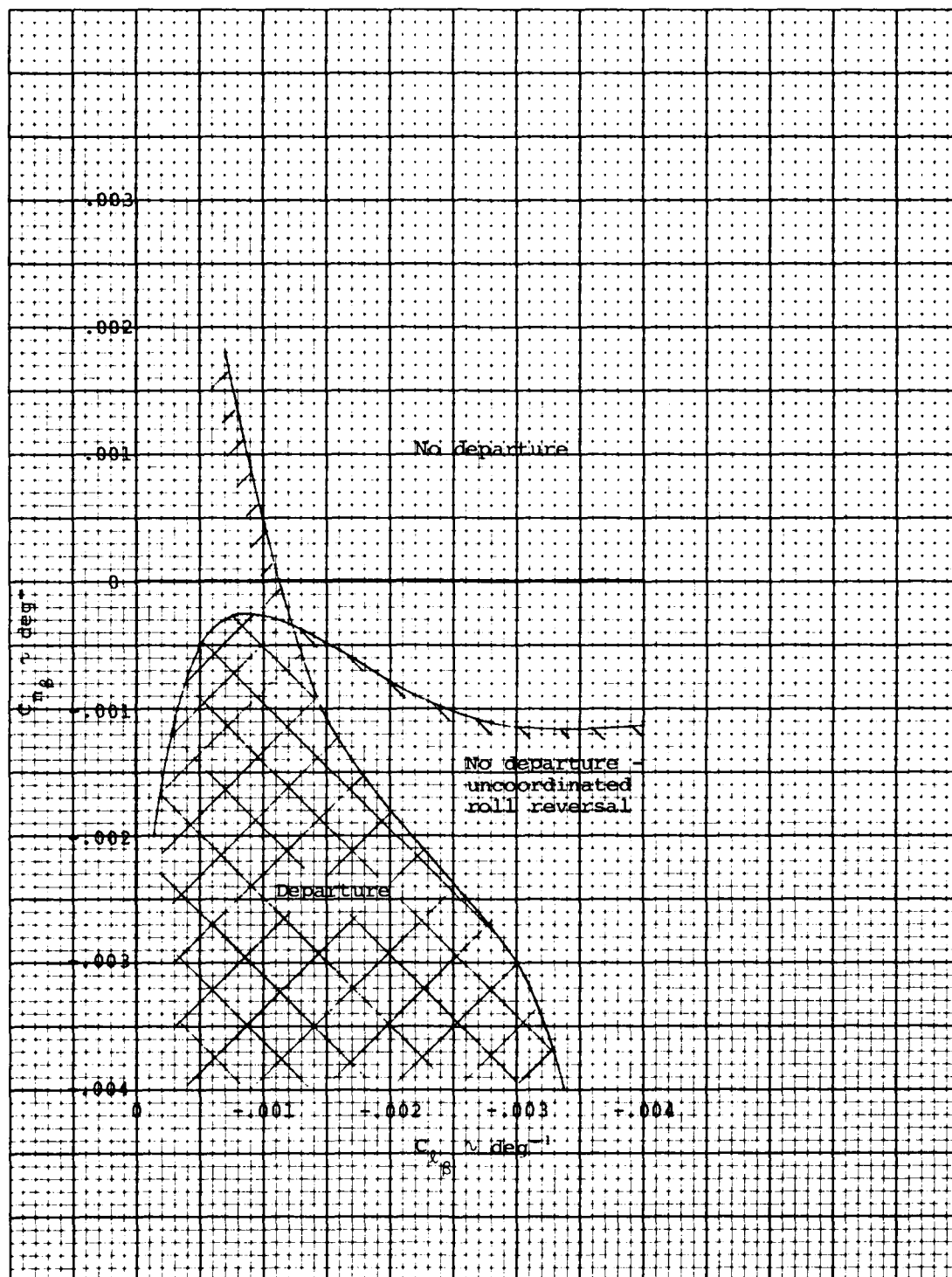
a) Proverse $C_{n_{\delta_a}}$

Figure 36. Departure and uncoordinated roll reversal
boundaries for fighter configurations

97
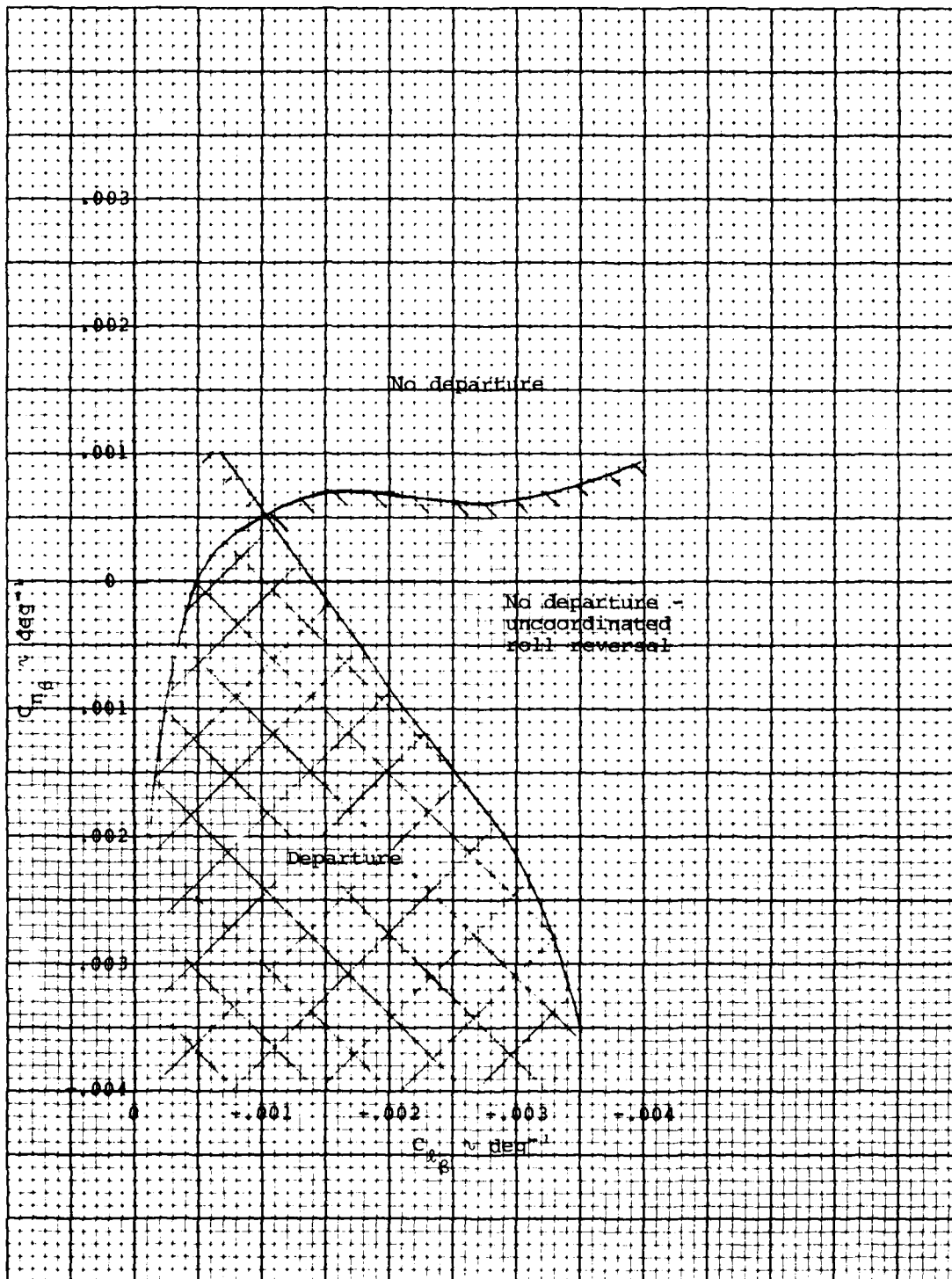
b) Neutral $C_{n_{\delta_a}}$

Figure 36. (Continued)

98
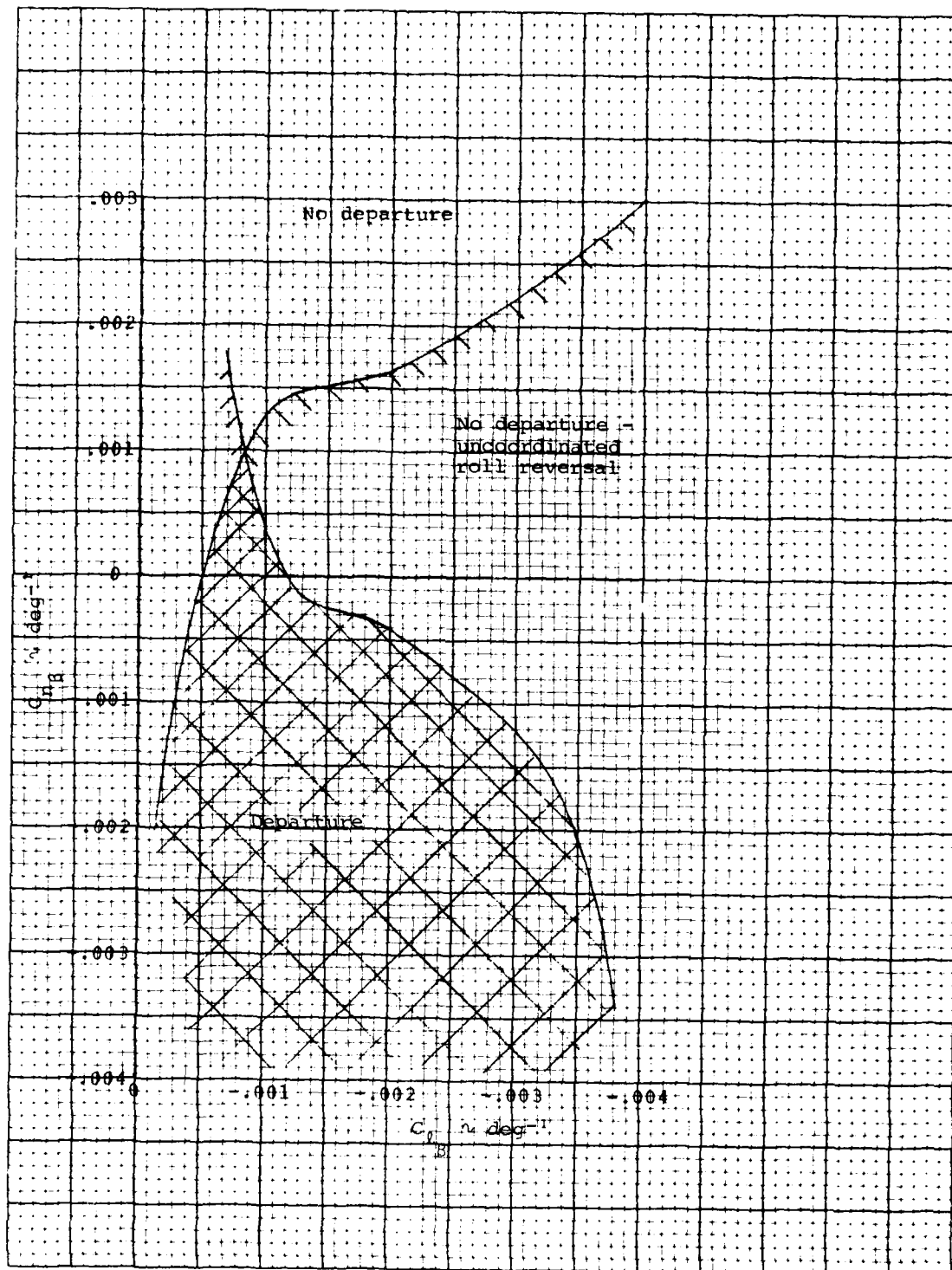
c) Adverse $C_{n_{\delta_a}}$

Figure 36. (Concluded)

99

APPENDIX

The aerodynamic parameters which were not varied during
the present study are presented herein. The normal, axial,
and side-force coefficients were programmed as functions of
angle of attack, sideslip angle and longitudinal control de-
flection as shown in Figures Al through A6. The lateral control
derivatives were programmed as functions of angle of attack and
lateral and longitudinal control deflections. The longitudinal
control deflection functional dependence results from the fact
that many current fighter configurations utilize differential
elevator deflection for lateral control. The $C_{\ell_{\delta_a}}$ model is
shown in Figures A7 and A8, the $C_{n_{\delta_a}}$ models in Figure A9 and the
$C_{Y_{\delta_a}}$ model in Figures A10 and A11. The dynamic derivatives,
C_{ℓ_p}, C_{n_p}, C_{ℓ_r} and C_{n_r}, are shown in Figures A12 through A15;
each is a function of angle of attack and represents character-
istic values for fighter type airplanes.

The familiar six-degree-of-freedom differential equations
representing the linear and angular accelerations of a moving
body axis system having its origin at the airplane center of
mass, as shown in Appendix A of Reference 3, were used to
generate the computer time histories for the study reported
herein. The aircraft geometric characteristics used in this
study are:

$$S = 400 \text{ ft}^2$$
$$\bar{c} = 10 \text{ ft}$$
$$b = 40 \text{ ft}$$

The maximum control deflections used during the study are:

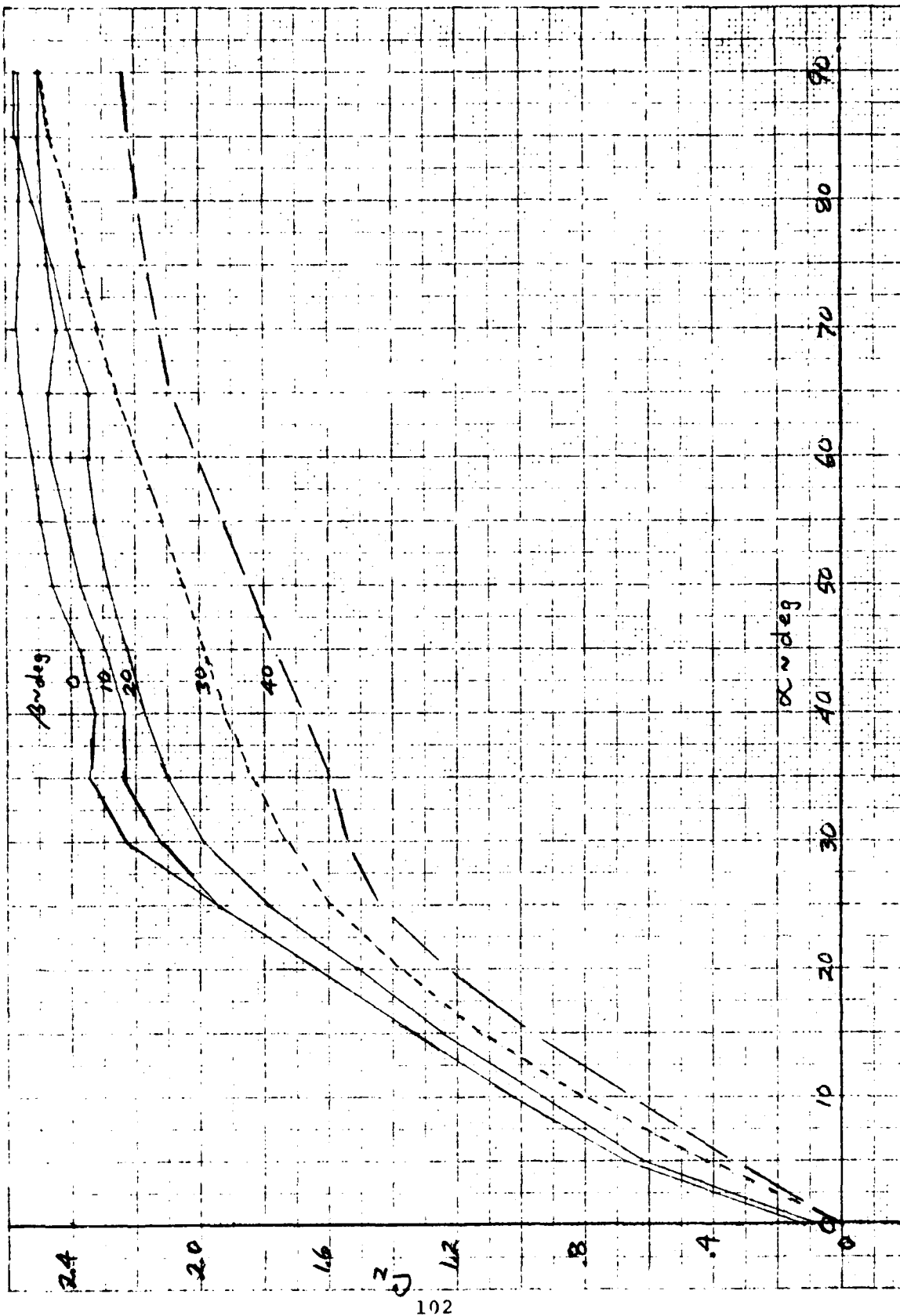| elevator | $\pm 30^\circ$ |
| lateral control | 12° per panel |

Figure A1.- Normal force coefficient as a function of angle of attack and sideslip angle. $i_s = 0$ deg
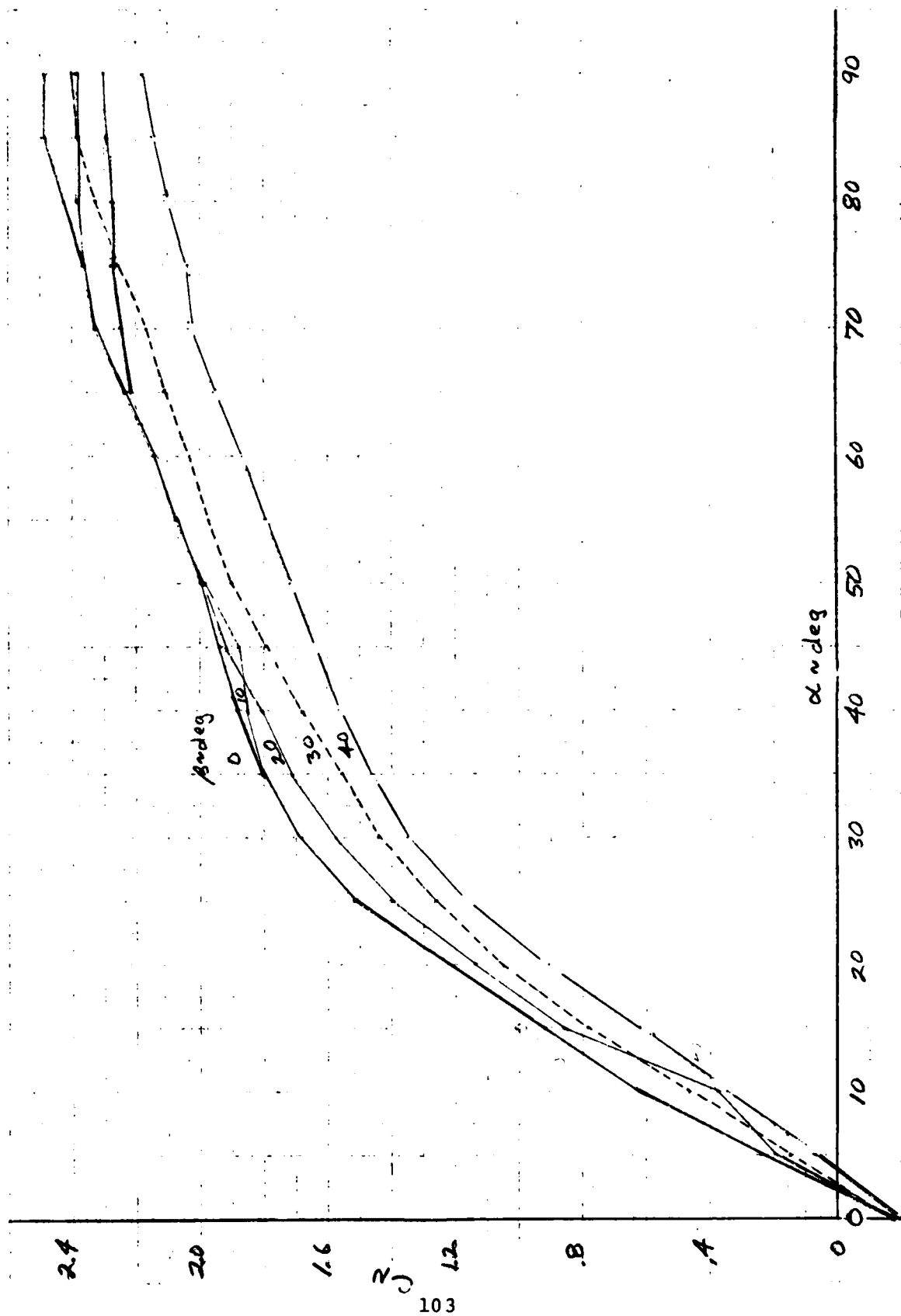
Figure A2.–Normal force coefficient as a function of angle of attack and sideslip angle. $i_s = -30$ deg
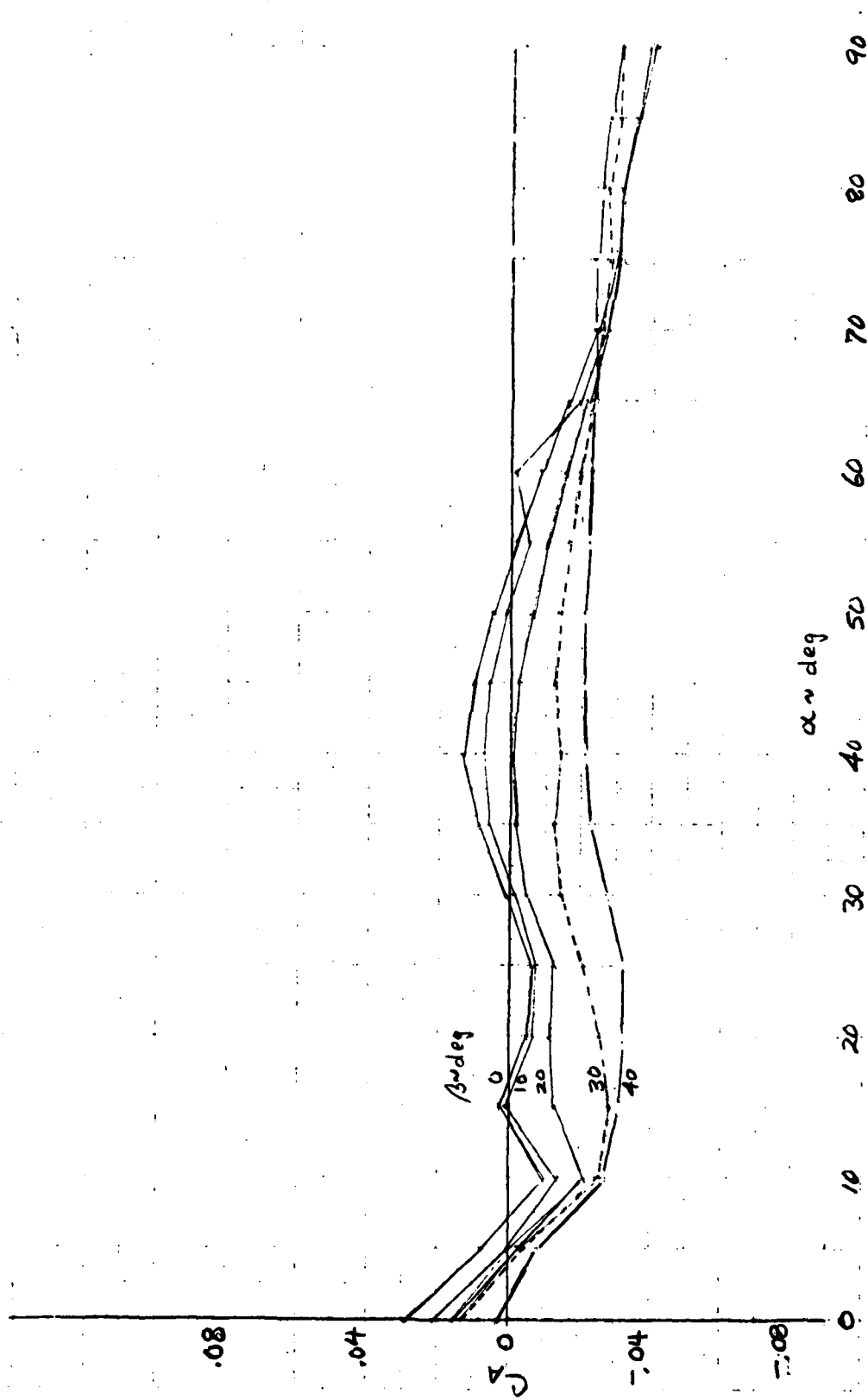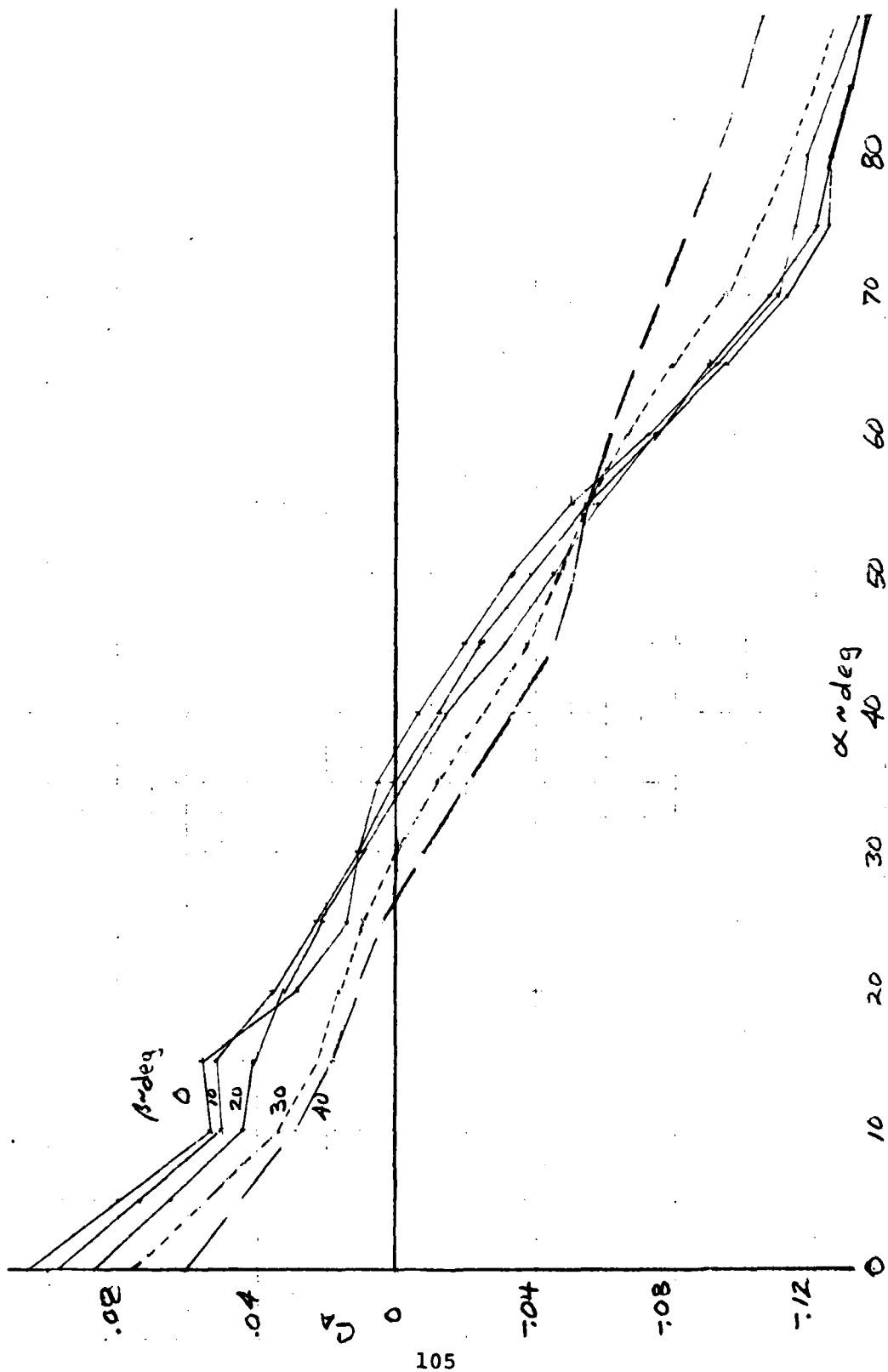
103

Figure A3. - Axial force coefficient as a function of angle of attack and sideslip angle. $i_s = 0$ deg

Figure A4. - Axial force coefficient as a function of angle of attack and sideslip angle. i_s = -30 deg
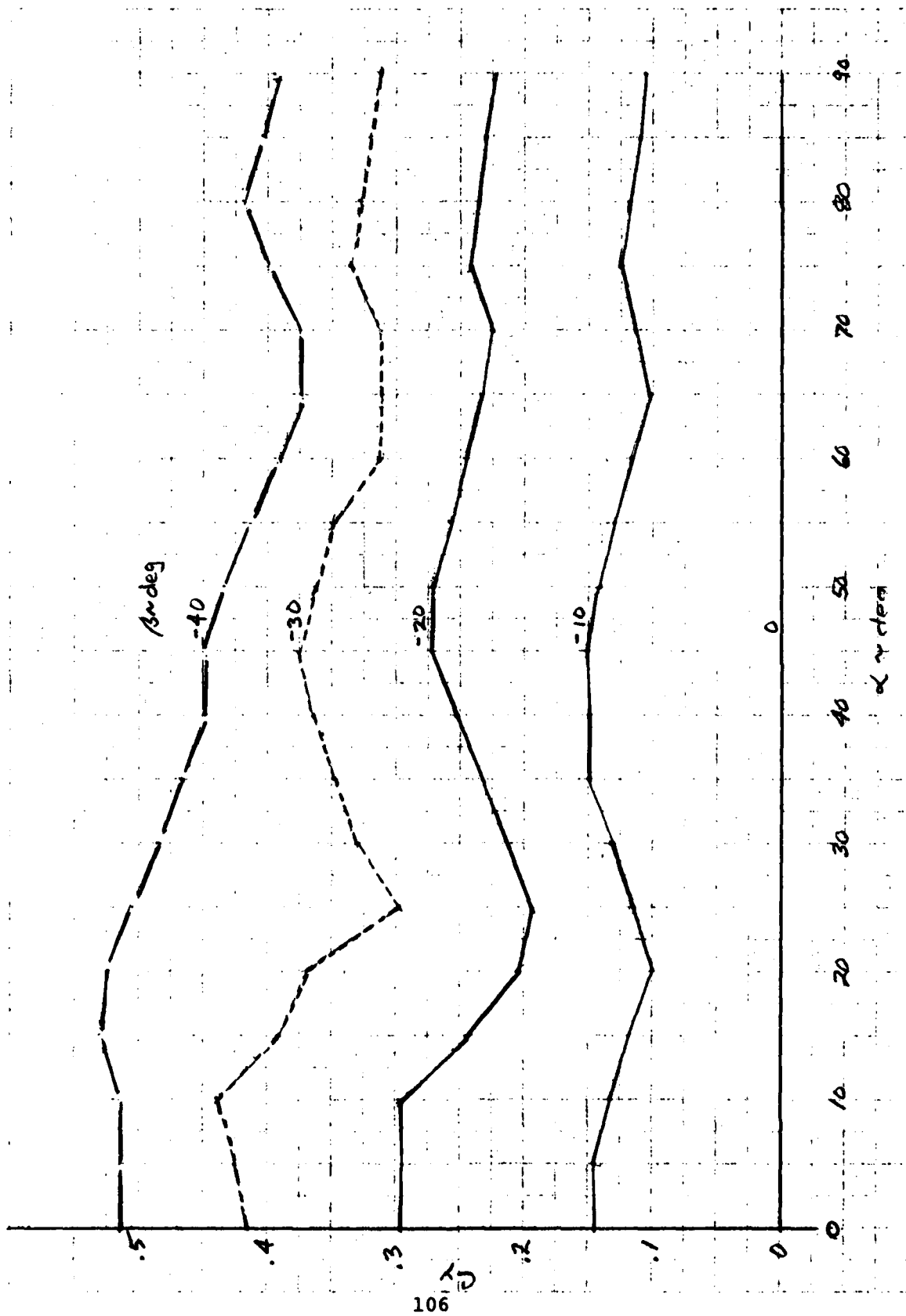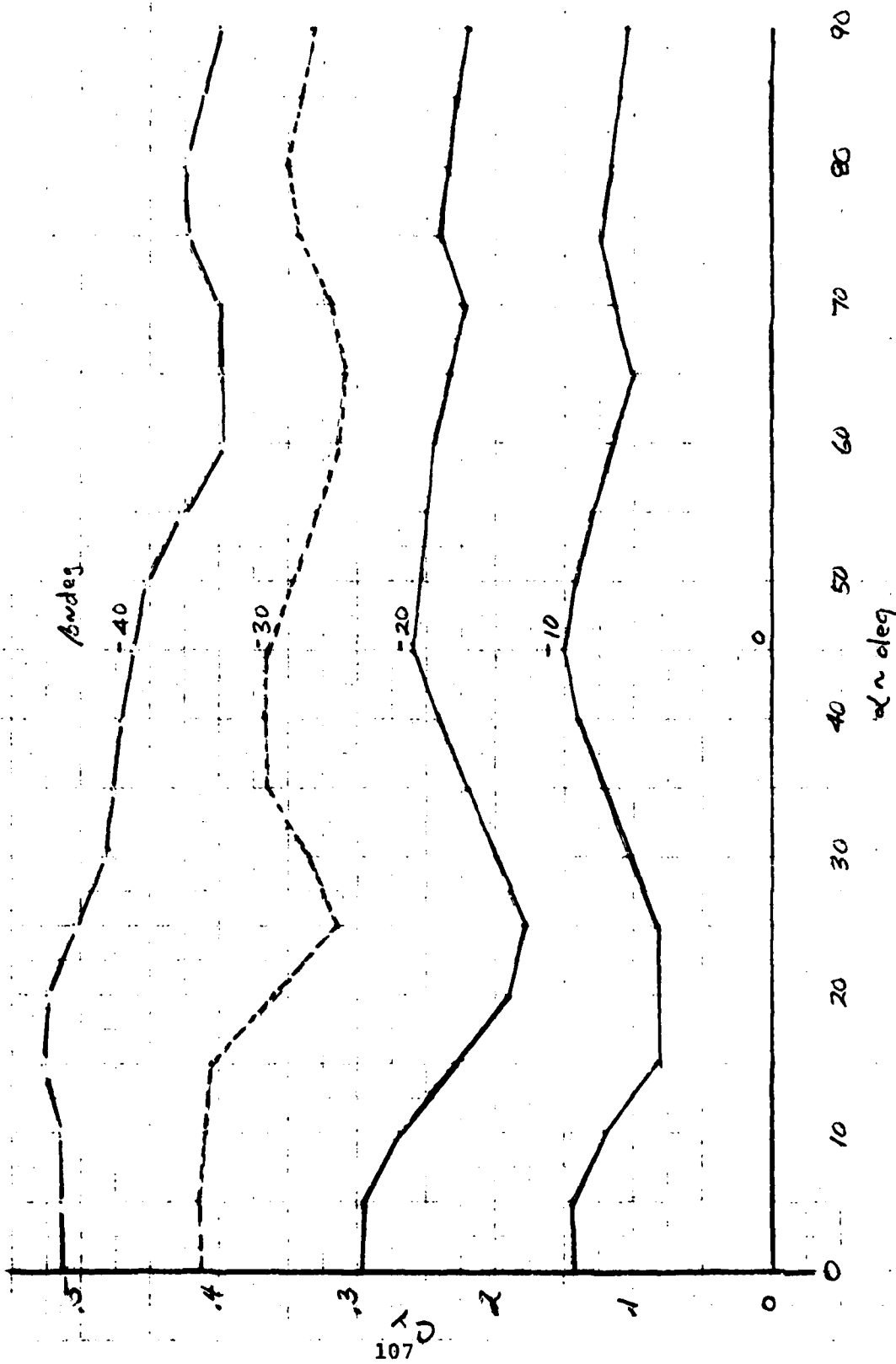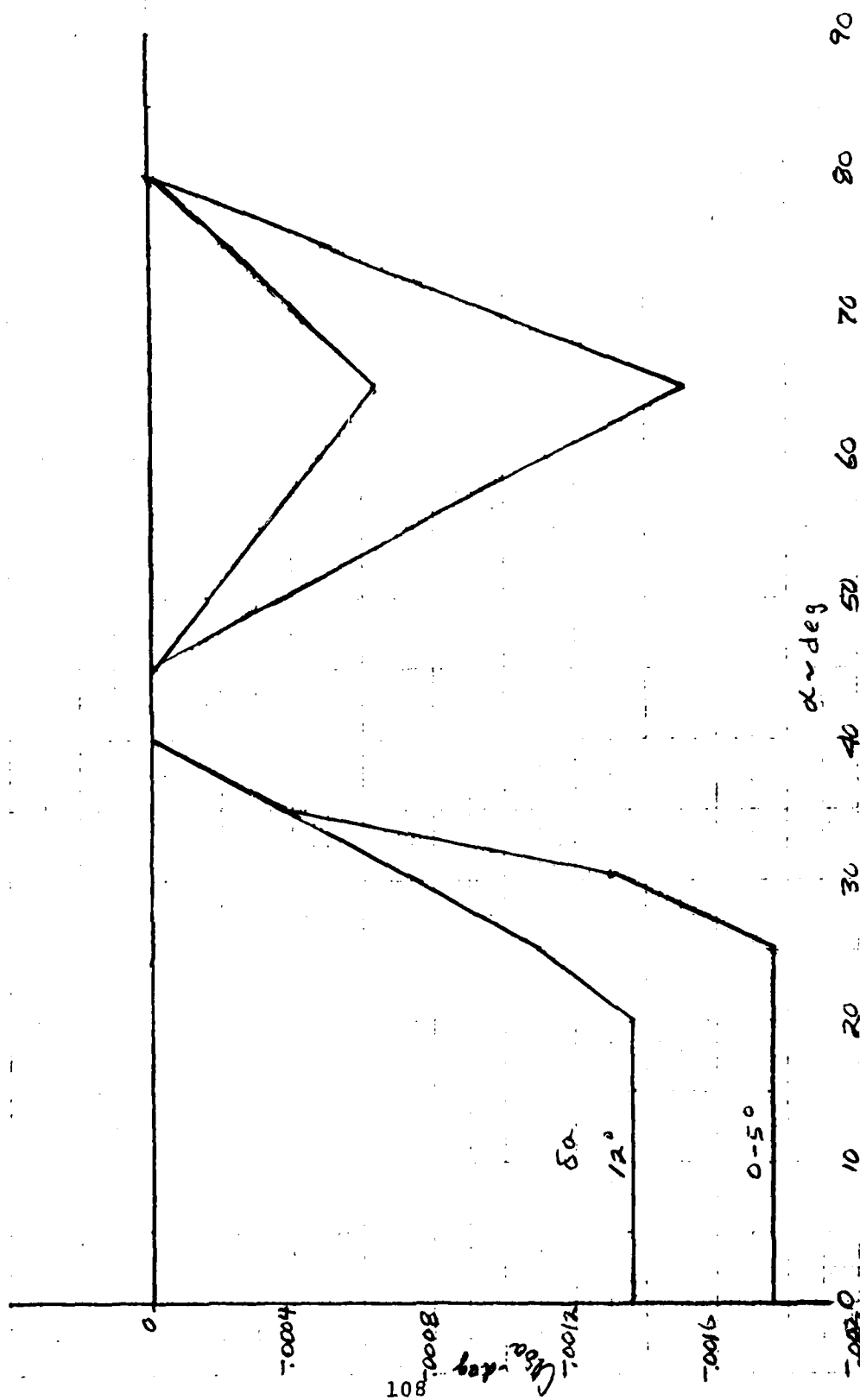
Figure A5. - Side force coefficient as a function of angle of attack and sideslip angle. $i_s = 0$ deg

Figure A6. - Side force coefficient as a function of angle of attack and sideslip angle. $i_s = -30$ deg

Figure A7. - Rolling moment due to lateral control derivative as a function of angle of attack and control deflection. $i_s = 0$ deg
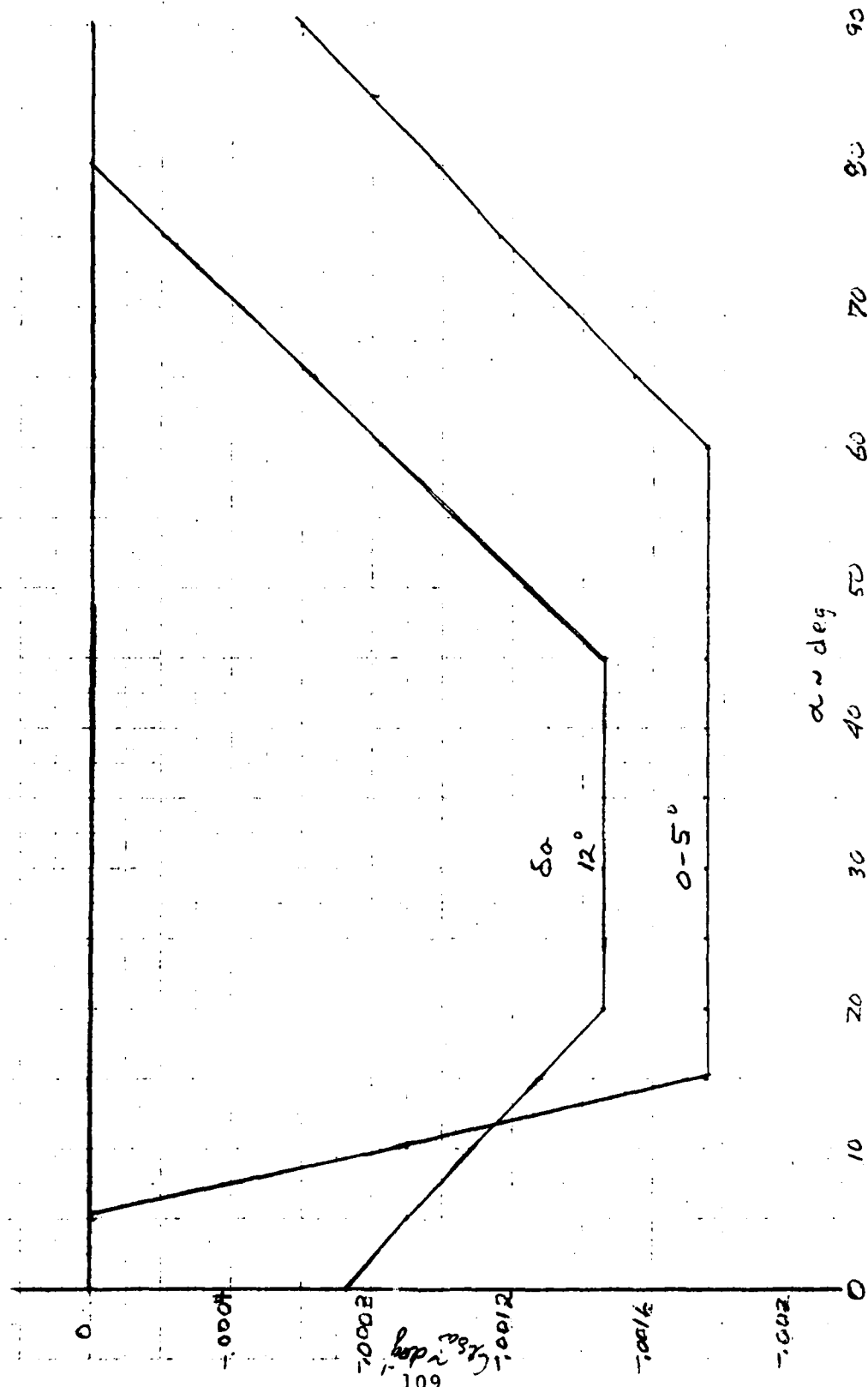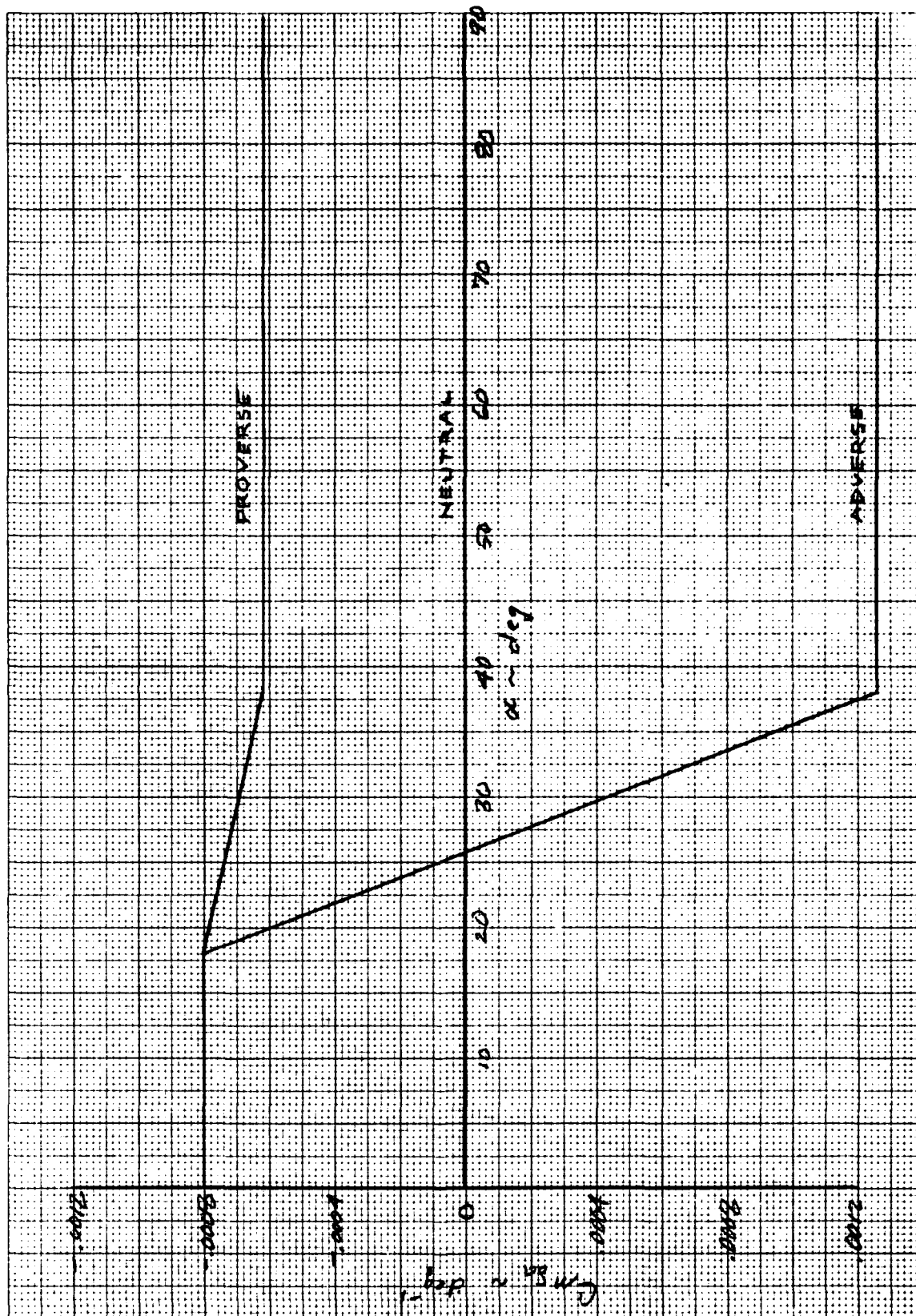
108

Figure A8. - Rolling moment due to lateral control derivative as a function of angle of attack and control deflection. $i_s = -30$ deg

Figure A9.-Yawing moment due to lateral control derivative as a
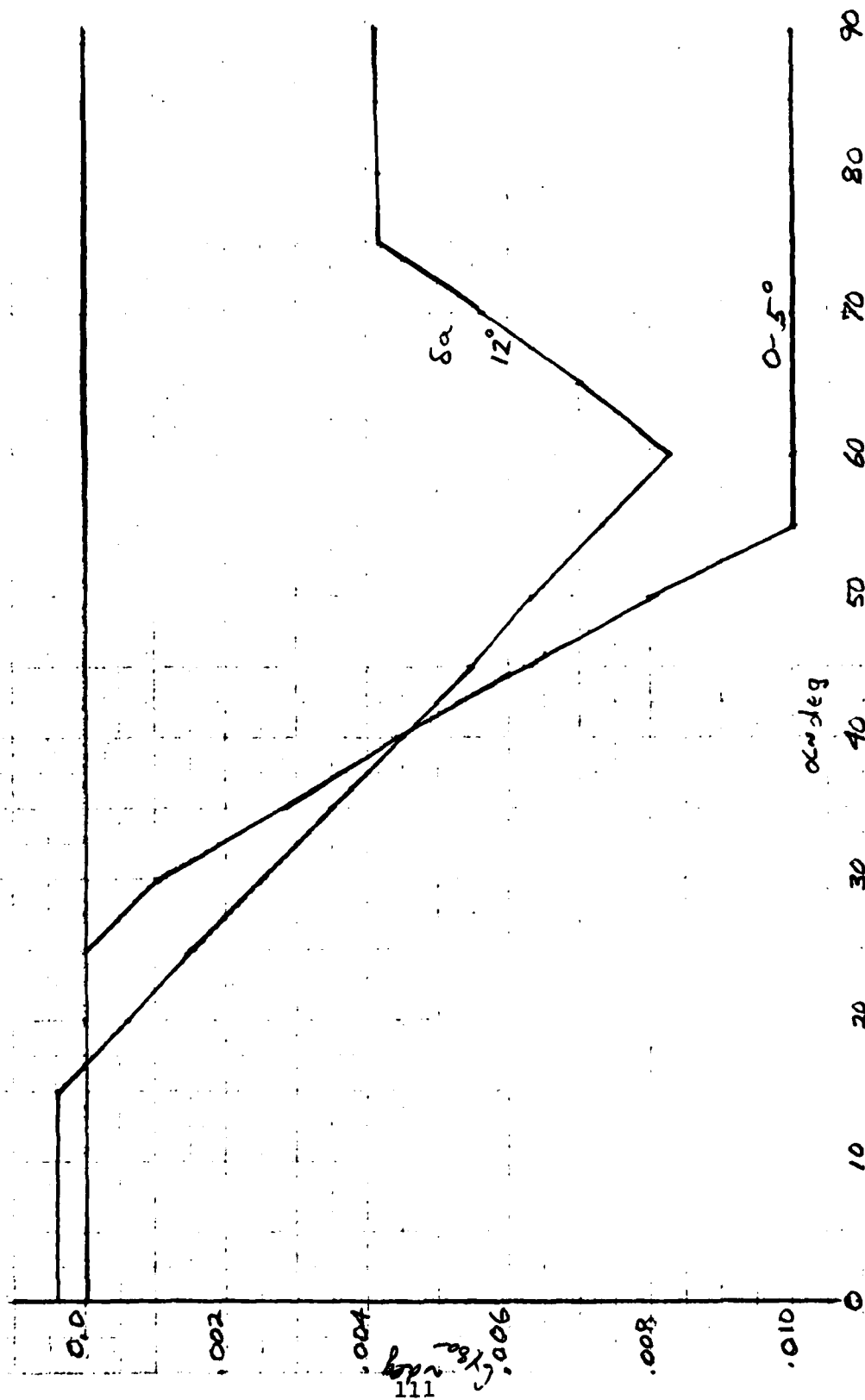function of angle of attack

110

Figure A10.- Side force due to lateral control derivative as a function of angle of attack and control deflection. $i_s = 0$ deg
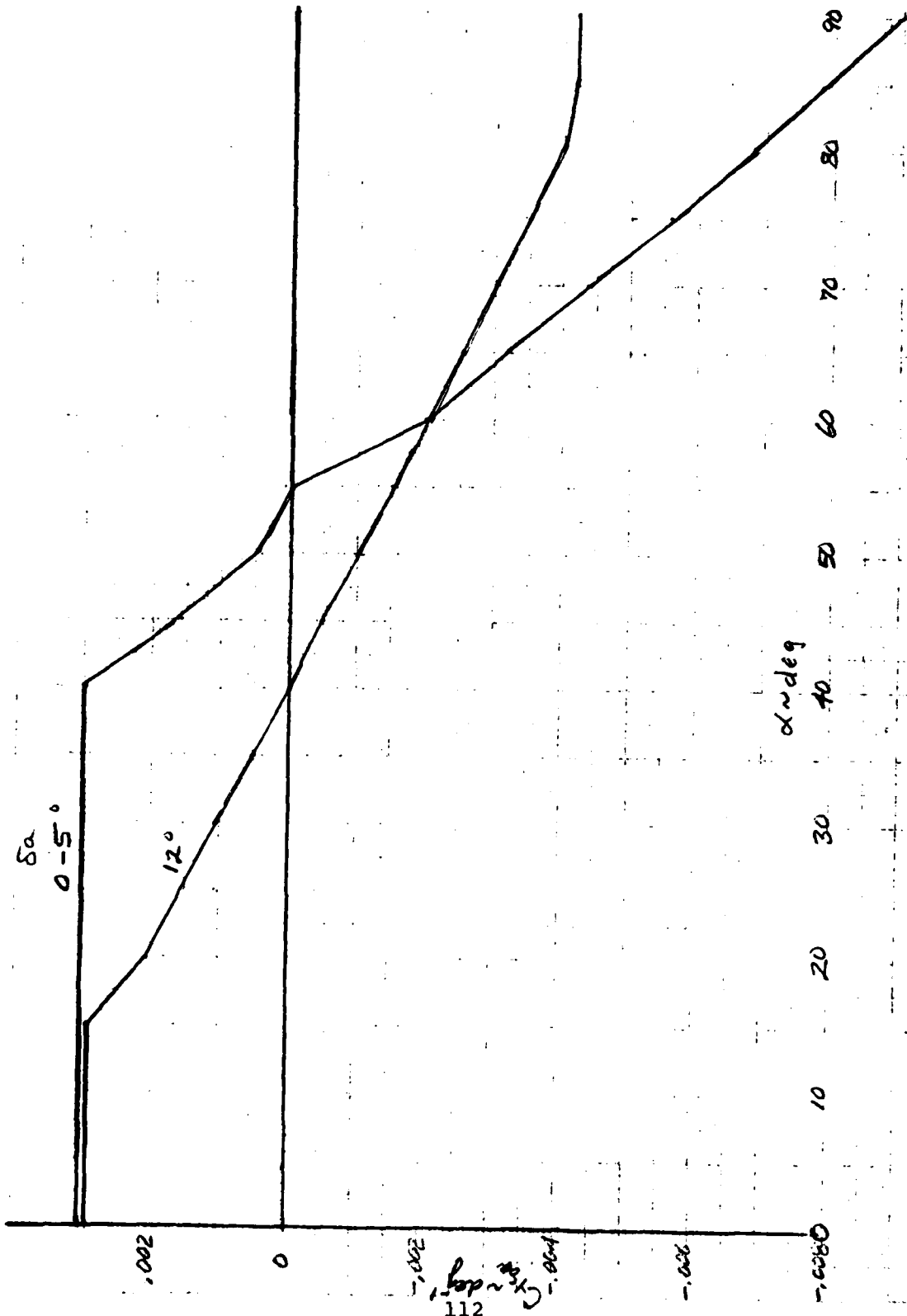
111

Figure A11.- Side force due to lateral control derivative as a function of angle of attack and control deflection. $i_s = -30$ deg
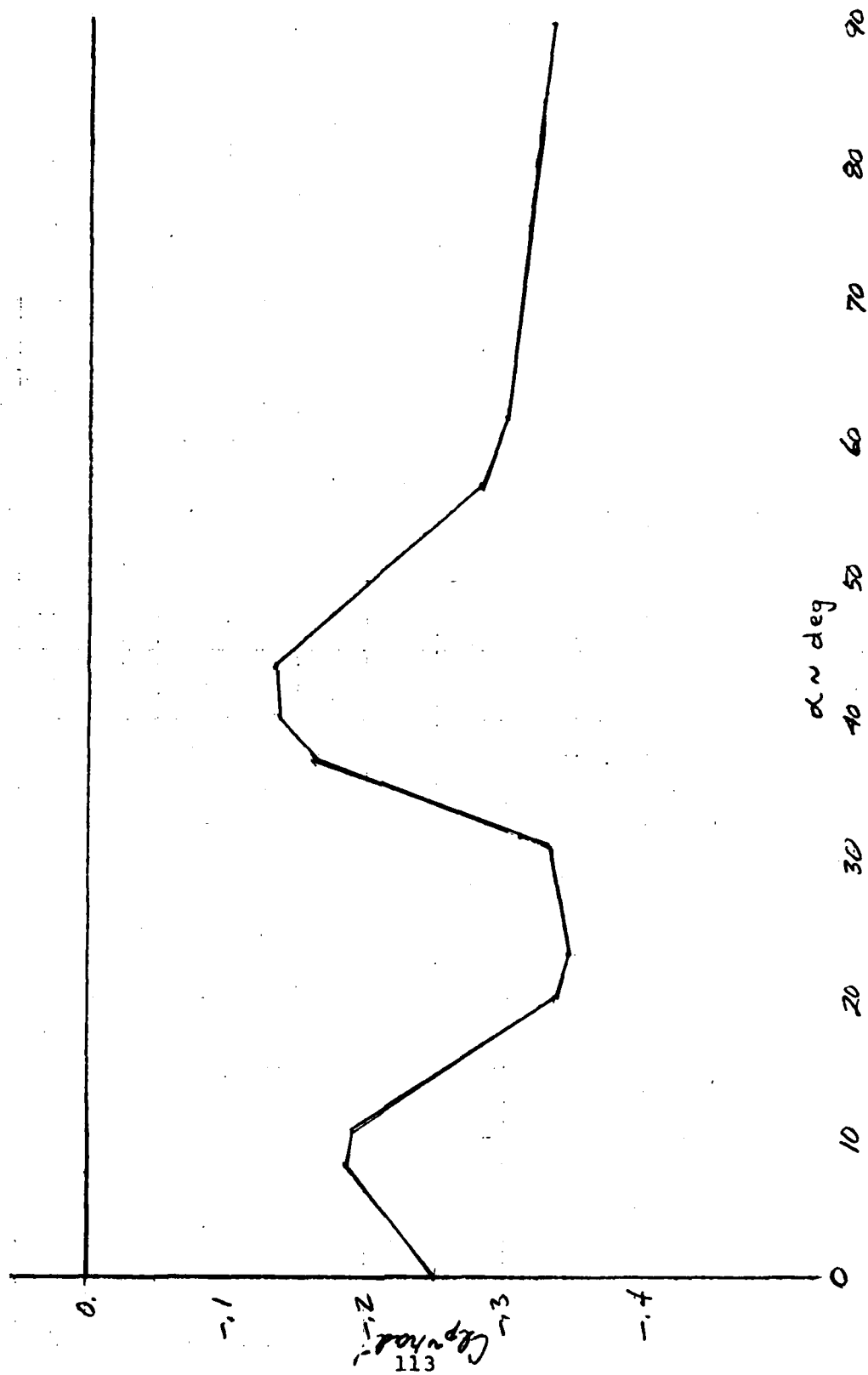
$\alpha \sim deg$

$C_{l_p} \sim rad^{-1}$

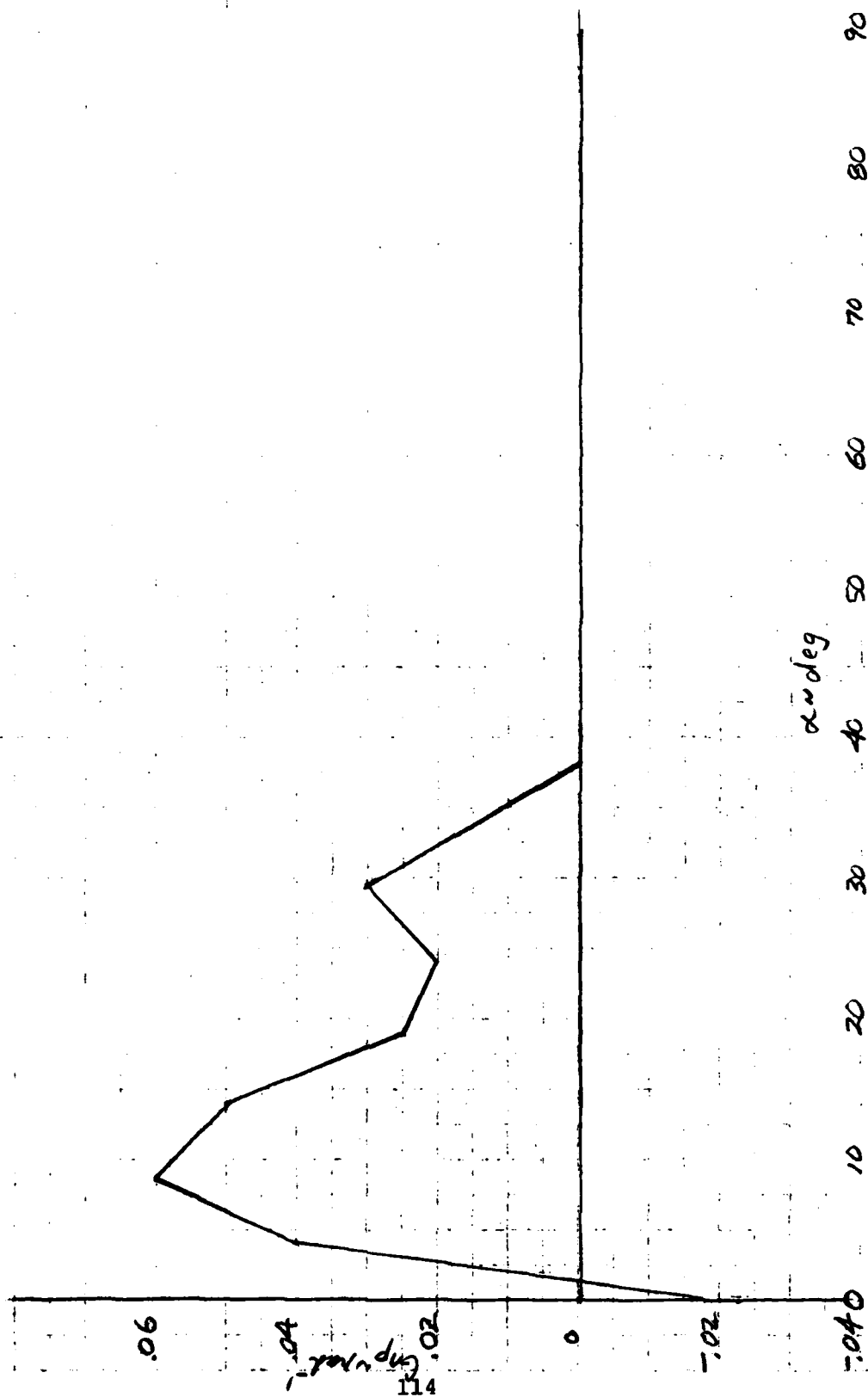Figure A12.- Damping derivative, C_{l_p}, as a function of angle of attack

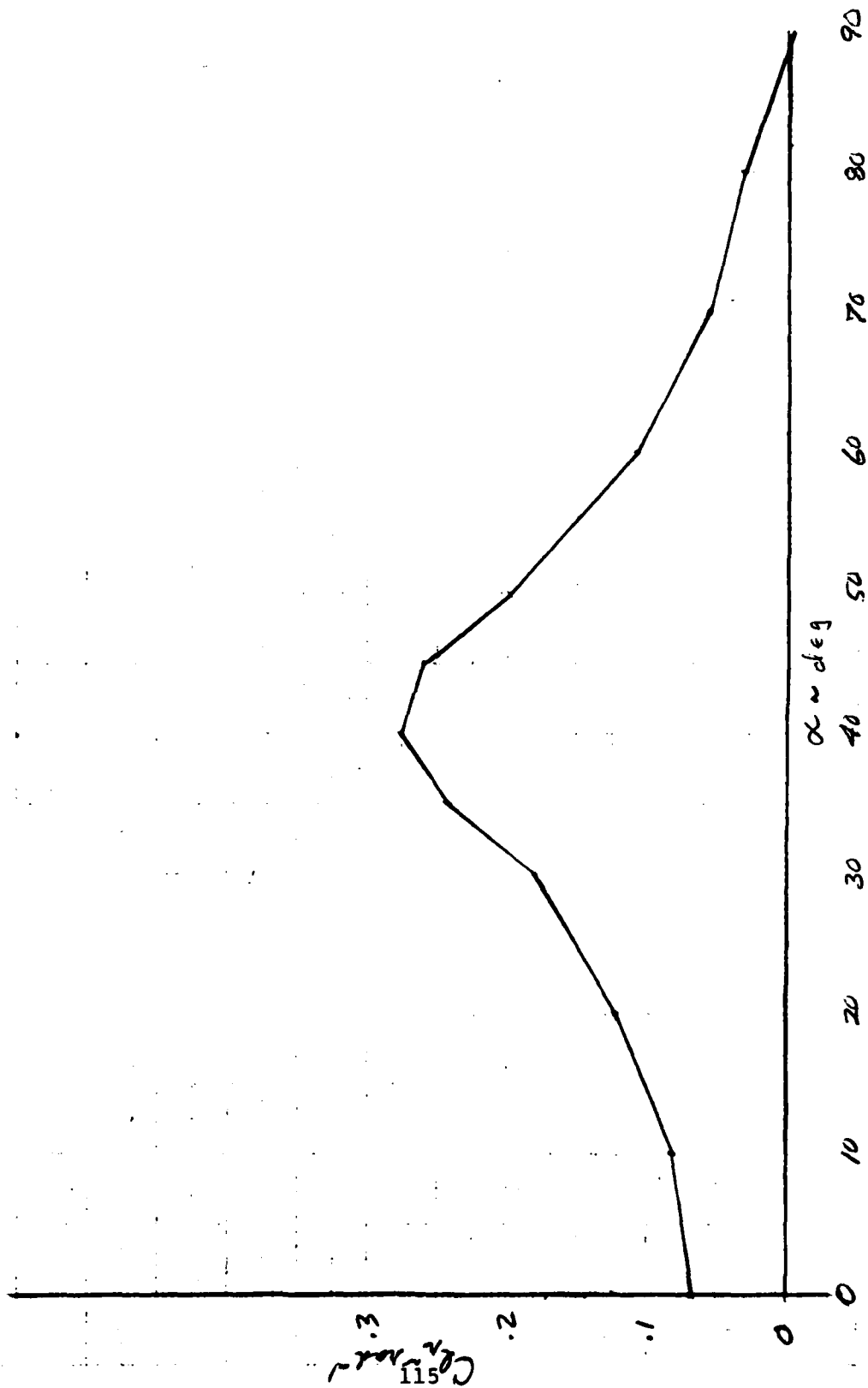Figure A13.- Cross derivative, C_{n_p}, as a function of angle of attack

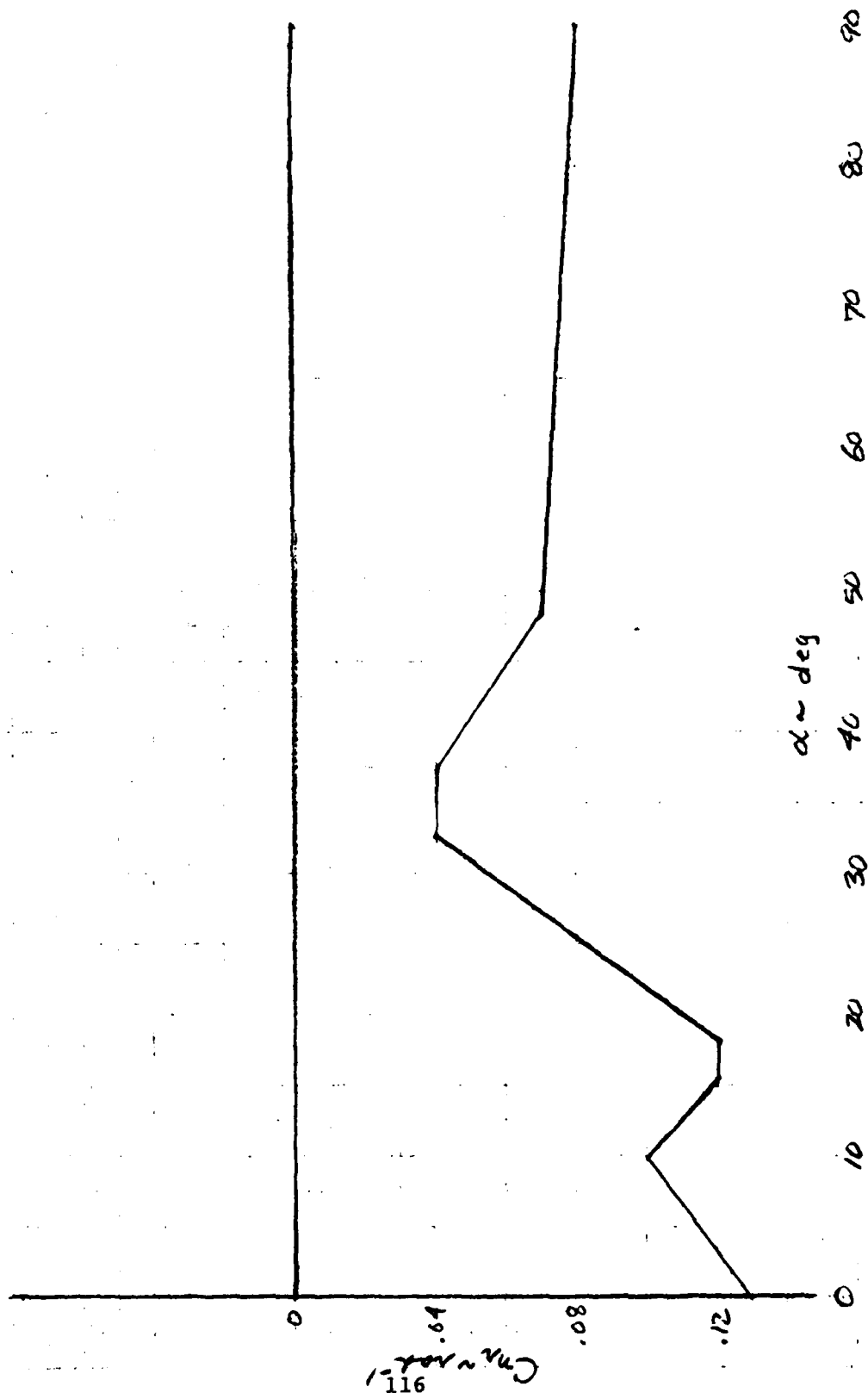Figure A14.- Cross derivative, C_{ℓ_r}, as a function of angle of attack

Figure A15.- Damping derivative, C_{n_r}, as a function of angle of attack

LIST OF REFERENCES

1.   Bihrle, William, Jr. and Barnhart, Billy: Design Charts
      and Boundaries for Identifying Departure Resistant
      Fighter Configurations, Naval Air Development Center,
      Warminster, Pennsylvania, 18974, Report No. NADC-76154-30,
      July 1978.

2.   Bihrle, William, Jr.: "Influence of the Static and
      Dynamic Aerodynamic Characteristics on the Spinning
      Motion of Aircraft", Journal of Aircraft, Vol. 8,
      No. 10, October 1971.

3.   Bihrle, William, Jr. and Barnhart, Billy: Effects of
      Several Factors on Theoretical Predictions of Air-
      plane Spin Characteristics, NASA CR 132521, August 1974.

4.   Moul, Martin T. and Paulson, John W.: Dynamic Lateral
      Behavior of High Performance Aircraft, NACA RM L58E16,
      August 1958.